

**ALGERIAN DEMOCRATIC AND POPULAR REPUBLIC
MINISTRY OF HIGHER EDUCATION
AND SCIENTIFIC RESEARCH**

**MENTOURI CONSTANTINE UNIVERSITY
FACULTY OF EXACT SCIENCES
DEPARTMENT OF PHYSICS**

Order number: 66/D3C/2024

Serial number:04/Phy/2024

THESIS

**Submitted to obtain the degree of
DOCTORATE OF THE THIRD CYCLE IN PHYSICS
Option: ENERGETIC**

Theme:

**CONTRIBUTION TO THE THEORETICAL STUDY OF HEAT AND
DYNAMIC TRANSFERS IN FINNED AND UNFINNED SOLAR
ABSORBERS**

By:

HASSEN HAITHEM

Defended on: 09/11/2024

Doctoral Committee:

President:	DJEZZAR Mahfoud	Pr	Frères Mentouri Constantine 1
Reporter:	BOUFENDI Toufik	Pr	Frères Mentouri Constantine 1
Examiners:	TOUAHRI Sofiane	MCA	Frères Mentouri Constantine 1
	FATEH MEBAREK Oudina	Pr	20 Août 1995 Skikda
	BENGUERBA Yacine	Pr	Ferhat Abbas Setif 1
	MAOUGAL Abdelaziz	Pr	Frères Mentouri Constantine 1

Acknowledgement

First and foremost, I want to express my gratitude to the Almighty **ALLAH** for His unwavering guidance and blessings throughout this journey.

I am deeply indebted to my late father, *Pr. HASSEN Djilani*, whose belief in my academic potential fueled my determination to pursue a PhD. Although he is no longer with us, his memory and encouragement continue to inspire me.

To my *mother*, whose steadfast support and encouragement have been my pillar of strength, I extend my heartfelt thanks. Her unwavering faith in me has been a source of motivation during the toughest of times.

A special acknowledgment is owed to my advisor, Professor *BOUFENDI Toufik*, whose mentorship and guidance have been invaluable from the very beginning of my doctoral studies. His expertise and dedication have played a pivotal role in shaping my academic journey. I am also deeply grateful to Professor *BEN GUERBA Yassin* for igniting within me a renewed passion for research through his unwavering dedication and enthusiasm. Furthermore, I extend my appreciation to *Dr. TOUAHRI Sofiane* for his valuable contributions, insightful discussions, and meticulous editing assistance throughout the thesis-writing process. I also would like to extend my thanks to all the professors who have imparted their knowledge and wisdom, each contributing in their own unique way to my academic growth and development. A sincere appreciation is extended to the respected members of my committee, with a special acknowledgment to *Pr. DJEZZAR Mahfoud*.

To my beloved *wife*, whose unwavering belief in me and unwavering support have been my rock, I owe the deepest gratitude. It is her love, encouragement, and sacrifices that have enabled me to pursue and complete this academic endeavor.

I extend my heartfelt thanks to my brother *Dr. HASSEN Naoufel*, my *two sisters*, *son*, and *daughter* for their unwavering support, understanding, and encouragement throughout this journey.

To my dear *friends*, whose companionship, encouragement, and occasional distractions have provided solace during the challenging times, I am truly grateful.

Last but not least, I want to express my gratitude to all those who have contributed in various ways, big and small, to my academic journey. Your support, encouragement, and belief in my abilities have played a significant role in helping me reach this important milestone.

Thank you all, from the bottom of my heart.

Table of contents

Nomenclature	III
List of figures	I
List of tables	I
General introduction	01
Brief history	02
Algeria’s energy	04
Problematic and structure of the thesis	05
Chapter 1	
Literature survey	06
1.1.Introduction	06
1.2. Convection in horizontal pipe	12
1.3. Convection in annular pipe	13
1.4. Convection in finned pipe	14
1.4.1. External fins	15
1.4.2. Internal fins	19
1.4.2.1.Internal helical fins	20
1.5. Summarized of the literature review	27
1.6. Conclusion	27
1.7. Objective	27
Chapter 2	
Mathematical modeling	29
2.1.Introduction	29
2.2.Model geometry	30
2.3.Governing equations	33
2.3.1. Conservation of Mass	34
2.3.2. Conservation of Momentum (Navier-Stokes Equations)	34
2.3.3. Conservation of Energy	34
2.3.4. Nusselt number	35
2.4. Important parameters	35
2.4.1. Pressure drop	35
2.4.2. Friction factor	36
2.4.3. Head loss	36
2.4.4. Colburn J-factor	37
2.4.5. Performance evaluation criterion “PEC”	37
2.4.6. Fin effectiveness	38
2.4.7. Fin efficiency	38
2.5. Geometrical characteristics	38

2.6. Benefit	40
2.7. Conclusion	41
Chapter 3	
Numerical resolution	42
3.1.Introduction	42
3.2.FIRST TEST: the mesh	43
3.2.1. Mesh elements size test	44
3.3.Results validation	48
3.4.Conclusion	48
Chapter 4	
Results and discussion	49
4.1.Introduction	49
4.2.SECOND TEST: fins number	50
4.2.1. Hydrodynamic	52
4.2.2. Thermal	54
4.2.3. Pressure drop	57
4.2.4. Heat transfer	59
4.2.5. Conclusion	61
4.3.THIRD TEST: helix angle	63
4.3.1. Hydrodynamic	64
4.3.2. Thermal	67
4.3.3. Pressure drop	71
4.3.4. Heat transfer	72
4.3.5. Conclusion	75
4.4.FOURTH TEST: heat flux	76
4.4.1. Hydrodynamic	77
4.4.2. Thermal	78
4.4.3. Nusselt number	83
4.4.4. Conclusion	84
4.5.FIFTH TEST: fluid velocity	85
4.5.1. Hydrodynamic	85
4.5.2. Thermal	87
4.5.3. Pressure drop	91
4.5.4. Heat transfer	92
4.5.5. Conclusion	94
General conclusion	95
Future studies	98
References	99
Annex I	107
Annex II	108

Nomenclature

Symbols

A	Surface area	m^2
b	Fin base distance	m
c	Fin top distance	m
C _p	Specific heat	J/kg.°C
D	Tube diameter	m
D _h	Hydraulic diameter	m
e	Fin height	m
ED _i	External diameter of inner tube	m
ED _o	External diameter of outer tube	m
EC _f	External circumference of fins	m
ES _f	External surface of fins	m^2
f	Darcy friction factor	-
g	Acceleration due to gravity	m/s^2
h	Convective heat transfer coefficient	w/m^2K
H _L	Helical fin length	m
HL	Head loss	m
H _p	Helical fin length	m
ID _i	Internal diameter of inner tube	m
ID _o	Internal diameter of outer tube	m
j	Colburn J-factor	-
k	Thermal conductivity	$W/m.K$
L	Tube length	m
N _s	Number of fins or number of starts	-
Nu	Nusselt number	-
p	Pitch of a helix	m
P	Static pressure	Pa
Pr	Prandtl number	-
q	Heat flux	w/m^2
Q	Heat transfer rate	W
R	electrical resistance of helical fin	Ω
Re	Reynolds number	-
S	cross-sectional area of the trapezoidal fin	m^2
t	Time	S

T	Temperature	°C or K
T_s	Distance between two fins	m
u, v, w	Velocity components in the r, θ , and z directions, respectively	m/s
V	Average velocity	m/s

Greek Symbols

α	Helix angle	°
ΔP	Pressure loss	Pa
ρ	Fluid density	Kg/m ³
ρ_e	Aluminum electrical resistivity	$\Omega \cdot m$
μ	Fluid viscosity	Pa.s
σ	electrical conductivity	S/m
ε	Tube roughness	m
ϵ	Fin effectiveness	
η	Fin efficiency	

Subscripts

b	Base area
f	Fin
h	Hydraulic
i	Inner
o	Outer
0	Reference case “smooth tube”
∞	Surrounding
W	Water

Units

GW	gigawatt	GW = 10 ⁹ watt
EJ	exajoule	EJ = 10 ¹⁸ joule

Abbreviation

(PV)	Solar Photovoltaic
(WHO)	World Health Organization
(RCREEE)	Regional Center for Renewable Energy and Energy Efficiency

(CFD)	Computational fluid dynamics
(GNP)	Gold nanoparticle
(AIFT)	arc-shaped inner finned tube
(PCM)	Phase change materials
(PEC)	Performance evaluation criterion
(HVAC)	Heating, Ventilation and Air Conditioning

List of figures

Figure 01:	A cross-section of a hot box	02
Figure 02:	First solar water heater	03
Figure 03:	The best research-cell efficiencies by the national renewable energy laboratory	03
Figure 04:	Current Installed Capacity of production of energy	04
Figure 05:	Oil and natural gas basins and pipeline infrastructure in Algeria	04
Figure 1.1:	Types of solar thermal collectors	08
Figure 1.2:	Different methods to enhance tubes of solar thermal collectors	09
Figure 1.3:	Different tubing geometry of solar thermal absorber	11
Figure 1.4:	Different finned geometries	14
Figure 1.5:	(A) simple schematic of air-cooling system - (b) external helical fins	15
Figure 1.6:	Forced draft air-cooled heat exchanger	15
Figure 1.7:	Characteristics and arrangement of finned tubes	16
Figure 1.8:	Finned-tube construction	16
Figure 1.9:	(a) Tubes with confuser-type bent fins – (b) Flat-oval tubes with incomplete finning	18
Figure 1.10:	Arrangements of profiled tubes in bundles and their slope	18
Figure 1.11:	Solar air heater with wavy finned absorber	18
Figure 1.12:	(a) Visualization of the Longitudinal fins - (b) Visualization of the transverse fins	20
Figure 1.13:	Fin geometries used by Deorah [68]	22
Figure 2.1:	Tube geometry, example of two helical fins	30
Figure 2.2:	Trapezoidal fins geometry	31
Figure 2.3:	Helical fins geometry details	31
Figure 2.4:	Illustration of helix angle	31
Figure 3.1:	Tetrahedral mesh structure illustration	44
Figure 3.2:	Outlet velocity and temperature elements size comparison	45

Figure 3.3: Illustration of mesh element size difference between (a) 0.0001 m and (b) 0.0005 m	45
Figure 3.4: Key parameters comparison between 0.0001 m and 0.0005 m cases	46
Figure 3.5: Velocity and temperature contours, element quality and fluid interface temperature for the 0.0001 m and 0.0005 m element size cases.....	47
Figure 3.6: Illustration of tetrahedral mesh with 0.0005 m element size for the case of 8 helical fins with 45° helix angle	47
Figure 3.7: Validation of the calculation code for a horizontal pipe: a comparison with the values of the average circumferential Nusselt obtained by Nazrul et al. [102]	48
Figure 4.1: Mind map of all tests done in the study	50
Figure 4.2: Cases studied geometries in test 02	51
Figure 4.3: Illustration of 8 fins 20° annulus geometry	51
Figure 4.4: Velocity contours of all cases in test 02	53
Figure 4.5: Average axial velocity for all cases in test 02	53
Figure 4.6: Temperature contours of all cases in test 02	55
Figure 4.7: Minimum fluid temperature along the axial direction of all cases in test 02.....	56
Figure 4.8: Average interface fluid-outer tube temperature along the axial direction for test 02	56
Figure 4.9: Average tubes walls temperature for test 02	57
Figure 4.10: Pressure drop variation along the axial direction for test 02	58
Figure 4.11: Wall shear stress versus pressure drop for all cases in test 02	59
Figure 4.12: Surface heat flux values of all cases in test 02	59
Figure 4.13: Heat flux versus heat transfer coefficient for all cases of test 02	60
Figure 4.14: Plot of Nusselt number along the axial direction for all cases of test 02.....	61
Figure 4.15: Cases studied geometries of test 03	64
Figure 4.16: Velocity contours of all cases in test 03	66
Figure 4.17: Average velocity along the axial direction	66
Figure 4.18: Temperature contours for all cases in test 03	68

Figure 4.19: Minimum fluid temperature along the axial direction of all cases in test 03.....	69
Figure 4.20: Average interface fluid-outer tube temperature along the axial direction for test 03	69
Figure 4.21: Average tubes walls temperature for test 03	70
Figure 4.22: Pressure drop variation along the axial direction for test 03	71
Figure 4.23: Wall shear stress versus pressure drop for all cases in test 03	72
Figure 4.24: Surface heat flux values of all cases in test 03	72
Figure 4.25: Heat flux versus heat transfer coefficient for all cases of test 03	73
Figure 4.26: Plot of Nusselt number along the axial direction for all cases of test 03.....	74
Figure 4.27: Velocity contours for all cases in test 04	78
Figure 4.28: Average velocity along the axial direction, test 04	78
Figure 4.29: Temperature contours for all cases in test 04	80
Figure 4.30: Minimum fluid temperature along the axial direction for all cases in test 04.....	80
Figure 4.31: Average interface fluid-outer tube temperature along the axial direction for test 04	81
Figure 4.32: Heat flux versus heat transfer coefficient for all cases of test 04	82
Figure 4.33: plot of Nusselt number along the axial direction for all cases of test 04.....	83
Figure 4.34: Velocity contours for all cases of test 05	86
Figure 4.35: Average velocity along the axial direction, test 05	87
Figure 4.36: Temperature contours for all cases in test 05	88
Figure 4.37: Minimum fluid temperature along the axial direction for all cases in test 05.....	89
Figure 4.38: Average tubes walls temperature for test 05	90
Figure 4.39: Pressure drop variation along the axial direction for test 05	91
Figure 4.40: Wall shear stress versus pressure drop for all cases in test 05	92
Figure 4.41: Heat flux versus heat transfer coefficient for all cases of test 05	93
Figure 4.42: Plot of Nusselt number along the axial direction for all cases of test 05.....	93

List of tables

Table 1.1: Helical groove tubes parameters used by Jamshed et al. [74]	23
Table 2.1: Finned tubes parameters for different helix angles	32
Table 2.2: The friction factor in different flow regimes	36
Table 2.3: Different geometry parameters of helical fin tubes from the previous works	
Table 3.1: Element size parameters comparison	40
Table 4.1: Parameters of the cases studied in test 02.....	45
Table 4.2: Average axial velocity values of the cases studied in test 02	41
Table 4.3: Parameters of the cases studied in test 03	54
Table 4.4: Average axial velocity of the cases studied in test 03	63
Table 4.5: Average axial velocity of the cases studied in test 04.....	66
Table 4.6: inlet and outlet values of Nusselt number for all case for the test 04	78
Table 4.6: Cases parameters for the test 05	84
Table 4.7: Average axial velocity of the cases studied in test 05.....	85
Table 4.8: Different temperatures walls at the outlet in test 05.....	87

General introduction

The human needs energy for his life, as the energy is the capacity of a physical system to perform work, energy sources are classified into three main groups: fossil fuels, alternative energy, and renewables. **Fossil fuels** are made from ancient plants and animals subjected to high heat and pressure over thousands of years, such as oil, gas, and coal. **Alternative energy** includes any type of energy that isn't derived from fossil fuels, encompassing renewables and nuclear energy. **Renewable energy** consists of sources that can be naturally replenished within a human lifespan [1]. As we know that renewable energy has five big categories such as solar, wind, hydraulic, biomass and geothermal.

The most plentiful renewable energy source globally is solar energy, which involves technologies that change sunlight or heat from the sun into usable energy. Utilizing sunlight, we employ Solar Photovoltaic (PV) technology to transform solar energy into direct current electricity using semiconductors. Additionally, harnessing the sun's heat, we utilize Solar Thermal technologies to capture solar heat energy for heating and/or generating electricity.

In recent decades, there has been a growing concern about energy consumption, driven by a rapid increase in demand for energy. Moreover, environmental issues associated with conventional energy sources, such as climate change and global warming, are prompting a shift towards alternative energy solutions. According to the World Health Organization (WHO), the direct and indirect consequences of climate change lead to the loss of 160,000 lives annually [2].

The sun's energy output is immense, delivering more energy to Earth in a single hour than humanity consumes in a year. This celestial body radiates an astounding 3.8×10^{26} kilowatts of power, with approximately 1.8×10^{14} kilowatts reaching our planet. About

60% of this incoming energy reaches Earth's surface, while the remaining portion is reflected back into space or absorbed by the atmosphere.

Even harnessing a small fraction of this solar energy, just 0.1% with a modest 10% efficiency, could generate electricity four times greater than the current global generating capacity, which is roughly 3000 gigawatts. The annual solar radiation received by Earth, exceeding 3,400,000 exajoules, far surpasses the world's total annual primary energy consumption of 450 exajoules by a factor of over 7500. This amount also significantly outweighs the combined reserves of all non-renewable energy resources, including fossil fuels and nuclear power. Despite this vast potential, fossil fuels still provide 80% of the world's energy needs [3].

Globally, the aggregate demand for different renewable energy sources for industrial purposes, excluding hydroelectric and biomass, accounts for only around 0.8% [4] This goes against plans aimed at increasing investment in renewable energy sectors and optimizing the utilization of fossil fuels.

Brief history

Researchers are embarking on studies to harness this abundant and free energy. The journey started in 1876 when William Grylls Adams and his student, Richard Evans Day, made a groundbreaking discovery: they found that light could produce an electric current in Selenium. Albert Einstein's work on the photoelectric effect, pivotal for solar cell electricity generation, earned him the Nobel Prize in Physics in 1921. In 1953, Gerald Pearson, Daryl Chapin, and Calvin Fuller introduced the silicon solar cell, marking the advent of the first material capable of directly converting sunlight into electricity to power devices.

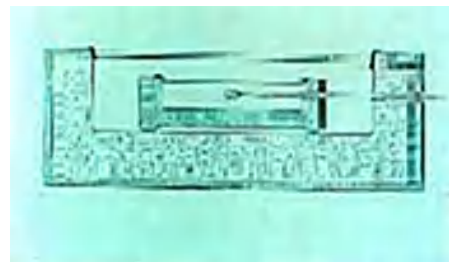


Figure 01: A cross-section of a hot box [5]

Dr. Hans Ziegler, an eminent expert in satellite instrumentation in the late 1950s, challenged the conventional belief held by the Navy. He argued that while traditional batteries would exhaust quickly, solar cells could sustain satellites for extended periods, saving millions of dollars in silent electronic equipment. In the 18th and 19th centuries, scientists utilized hot boxes to measure the sun's heat trapped by glass-covered enclosures. (figure 01).

No easy method existed for heating water during that time. Typically, people relied on a cook stove for this purpose, involving chopping wood or lifting heavy coal hoods, kindling the fuel, and periodically stocking the fire. In urban areas, the wealthier individuals used gas manufactured from coal to heat their water, although the fuel burned uncleanly and the heater required relighting each time. In many regions, wood, coal, or coal-gas were expensive and often difficult to obtain. To address these challenges, resourceful farmers, prospectors, and outdoor enthusiasts devised a safer, simpler, and more cost-effective solution – placing a black-painted metal water tank in the sun to absorb maximum solar energy. These were the earliest recorded solar water heaters, consisting of bare metal tanks painted black and tilted to face the sun (figure 02). By 1983, 60% of the Israeli population heated their water using solar energy. Even when the price of oil dropped in the mid-1980s, the Israeli government mandated solar water heating to prevent a regression in energy practices observed elsewhere. Consequently, today, over 90% of Israeli households own solar water heaters [5].



Figure 02: first solar water heater [5]

The evolution of solar energy technologies has progressed significantly from that time until now and into the future. However, various efficiency issues persist, such as the maximum efficiency achievable by photovoltaic cells, which, as of 1976 to 2024, stands at

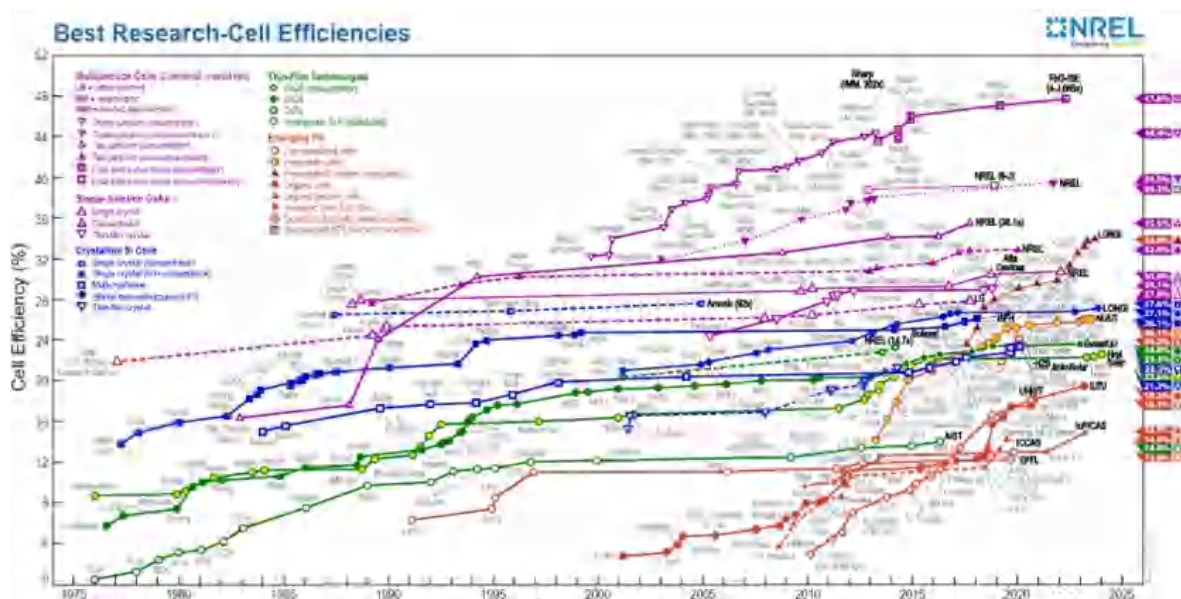


Figure 03: the best research-cell efficiencies by the national renewable energy laboratory [6]

just 47% for the four-junction or more "concentrator" type at the Fraunhofer Institute for Solar Energy Systems/Soitec (figure 03) [6]. Additionally, the best efficiency attained by a silicon single crystal is only 26.1%, achieved by the Institute for Solar Energy Research Hamelin. Considering these limitations, the prospect of reaching efficiencies of 80% or even 100% remains an ambitious goal.

Algeria's energy

Algeria possesses substantial natural gas reserves, estimated at approximately 159 trillion cubic feet, representing nearly 2.3% of global reserves as of January 1, 2016 [7]. The nation's economy heavily depends on its position as the third-largest oil producer in Africa, with fossil fuels serving as the primary energy sources. These resources contribute about 30% to Algeria's gross domestic product.

However, renewable energy sources, such as hydro and solar, account for only a small portion of the country's installed energy capacity, at approximately 2% (figure 04) [8]. The government has set ambitious goals to diversify the energy mix, aiming to increase the share of electricity generation from renewable energy sources to 6% by 2020 and further to 40% by 2030.

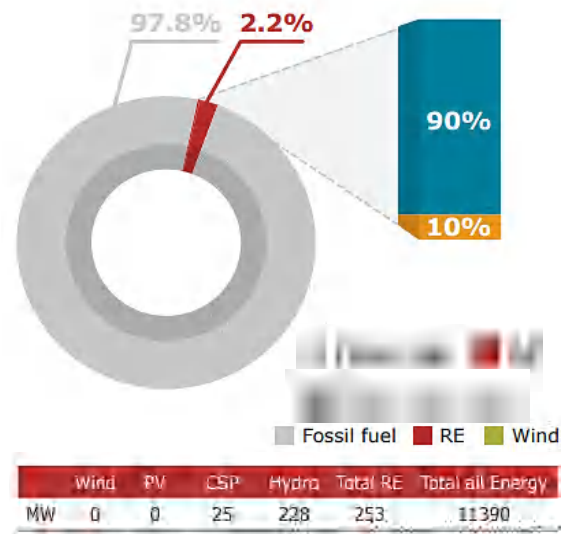


Figure 04: Current Installed Capacity of production of energy [8]

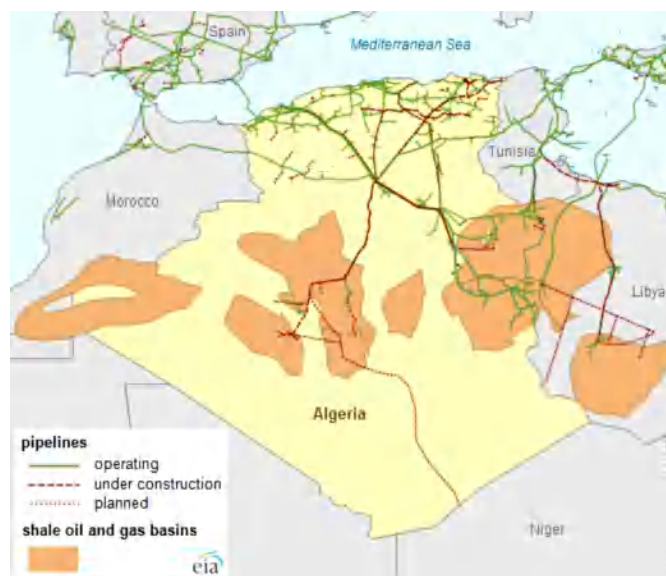


Figure 05: Oil and natural gas basins and pipeline infrastructure in Algeria [7]

Problematic and structure of the thesis

Year after year, the problem of forced convection with different conditions is been treating at the Laboratory of Energy Physics at Mentouri Constantine University and they progressing with considerable results, it start by **Boufendi & Afrid [9]** with their Three-dimensional Conjugate Conduction-Mixed convection study, **Boufendi [10]** continue with this problem in his Ph.D. thesis concerning the mixed convection in cylindrical horizontal conduit, in 2010 **Benkhadda [11]** worked on annular cylindrical duct with fins, after him **Chahboub [12]** treated the influence of parietal conduction on the conjugate heat transfer in horizontal duct, the development is steel continuing, in 2012 **Touahri [13]** advanced in his Ph.D., he treated the three-dimensional mixed convection combined with fluid flows in cylindrical horizontal ducts with and without fins, this amount works have done a considerable development and made the way more easy for us and for the next generation.

In light of previous studies, our research endeavors to further explore and enhance a similar topic by selecting an annulus with comparable characteristics as our model. The novelty of our research lies in the inclusion of helical fins geometry, thus we undertake an investigation into varying the number and helix angle of these fins. However, this thesis comprises four chapters structured as follows: Chapter 1 provides a comprehensive review of existing research on solar thermal collectors, highlighting various methods aimed at enhancing heat transfer within the tubes, including the use of nanofluids, innovative tube geometries, and the integration of fins. Chapter 2 lays the groundwork by developing a robust mathematical framework to accurately model the physical processes involved, incorporating essential equations governing fluid flow and heat transfer. Chapter 3 transitions to computational fluid dynamics (CFD) simulations, meticulously constructing the simulation environment and conducting tests to investigate the system's thermo-hydraulic behavior. Throughout Chapter 4, a series of experiments and analyses are meticulously designed and executed to answer key research questions, exploring the impact of parameters such as fins number, helix angle, heat flux, and fluid velocity on heat transfer performance and pressure drop. Finally, Chapter 5 synthesizes the findings, revealing the superiority of tetrahedral mesh structures, optimal mesh element sizes, and the nuanced effects of varying parameters, offering valuable insights for optimizing similar systems in practical applications.

Chapter 1

Literature survey

1.1 Introduction

The phenomenon of heat transfer, the movement of energy from hotter to colder objects, has long been recognized. In 1822, Joseph Fourier's seminal work, "Théorie Analytique de la Chaleur," laid the foundation for the theory of heat conduction, known as Fourier's Law. This law describes the microscopic agitation and propagation of particles that underlies heat transfer. Beyond conduction, objects continuously emit energy through electromagnetic radiation. This process, known as radiation, has been a subject of scientific inquiry for centuries. Before Fourier's work, in 1701, Isaac Newton examined the process of convection, the transfer of heat through the movement of a fluid. Convection occurs when a fluid, such as air or water, carries heat away from a solid object [14].

There are three types of convection: natural convection (also known as free convection), forced convection, and mixed convection. Natural convection occurs spontaneously due to temperature differences, leading to density variations within the fluid. Forced convection happens when the fluid is subjected to increased pressure through mechanical means such as pumps or fans. Mixed convection arises when both natural and forced convection occur simultaneously, with comparable magnitudes. In mixed convection, if the effects of natural convection and forced convection align, it's termed favorable mixed convection. Conversely, if the effects of Archimedes forces and the fluid movement imposed by mechanical systems oppose each other, it's termed unfavorable mixed convection. [15]. Just after 1960 researchers consider the effect of natural convection on the mixed convection in ducts, in our study we consider this effect, taking into account the studies related.

Starting with renewable energies, derived from natural sources like sunlight, wind, and water, offer a sustainable alternative to traditional fossil fuels. Harnessing these resources for power generation minimizes environmental impact and addresses the growing concerns of climate change. Solar energy utilizes sunlight to produce electricity, while wind power harnesses the kinetic energy of the wind. Hydropower taps into the energy of flowing water, and other sources like geothermal and biomass contribute to the diverse portfolio of renewable energy options. Embracing these clean and inexhaustible sources not only reduces carbon emissions but also fosters a more resilient and environmentally friendly energy landscape, paving the way for a sustainable future.

Renewable energy sources have emerged as a crucial avenue in addressing global energy demands while mitigating environmental impacts. Within the realm of renewable resources, solar energy stands out as a beacon of sustainability, harnessing the sun's inexhaustible power. Solar thermal collectors play a pivotal role in capturing and converting this abundant solar energy into heat. These collectors, ranging from flat-plate designs to concentrated systems (figure 1.1), facilitate the transformation of sunlight into thermal energy. As a cornerstone of sustainable technology, solar thermal collectors contribute to reducing dependence on non-renewable resources and curbing carbon emissions. The overarching goal is to enhance energy efficiency, foster energy independence, and propel a transition towards cleaner and greener energy solutions. As research and innovation progress, the

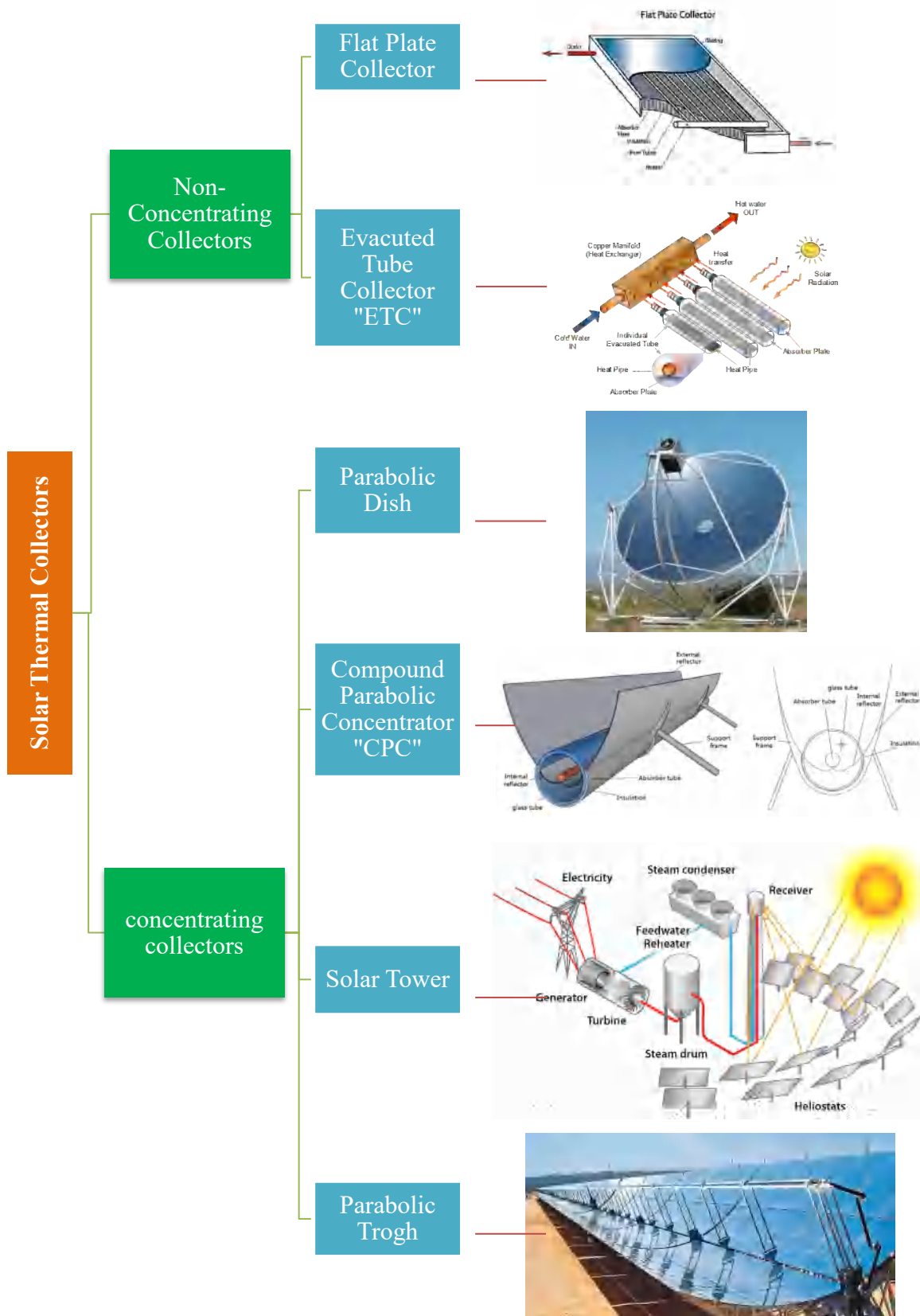


Figure 1.1: types of solar thermal collectors

integration of solar thermal collectors continues to yield promising results, aligning with broader objectives to create a more sustainable and resilient energy future.

It is clear that heat transfer had numerous problems, these problems can be differentiated according to their goals as the following:

- The increase of the energy that is either transmitted or absorbed by a surface.
- The obtaining of a better efficiency of the heat source.
- The reduction or increase of the heat flow passage from one setting to another [16].

Many researches were published in order to solve those problems and to reach a high efficiency, those studies are divided into experimental and theoretical, and they touched all the parts of a solar thermal collector. With a view to enhance the efficiency, **Klein [17]**, **HOLLANDS & al [18]** and **WIJEYSUNDERA & al [19]** studied the energy loss in the insolation and cover of a flat-plate collector, **Oliva et al [20]** and **Michaelides & al [21]** determined the thermal behavior of a solar collector, while **De Ron [22]**, **Hilmer & al [23]**

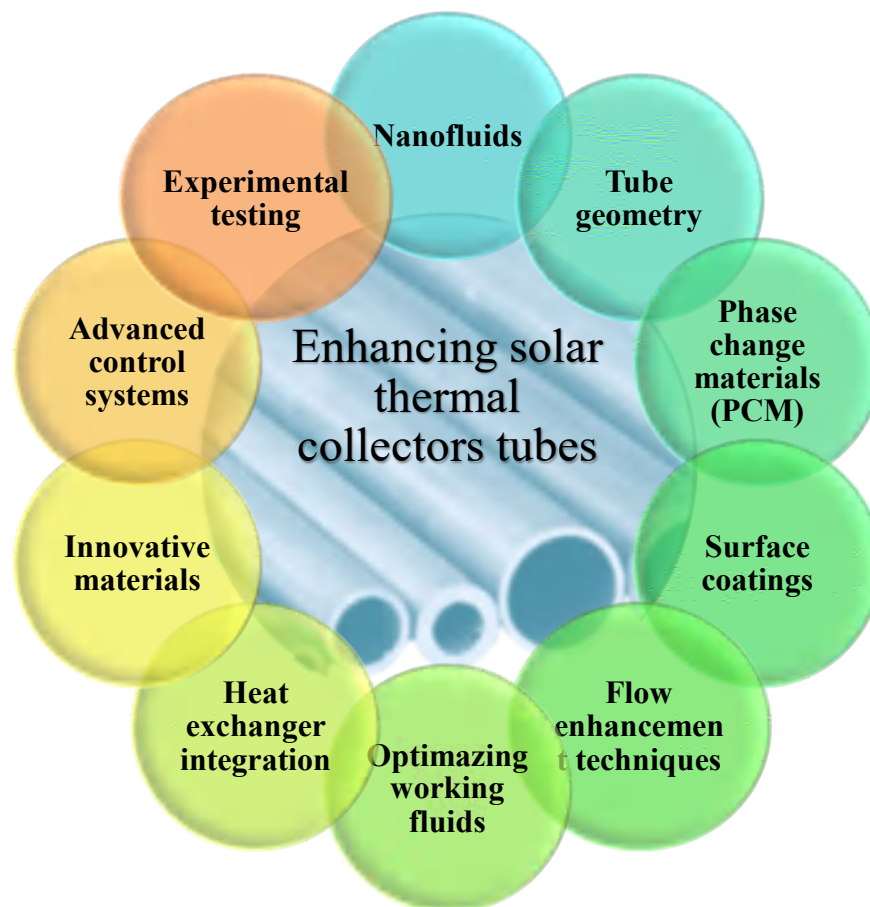


Figure 1.2: different methods to enhance tubes of solar thermal collectors

and **kalogirou & al [24]** studied it experimentally. Solar collectors are also used for cooling purposes. As such as, **Florides & al [25]**, **Lu & al [26]**, **Balghouthi & al [27]** and **Florides & al [28]** who presented studies of solar cooling system. Although, inside the solar collectors we found many studies on enhancing the conductivity of the transportation fluid by adding Nano-Particles, we mention the studies of **Choi [29]**, **Eastman & al [30]**, **Choi & al [31]** and **Zhang & al [32]** who used Gold nanoparticle (GNP), and many other researchers who studies different parts of different types of solar collectors.

Focusing on a simple component of the solar thermal collector, which are the tubes, we can improve them through several methods, as explained below (figure 1.2). Different types are used for the aim of enhancing heat transfer inside tubes of solar collectors:

- 1) **Nanofluids for Improved Heat Transfer:** Investigating the use of nanofluids (fluids containing nanoparticles) to enhance heat transfer efficiency within the tubes. Research could focus on different types of nanoparticles, concentrations, and their impact on heat transfer rates.
- 2) **Enhanced Tube Geometry:** Exploring novel tube designs and geometries, such as ribbed or corrugated tubes, to increase turbulence and improve heat transfer. Computational fluid dynamics (CFD) simulations can be employed to optimize these designs.
- 3) **Phase Change Materials (PCM):** Studying the integration of phase change materials within the tubes of solar collectors to store and release heat efficiently. This can help extend the availability of hot water or energy during cloudy periods.
- 4) **Surface Coatings:** Investigating the application of advanced coatings on the inner surfaces of collector tubes to improve heat absorption and transfer. These coatings may include selective absorber coatings or superhydrophobic coatings.
- 5) **Flow Enhancement Techniques:** Researching techniques like swirl flow or using inserts (e.g., twisted tapes) within the tubes to enhance heat transfer by increasing turbulence and mixing of the working fluid.
- 6) **Optimizing Working Fluids:** Analysing the use of different working fluids, such as organic fluids or refrigerants, to maximize heat transfer efficiency in varying temperature conditions.

- 7) **Heat Exchanger Integration:** Exploring the integration of heat exchanger designs within the collector tubes to extract and transfer heat more effectively to the desired application, such as space heating or electricity generation.
- 8) **Innovative Materials:** Investigating advanced materials, including carbon nanotubes or graphene-based materials, for both the tube construction and the working fluid to improve thermal conductivity and heat transfer.
- 9) **Advanced Control Systems:** Developing smart control systems that optimize the operation of solar collectors based on real-time weather conditions and demand, ensuring efficient heat transfer and energy utilization.
- 10) **Experimental Testing:** Conducting experimental studies in real-world conditions to validate theoretical models and assess the performance of various heat transfer enhancement techniques.

These research avenues address different aspects of enhancing heat transfer within solar collector tubes and can contribute to improving the overall efficiency and effectiveness of solar thermal systems.

In our study we are interested in enhancing the heat transfer inside tubes of solar thermal collectors by adding external surfaces such as fins, There are several types of solar thermal collector tubes, the most common type is the horizontal or inclined pipe in which the cold fluid pass through it and back hotter (Figure 1.3 A), the second type is the annular one where two tubes are attached one inside the other with different diameters (figure 1.3 B), in these two types we can add external surfaces like fins, this goal is a focal point of interest for numerous researchers as we mentioned in the following paragraphs.

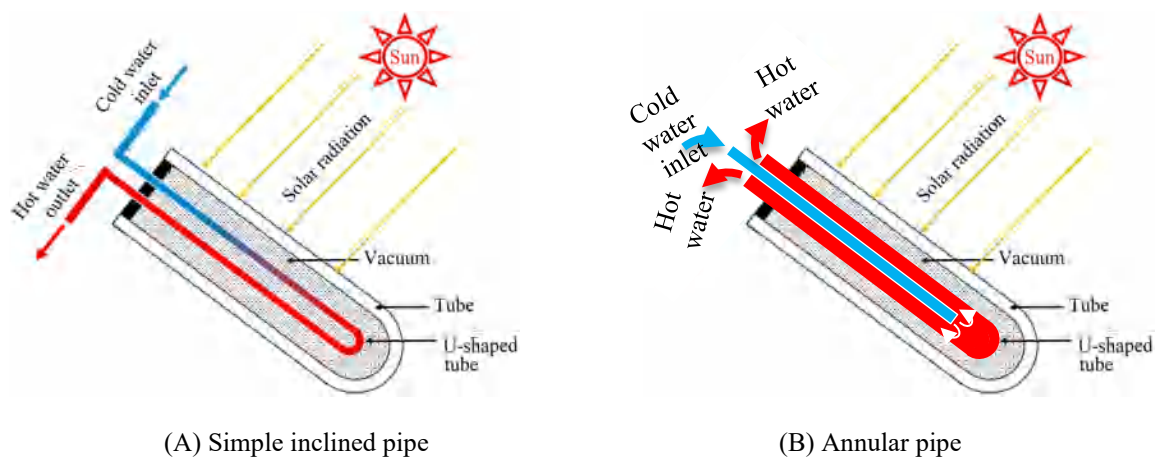


Figure 1.3: different tubing geometry of solar thermal absorber

1.2 Convection in horizontal pipe

Several experimental, theoretical, analytical and numerical works, have been published by researchers on the problem of mixed convection in full cylindrical ducts, and that's because of its large applications such as heat exchangers, nuclear reactors cooling system, heating water in solar thermal collectors etc. However, there exist two types of applications of boundary conditions: thermal conditions applied to the interface solid-fluid and thermal conditions applied to the external surface (conjugated problem) which is the subject of our current study.

Neglecting the conduction in mixed convection is common treated problem, its first appearance by **Martinelli et Boelter [33]** in which they studied the laminar developed flow in vertical cylindrical pipe, thus, in inclined pipe, the laminar mixed convection was studied numerically by **Orfi et al. [34]**. However, **wang et al. [35]** analyses numerically the mixed convection in horizontal and vertical pipes, it is clear that considering conduction in the pipes thickness make the study close to reality more than neglecting it, however, many authors **Boufendi & Afrid [36,37]**, **Touahri & Boufendi [38]**, **Abboudi & Papini [39]**, **Mokrane [40]** and others, determined that taking the thermal conduction into account makes the numerical results in excellent agreement with those obtained experimentally.

Boufendi & Afrid [9] conducted a comprehensive three-dimensional numerical simulation to model heat transfer in a horizontal pipe with a thin wall. This simulation focused on mixed laminar convection coupled with conduction within the pipe wall, which experiences constant and uniform volumetric heating. The study incorporated the thermal dependence of fluid properties and considered thermal losses between the pipe's outer surface and the surrounding environment. The governing equations for continuity, momentum, and energy were solved using a first-order discretized finite volume method. The results revealed that both thermal and dynamic fields exhibit three-dimensional behavior. A significant non-uniformity in heat flux was observed at the wall-fluid interface. The average Nusselt number within the pipe showed a substantial increase as volumetric heating within the pipe wall intensified. Importantly, these numerical findings were found to be consistent with experimental data obtained under identical geometric, dynamic, and thermal conditions.

Chehboub [12] and **Chehboub & Boufendi [42]** conducted numerical studies to investigate the impact of wall conduction on heat transfer within a horizontal duct. Their research focused on three different materials: **Inconel** ($K= 15 \text{ W/m.K}$), **steel** ($K= 48.5 \text{ W/m.K}$), and **tantalum** ($K= 57.5 \text{ W/m.K}$). The researchers numerically solved the conservation equations for mass, momentum, and energy, incorporating appropriate initial and boundary conditions using the finite volume method.

Their model accounted for mixed convection within the fluid coupled with thermal conduction in the duct wall. The fluid properties were considered thermally dependent, with a fixed geometric aspect ratio (L / D_i) of 104.17. The Reynolds and Prandtl numbers were calculated using the properties of water at a reference temperature ($T_0= 288 \text{ K}$ at the tube inlet), resulting in $Re=143.28$ and $Pr=8.082$.

The results demonstrated that mixed convection, under the studied control parameters, leads to a significant circumferential temperature variation in the wall further from the inlet. This variation is mitigated as the thermal conductivity of the material increases. The study further revealed that heat transfer enhances with increasing wall conductivity.

1.3 Convection in annular pipe

Recent scientific investigations into convection in annular pipes have yielded important insights into heat transfer phenomena within this geometry. Notably, the study by **Chen et al. [43]** employed computational fluid dynamics (CFD) simulations to analyze laminar flow and heat transfer in concentric annular pipes. Their findings revealed the impact of geometrical parameters, such as the aspect ratio and eccentricity, on heat transfer performance, emphasizing the importance of optimizing annular channel designs in thermal systems. Additionally, a comprehensive experimental investigation conducted by **Kim and Park [44]** examined turbulent heat transfer in annular channels with twisted tape inserts. Their work demonstrated substantial enhancements in heat transfer coefficients, illustrating the potential of passive techniques for improving the thermal efficiency of annular pipe systems. These recent studies underscore the significance of convection research in annular pipes for applications in various engineering and industrial contexts.

Back to 1980, **Mojtabi and Calatagirone [45]** examined laminar flow with varying Rayleigh numbers and inclination angles, finding that the axial flow in mixed convection

becomes more pronounced with higher Rayleigh numbers and is optimized when cylinders are horizontally oriented. Another numerical study was conducted by **Kotake and Hatorry [46]** where they analyzed mixed convection with different thermal boundary conditions and validated their results against experiments. However, **Habib et al. [47]** investigated mixed convection with non-uniform heat flux, and **Teamah et al. [48]** examined a wide range of parameters, showing the dominance of natural convection at low Prandtl numbers. **Padilla et al. [49]** explored the transition from conduction-dominated to convection-dominated heat transfer as Rayleigh numbers increased. These studies collectively contribute to understanding mixed convection in concentric cylinders under various conditions, offering valuable insights into heat transfer phenomena.

1.4 Convection in finned pipe

Based on the **FOURIER** law, the heat flux rises with the increase of heat exchange surface, a more popular method to extend heat transfer rate and promote the fluid turbulence is by attaching fins to the absorber. Moreover, we use finned tubes when the convective transfer coefficient is low outside comparatively to the inside coefficient.

In studies found in the literature concerning the ducts with fins, we found two models of fin location: a generally **internal location** (Figure 1.4: a) valid when the fluid in the pipe absorbs heat and an **external location** (Figure 1.4: b) valid when the fluid in the pipe releases heat to another external fluid, different models of ducts with fins presented by **Lienhard & al [14]** shown in Figure 1.4.

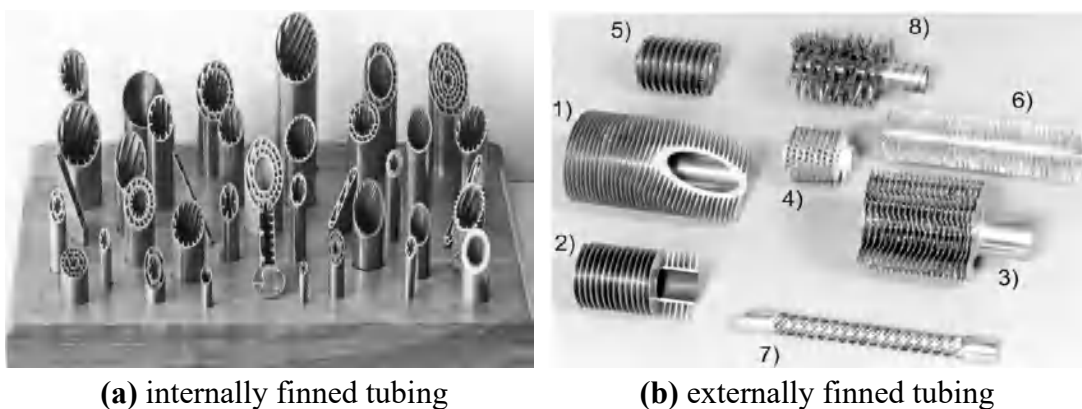


Figure 1.4: different finned geometries [14]

1.4.1. External fins

In “SONATRACH” (the first big Algerian company of petroleum and gas industry), after boosting gas to increase its pressure it should be cooled because it has a high temperature, so they use a system of gas cooling based on an exchanger, this is made by cylindrical tubes with helically fins (figure 1.5: b) that are attached on the external surface, the hot fluid - which is generally gas - pass inside the tubes from the inlet to the outlet in a horizontal direction (figure 1.5: a), and the cold fluid - which is generally air - is forced to pass in perpendicular direction with the tubes by ventilator in a vertical direction, the tubes has a distributor (stationary header) in the inter to dispatch the charge in the tubes, and a collector at the exit to collect all the charge on the tubes (figure 1.6) [50].

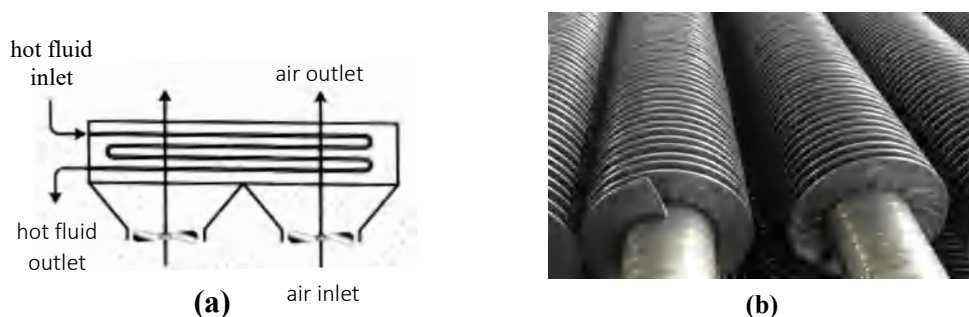


Figure 1.5: (a) simple schematic of air-cooling system - (b) external helical fins [50]

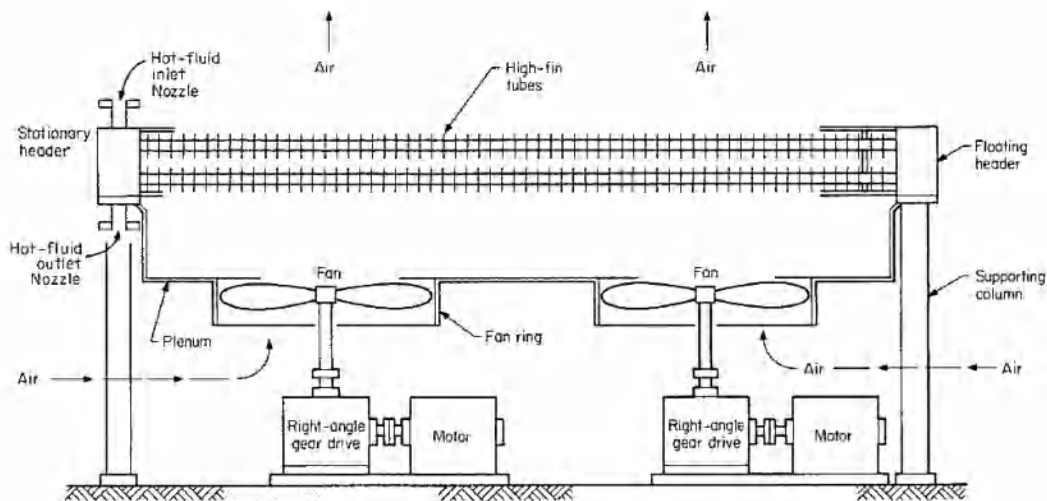


Figure 1.6: forced draft air cooled heat exchanger [50]

The tubes are made generally by rustproof metals (carbon steel, chrome moly steels, stainless steel...) with a length between 6 – 9 m, a diameter range from 12 to 16 mm and thickness of 2.8 mm, and they are arranged in a triangular structure (60°) (figure 1.7).

Besides, the fins are generally made by aluminum, with a height of about $5/8$ in, and thickness of 0.12 in each inch of the tube contain about 9 fins.

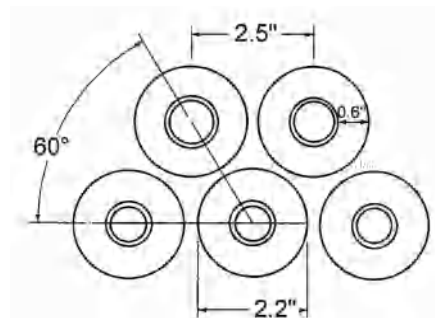


Figure 1.7: characteristics and arrangement of finned tubes [50]

This technology gives a good efficiency of cooling gas in the industrial domain referring to the effect of the fins, and its function of the geometry and type of materials used. On the other hand, the problem of closing tubes is not existing in this case, but the smaller distance between the fins (9 fins in 2.5 cm) causes some problems when they closed by sands or other deposits, especially it decreases the efficiency of the exchanger (figure 1.8).

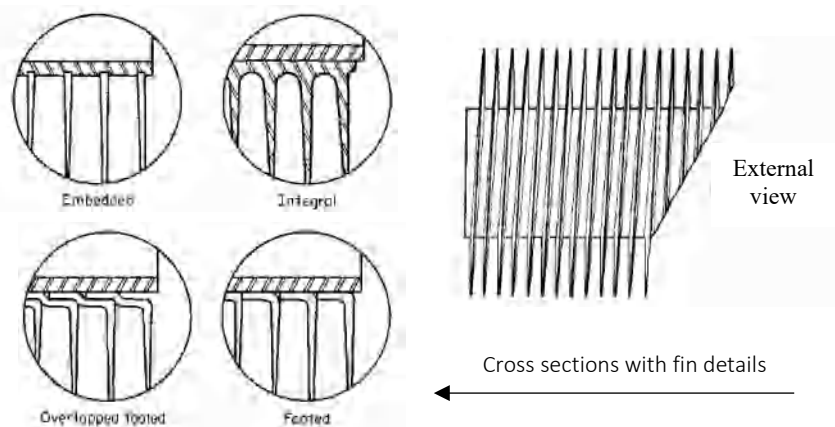


Figure 1.8: finned-tube construction [51]

Fins that are closer together and narrower tend to perform better than larger and more widely spaced fins. However, we face limitations due to increased pressure drops when the fins are spaced too closely. A fin's efficiency improves with higher thermal conductivity. Therefore, selecting fins involves finding a balance between cost, space limitations, pressure drop, and heat transfer efficiency [51].

In the Ph.D thesis of **Ouzzane** [52], the author studied numerically the heat transfer by mixed convection of a developed flow, laminar in steady state inside a horizontal or

inclined cylindrical pipe with a heat flow Non-uniform on its external surface, two cases are studied: with and without longitudinal fins, differential equations have been integrated and discretized in his study using the finite volume approach. The results obtained show that in the case of a pipe with two fins, the asymptotic value of the Nusselt number has increased by 37 % compared to a pipe without fins. However, in a pipe equipped with eight outer longitudinal fins, the upper fin evacuates approximately twice as much heat as the fin situated at the bottom of the section, in this case a finned duct of 0.848 meters in length evacuates the same amount of energy That a smooth line (without fins) having a length of 2.139 meters.

“Ouzzane” has also studied the effect of parietal conduction on the evolution of thermal and hydrodynamic fields, he finds that in the case of materials having good thermal conductivity, the temperature of the solid-fluid interface tends to become uniform. Nevertheless, a relatively high differential temperature between the top and the bottom in the case of a material with low thermal conductivity, while in the case of a horizontal or inclined conduit for the improvement of heat exchange, the author recommends placing more fins on the upper part of the section in the case of cooling and on the lower part in the case of warming.

A novel concept, known as "cutting fins," has recently emerged as a promising technique for enhancing heat transfer, introduced by **Pis'mennyi [53]**. This approach proposes two distinct designs for improved heat transfer surfaces. The first design involves tubes with fins shaped like a diffuser (see Figure 1.9: a), while the second type utilizes flat-oval tubes with incomplete finning (see Figure 1.9: b).

Pis'mennyi conducted extensive investigations to evaluate the influence of the angle (γ) on the thermal and hydraulic performance of finned tube bundles. He fabricated four sets of tubes with angles ranging from 0° to 20° . His research indicated that replacing smooth fins with corrugated fins on a single finned tube at a Reynolds number (Re) = 104 led to a 12-15% increase in heat transfer. However, this enhancement came at the cost of a significant 65-70% increase in drag.

Importantly, the cutting of fins did not diminish the fin surface area. Instead, it resulted in a notable 12-36% improvement in heat transfer, with the degree of enhancement dependent on the specific finning parameters and cutting method employed.

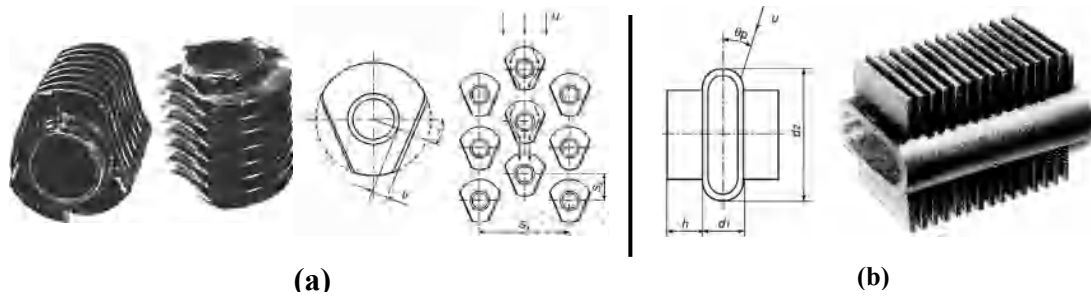


Figure 1.9: (a) Tubes with confuser-type bent fins – (b) Flat-oval tubes with incomplete finning [53]

Furthermore, Pis'mennyi proposed another method to enhance heat transfer by tilting bundle finned tubes towards the incoming flow direction (see figure 1.10). This approach resulted in a significant reduction in the size of the stern vortex zone, thereby improving overall heat transfer efficiency.

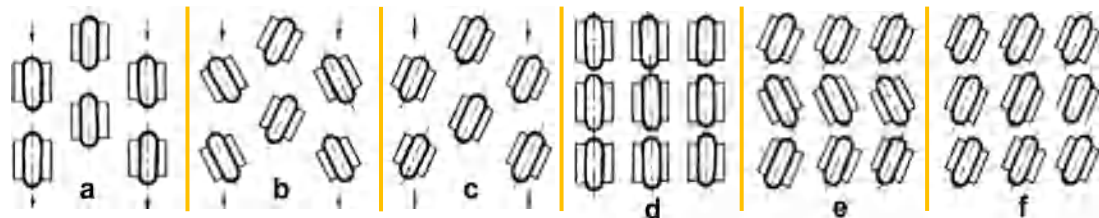


Figure 1.10: Arrangements of profiled tubes in bundles and their slope [53]

Wavy fins are used by **Priyam & Chand [54]**, For their study on how well finned absorber solar air heaters perform, they consider factors like how much air flows through and how close together the fins are. They use these factors in a formula to calculate how efficient the collector is. They also look at another factor, which is how well the heater works in terms of both heat and water flow. Their math model gives a good estimate of how well a solar air heater with wavy fins works. They found that when more air flows through the heater, it increases pressure but also makes the collector more efficient. They also discovered that a solar air heater with wavy fins (see figure 1.11) is more efficient than a flat plate collector in similar conditions.

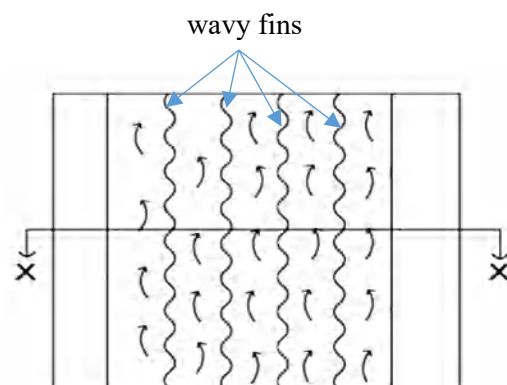


Figure 1.11: Solar air heater with wavy finned absorber [54]

1.4.2. Internal fins

Using internal fins is the best and most cost-effective method to boost heat transfer within a duct. This is because they significantly improve heat transfer without causing a substantial increase in pressure, and they are also inexpensive to produce. However, a large number of internal fin geometries have been proposed for use in several domains, and more are still being developed, these fins can take a variety of forms such as longitudinal fins [55], wavy fin array [56], sinusoidal wavy fin [57], plain fin [58], longitudinal thin, triangular and V-shaped fins [59], S-shaped, Z-shaped and V-shaped lateral fin [60], arc-shaped fin [61], three-dimensional integral roughness tubes [62], three-dimensional dimpled tubes [63], straight fins and circular-sector fins [64], Blossom-shaped internal fins [65], spirally fluted tubes (extended surface obtained by deforming the tube wall to form spiral flutes) [66], circular, trapezoidal and rectangular grooves shapes [67], vertical helical fins [68] and finally the geometry that we are interested in in this study: the internal helical fins [69].

Touahri [13] conducted a numerical investigation of three-dimensional mixed convection within cylindrical horizontal ducts. The study explored three distinct geometric configurations:

1. **Horizontal pipe with a finite wall thickness:** This case considered a pipe with a wall of measurable thickness.
2. **Annular space between two concentric horizontal pipes:** This scenario focused on the space between two horizontally aligned, concentric pipes.
3. **Horizontal pipe and an annular space with fins:** This configuration involved a horizontal pipe with an annular space surrounding it, and the presence of longitudinal and transversal fins within the annular space.

The continuity, momentum, and energy equations, along with their initial and boundary conditions, are solved numerically using a finite volume method for conjugate mixed convection in a cylindrical coordinate system. The Reynolds and Prandtl numbers are kept constant while the Grashof number varies. The SIMPLER algorithm is employed to solve a system of nonlinear partial differential equations with second-order spatiotemporal discretization.

Concerning the first part the results shows that it possible to obtain a simple correlation of the average Nusselt number with the Richardson number ($Nu_m = 12.753 Ri^{0.156}$), it shows also that the decrease in the thickness of the annulus increases the heat transfer, this is justify by the increase in the average Nusselt number by decreasing the hydraulic diameter. He found in the second part that the average Nusselt number is increased to 74.5 % in the case of an annular space. In this case, the correlation will be $Nu_m = 12.8678 Ri^{0.1426}$.

The use of fins in the last part improves the heat transfer, this improvement is very important in the case of longitudinal fins (figure 1.12: a) and it is moderate in the case of transverse fins (figure 1.12: b), he also proved that the fins used in the annular spaces are more participate in the heat transfer to those of a horizontal duct due to the increase of the exchange surface between the fluid and the fins in the case of an annular space.

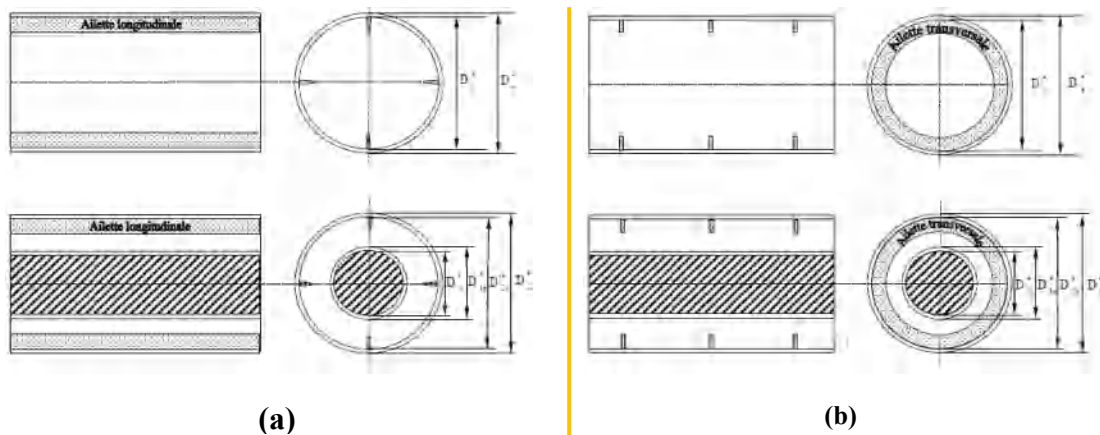


Figure 1.12: (a) Visualization of the Longitudinal fins - (b) Visualization of the transverse fins [13]

Soliman & al [71] conducted a numerical study to investigate the temperature distribution within fins, the fluid temperature, and the local heat flux, assuming a uniform outer wall temperature. They compared both finned and finless configurations. The results highlighted the significant influence of the number and size of the fins on the heat distribution and flux. Notably, the finned tube exhibited superior heat transfer capabilities at the surface compared to the smooth tube.

1.4.2.1. Internal helical fins

For our study, we define a "micro-fin" as a fin with a height less than 1 mm, with our shortest fin height being 1.2 mm. Numerous researchers have investigated the characteristics

of micro-fins and their impact on dynamic and thermal fields during heat exchange processes.

This research began in 1977 when **Fujie et al. [69]** introduced internal helical micro-finned tubes. This geometry has since been widely adopted for heat transfer enhancement. **Schlager et al. [72]** carried out an experimental study in 1990 to evaluate the condensation heat transfer performance of R22 refrigerant in three different micro-fin tubes. They adjusted the fin heights (ranging from 0.15 to 0.3 mm) and helix angles (15°, 18°, and 25°). The results demonstrated that the micro-fin tube with a 0.3 mm fin height and an 18° helix angle achieved the highest condensation coefficient. This indicates that both fin height and helix angle are crucial factors in optimizing condensation heat transfer performance in micro-fin tubes

Webb and Li [73] compared seven different internal helical ridge tubes, including a smooth tube, to assess long-term fouling behavior using 800-ppm calcium hardness water in a chiller/cooling tower system. These seven tubes also featured external circular fins with a height of 0.9 mm. The internal fin height, helix angle, and number of starts varied across the seven tubes (0.33-0.55 mm, 25-45°, 10-45, respectively). The researchers observed that the potential for fouling increased as both the number of starts and the helix angle increased. The most significant fouling occurred in three tubes with higher numbers of starts and helix angles ranging from 35° to 45°. Based on these findings, they concluded that the tube with 45 starts, a 45° helix angle, and a 0.33 mm fin height was the most suitable choice for their study, likely due to a balance between heat transfer performance and fouling resistance.

Deorah [68] investigated the influence of various fin patterns on heat transfer in a vertical direction. The study compared a single coiled fin, a tube with 10 equally spaced fins with a single turn, and a reference tube without fins. The analysis focused on parameters such as heat transfer coefficient, heat transfer rate, fin effectiveness and surface Nusselt number.

Three distinct fin geometries were examined using ANSYS 13.0 simulation software: rectangular, concave parabolic, and trapezoidal (see Figure 1.13). Aluminum was selected as the fin material, with air serving as the fluid flowing inside the tube under laminar flow conditions.

The analysis was conducted on five tubes with identical dimensions (inner diameter 50 mm, outer diameter 53 mm), but with different fin configurations or profiles. All tubes had the same fin height (5 mm) and fin thickness (2 mm), with variations in the concave parabolic and trapezoidal geometries (2-4 mm).

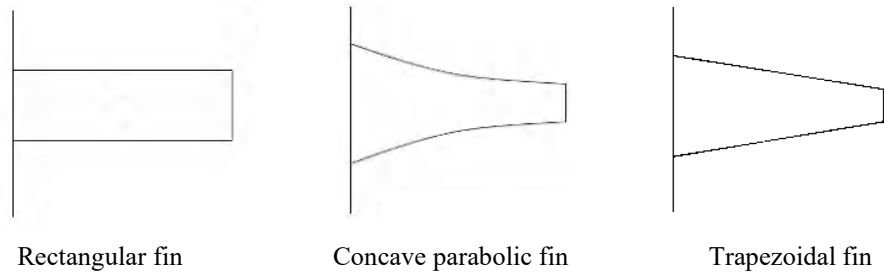


Figure 1.13: fin geometries used by **Deorah [68]**

The author observed that the single fin with a large number of turns restricts the airflow path, increasing flow resistance and reducing airflow rate, which decreases heat transfer rate. Consequently, configurations with a large fins number with one turn performed better efficiency than other fin configurations, as they offer a smaller flow resistance, higher heat transfer rates, and maximum surface Nusselt number. Among the fin geometries studied, the trapezoidal geometry exhibited the highest values of surface Nusselt number, heat transfer rate, and surface heat transfer coefficient compared to the concave parabolic and rectangular geometries.

Huang et al. [61] conducted an experimental study on the single-phase thermal performance of arc-shaped inner finned tubes (AIFT). They used a rolling-extruding (R-E) method to create these new inner finned tubes. In their study, they constructed three types of tubes with different numbers of arc fins: 35, 40, and 45 fins, all with a fin height of 0.7 mm. They compared these tubes with an inner helical finned tube containing 45 fins with a fin height of 0.35 mm. All tubes were 2 meters long and had a fin helix angle of 42° . They also compared them with a smooth tube. The Reynolds number in their study ranged from 4000 to 14200.

A numerical study on helical groove tubes was performed by **Jamshed et al. [74]** to assess entropy generation minimization, they studied four tubes with different pitch length and helix angle showed in Table 1.1, with Reynolds number $5000 \leq Re \leq 10000$, and compared them with a smooth tube, they discovered that the friction factor didn't display a notable difference compared to the smooth tube, with a maximum difference of around 5%

for GT02. However, their Nusselt number exhibited a significant variation, with a maximum difference of 42% for GT02 tube at Re 10000. The most substantial enhancement was observed in GT02, as it showed the best overall performance among the tubes tested, with a 33% increase in thermal performance

Table 1.1: helical groove tubes parameters used by **Jamshed et al. [74]**

	Tube length (m)	Pitch (m)	Helix angle (°)
GT02	2	0.051	23.6
GT04	2	0.102	12.3
GT06	2	0.152	8.3
GT08	2	0.203	5.4

The flow regime plays a crucial role in the thermodynamics of internal helical finned tubes. Research indicates that these tubes demonstrate limited effectiveness in the laminar flow regime, with no noticeable improvement in heat transfer efficiency [75, 76, 77, 78].

However, as the flow transitions to turbulent, a different picture emerges. Studies have observed that helical finned tubes exhibit higher friction factors compared to plain tubes [79, 80, 81, 82, 83]. This suggests that while turbulent flow may enhance heat transfer in helical finned tubes, it also comes with increased energy losses due to higher friction.

Furthermore, investigations focused on the fully turbulent regime have shown that the friction factor of helical finned tubes becomes comparable to that of plain tubes [84, 79, 85, 86, 81, 87, 88]. This suggests that the increased friction factor observed in the transitional regime may be a temporary phenomenon, and the long-term effect of helical fins on friction in turbulent flow is less pronounced.

Solanki and Kumar [89] conducted an experimental study comparing the performance of a smooth straight copper tube to a micro-fin helical coiled copper tube during condensation heat transfer. Cooling water flowed through the outer shell in the opposite direction. Their research focused on examining the heat transfer coefficients and frictional pressure drops, and exploring the flow regime transitions within the micro-fin helical coiled tube. Their results showed that the highest heat transfer coefficient was exhibited in the case of micro-fin helical coiled tube compared to the smooth tube, with an improvement ranging from 160% to 255%. However, this enhanced heat transfer came at the cost of higher

frictional pressure drops, which were found to be 69% to 155% greater than those of the smooth tube.

Maakoul et al. [90] conducted a 3D Computational Fluid Dynamics (CFD) simulation to evaluate the thermohydraulic performance of a gas-to-liquid double-pipe heat exchanger. Their research focused on comparing the performance of heat exchangers equipped with both helical fins and longitudinal fins. Using FLUENT software, they investigated various aspects of the heat exchanger, including gas-side fluid flow, turbulence, heat transfer, and power consumption. Their study specifically focused on analyzing the flow field characteristics of helical fins under turbulent flow conditions, using Reynolds numbers ranging from 1.24×10^4 to 1.77×10^4 and helical fin spacings between 0.05–0.2 m.

When comparing helical and longitudinal fin designs, researchers discovered that helical fins provided a substantial advantage in heat transfer rate. For the same unit weight, helical fins achieved a significantly higher heat transfer rate than longitudinal fins. However, this benefit was accompanied by an increased pressure drop. Further analysis showed that the heat transfer surface area of the helical fins was 3%–24% larger than that of the longitudinal fins. This increased surface area played a major role in the improved heat transfer efficiency observed with the helical fin design.

The impact of internal helical fin geometry, particularly the helix angle, has been a subject of interest for researchers. **Ito and Kimura [91]** conducted a study in 1979 to examine the effects of helix angle on heat transfer in internal spiral grooved tubes using R22 as a refrigerant. Their experiments, performed under various heat and mass flux conditions, involved helix angles ranging from 0° to 90° . They observed that the heat transfer coefficient increased with the helix angle until reaching 7° . After this point, it decreased to a minimum value around 45° , and then increased again towards 90° .

Yang and Hrnjak [92] investigated the influence of micro-fin geometries on two-phase flow behavior during evaporation, using a transparent micro-fin tube fabricated via 3D printing. Their experiments involved comparing a smooth tube with three micro-fin tubes with different helix angles (0° , 10° , and 18°). They used R410A flow boiling at a saturation temperature of 10°C .

The researchers observed a distinct flow pattern in the helical micro-fin tube. Compared to both smooth and axial micro-fin tubes, the helical micro-fin tube exhibited an

annular flow pattern at a lower vapor quality. This suggests that the helical design promotes annular flow earlier in the evaporation process. Furthermore, they found that the helix angle played a significant role in influencing the transition boundary between stratified wavy flow and wavy annular flow. As the helix angle increased, this transition shifted downward, meaning it occurred at lower mass fluxes and vapor qualities. This indicates that a higher helix angle promotes the transition to wavy annular flow at earlier stages of the evaporation process.

Mann and Eckels [93] conducted a multi-objective optimization study for 2D helical micro-fin surfaces using computational fluid dynamics (CFD) simulations. Their objective was to find the optimal balance between minimizing friction enhancement and maximizing heat transfer enhancement. They varied three input parameters: fin height, helix angle, and the number of starts. After evaluating over 700 simulations and comparing their results with available data, they identified distinct differences in flow characteristics between geometries with helix angles above and below approximately 45° .

Zdaniuk et al. [94] conducted an experimental study to determine the heat transfer coefficients and friction factors of eight helically-finned tubes and one smooth tube using liquid water. They covered a wide range of Reynolds numbers, from 12,000 to 60,000, and varied the design parameters of the helically-finned tubes, including helix angles (25° to 48°), numbers of fin starts (10 to 45), and fin height-to-diameter ratios (0.0199 to 0.0327). Their results for the plain tube showed satisfactory agreement with the well-established Blasius and Dittus–Boelter equations, validating the reliability of their experimental methodology. This provides confidence in the accuracy of their findings for the helically-finned tubes

Among the tested helically-finned tubes, tube 8, with $N_s = 45$, $a = 48^\circ$, and $e/D = 0.0244$, achieved the highest j -factor, indicating its superior heat transfer performance. In contrast, tube 1, with $N_s = 10$, $a = 48^\circ$, and $e/D = 0.0244$, had the lowest f -factor, signifying its lower friction losses. Based on these findings, the researchers recommended tube 8 ($N_s = 45$, $a = 48^\circ$, $e/D = 0.0244$) for heat exchange applications due to its combination of high heat transfer capability (high j -factor) and moderate friction losses (moderate f -factor) across all Reynolds numbers.

Yang and Hrnjak [92] utilized a unique approach to study the impact of micro-fin geometries on two-phase flow behavior during evaporation. They employed a transparent micro-fin tube, created using 3D printing, which allowed for direct visualization of the flow. Their experiments involved comparing a smooth tube with three micro-fin tubes, each with different helix angles (0° , 10° , and 18°), all made of clear resin. They focused on R410A flow boiling at a saturation temperature of 10°C . Their findings revealed that the annular flow pattern occurred at a lower vapor quality in the helical micro-fin tube compared to both the smooth and axial micro-fin tubes. They also observed that the helix angle played a significant role in influencing the transition boundary from stratified wavy flow to wavy annular flow. As the helix angle increased, this transition shifted downward (towards lower mass flux and vapor quality conditions).

Wang et al. [60] developed a correlation to predict the critical Reynolds number for turbulent flow in horizontal helically finned tubes. Their study focused on two tubes with distinct characteristics:

- Tube 1: 38 fins, helix angle of 60° , fin height-to-diameter ratio of 0.89
- Tube 2: 60 fins, helix angle of 45° , fin height-to-diameter ratio of 0.5

The study found that the critical Reynolds numbers for turbulent flow in Tube 1 and Tube 2 were 11,000 and 17,000, respectively. Importantly, they observed that the critical Reynolds number decreased as the helix angle or the fin height-to-diameter ratio decreased..

Muñoz and Abánades [95] conducted a comprehensive analysis of incorporating internal helically finned tubes into parabolic trough solar collectors, leveraging computational fluid dynamics (CFD) tools. Their study considered various factors influencing the performance of these systems, including pressure drops, thermal losses, thermo-mechanical stress, and thermal fatigue. Their analysis suggested a promising potential improvement in the efficiency of parabolic trough solar plants by 2% through the implementation of internally finned tubes. While they observed an increase in parasitic losses associated with pressure drops in the tube, primarily driven by the number of fins and helix angle, this was offset by a reduction in thermal losses and temperature gradients. Consequently, the overall thermal and exergetic efficiency of the collector was enhanced.

1.5. Summarized of the literature review

In the theoretical background we found that it's better to start with some general concepts, concerning the main parts of a solar collector because of their important role on the collector efficiency, our aim is to study the enhancement of the tubes transporting the fluid in those collectors, one of the methods of increasing the heat transfer efficiency in the tube is to enhance the dynamic-thermal effect by adding external surfaces.

The mixed convection has been studied numerically as we mentioned before, in fill conduit with variable physical properties, in a finned conduit. However, the fins have two positions external and internal, the external fins are used generally in the case of extracting heat from inside to outside the tube, while the internal fins are used to increase the heat transfer from outside to inside the tube.

The problems encountered in the literature are the geometry and the location of the fins. In the case of internal finned tubes, the objective of the majority of authors is to find the ideal case between the gain in heat transfer and the pressure drops (which costs more pumping energy). In addition, despite the richness in the bibliography, we found that the fins play their traditional role, that is to increase the exchange surface to improve the heat transfer and we have not found studies in that even the fin generates heat.

Numerous experimental and theoretical investigations are reviewed previously, those studies examined the performance of heat transfers and pressure drops of internal helical finned tubes, most of the works listed above have visualized the influence of this geometry of fins in the enhancement of heat transfer efficiency.

1.6. Conclusion

In this chapter, we reviewed the important works (Whether ancient or current) on solar thermal collectors with their essential parts, the mixed convection in fill conduit with variable physical properties, the external and internal finned tubes are also underscored, while the internal helical finned tubes were taken with more details.

1.7. Objective

The main objective of the present work is to study the heat transfer in forced convection, combined with fluid flows in horizontal cylindrical annulus, traversed by a Newtonian and incompressible fluid, with helical fins attached in the inner surface of the

conduits, the thermal conditions are as follows: a constant heat flux applied throughout all the thickness of the outer tube, the temperature is constant at the entrance of the duct while at the exit it will be considered that the duct is long enough to admit a near development. Moreover, radiative and convective losses to the surrounding environment will not be taken into account. the originality of this work lies in the introduction of a new type of fins considered as a heat-generating device allowing the increase of heat transfer between the fins and the fluid, and also a better heating of the fluid.

Chapter 2

Mathematical modeling

2.1.Introduction

The present study treats the laminar forced convection, we focused on the conjugated heat transfer (taking into account the heat transfer in both solid and fluid domains) in a horizontal annulus submitted to a uniform heat flux with the presence of longitudinal and helical fins, we studied the influence of varying fin parameters as their number of starts or the helix angle on the thermodynamics of the fluid. However, the studies mentioned in the previous chapter could give us a specific destination in the research if we took in consideration that the best fin shape that gives better results is the trapezoidal, and according to **Deorah [68]** the large number of fins with single turn is preferred more than the single fin with a large number of turns, this means that increasing the number of fins is preferred more than increasing the helix angle, but increasing booth of them is better. Thus, the geometry

and the systems of conservation equations, with their initial and boundary conditions are presented in this chapter.

2.2. Model geometry

The problem addressed in our study involves the three-dimensional steady, laminar forced convection of distilled water flowing in a long horizontal cylindrical annulus, as illustrated in Figure 2.1.

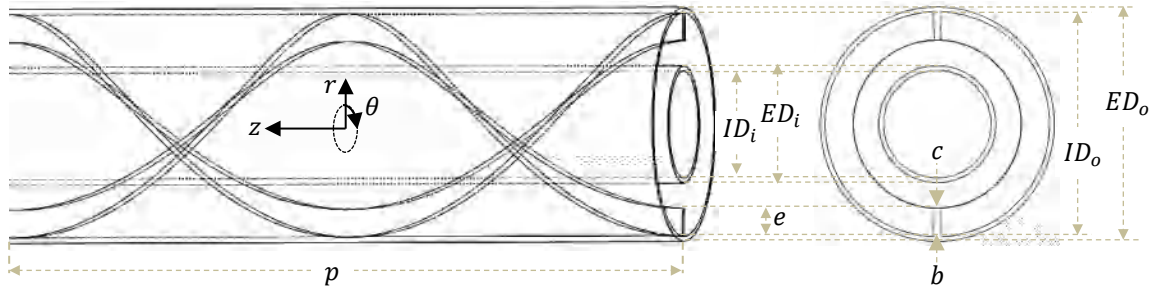


Figure 2.1: Tube geometry, example of two helical fins

The working fluid is considered Newtonian and incompressible, with constant thermophysical properties. The tube has a length (L) of 1000 mm, with an external diameter (ED_o) of 10 mm and an internal diameter (ID_o) of 9.6 mm for the outer tube. The inner tube has an external diameter (ED_i) of 5 mm and an internal diameter (ID_i) of 4.6 mm. The outer tube is equipped with longitudinal or helical fins on its inner surface, featuring a height (e) of 1.2 mm, a base (b) of 0.343 mm, and a top (c) of 0.257 mm, these fins dimensions are chosen from the work done by **Touahri [13]** to be compared with his results. However, four helix angles are considered (0° , 20° , 30° , and 45°) and three numbers of starts ($N_s = 2, 4$ and 8) for the helical fins. The tubes and fins are made of Aluminium with an electrical conductivity $\sigma = 3.541 \times 10^7 S/m$, a thermal conductivity $k = 202.4 W/m.K$. a heat generation equal to $1000 w/m^2$ applied to the external surface of outer tube, this heat is transferred to the flow of distilled water into the duct. At the entrance, the average axial velocity equal to $9.88 \times 10^{-2} m/s$ and a constant temperature of $15^\circ C$ with a thermal conductivity $k_w = 0.5769 W/m.K$.

Identical helical fins are attached to the inner wall of the tube (shown in figure 2.2) for the case of two helical fins are positioned at $(\theta = 0)$ and $(\theta = \pi)$, the case of four helical fins at $(\theta = 0)$, $(\theta = \pi/2)$, $(\theta = \pi)$ and $(\theta = 3\pi/2)$, and the eight helical fins case at $(\theta = 0)$, $(\theta = \pi/4)$, $(\theta = \pi/2)$, $(\theta = 3\pi/4)$, $(\theta = \pi)$, $(\theta = 5\pi/4)$, $(\theta = 3\pi/2)$ and $(\theta =$

$7\pi/4$), the fins are made by the same material of the tube, the axial section of each fin is in the form of a trapezium where the large base is attached to the inner wall of the outer tube (figure 2.3).

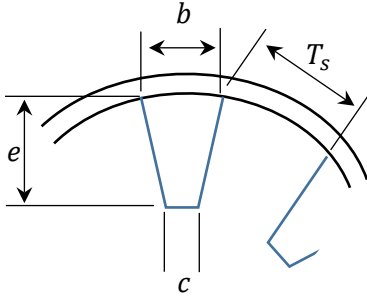


Figure 2.2: trapezoidal fins geometry

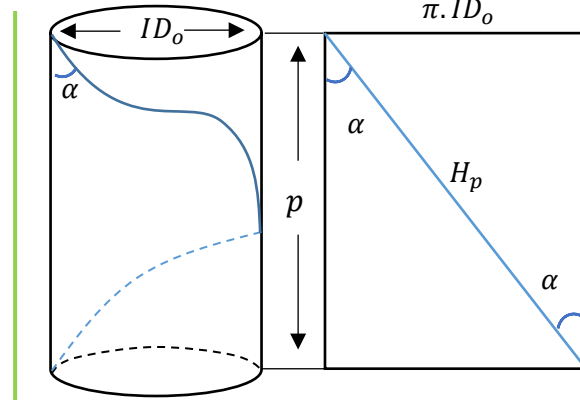


Figure 2.3: helical fins geometry details

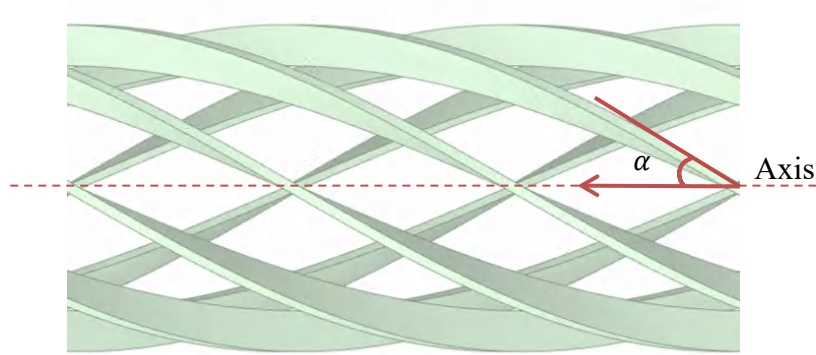


Figure 2.4: illustration of helix angle

The helix angle (α) is the angle between the tube axis and the helical fin, it is confined between 0° and 90° , using equation 2.1 we found 82.86, 52.23 and 30.16 mm values of pitch for the helix angle 20° , 30° and 45° respectively.

$$\tan(\alpha) = \frac{\pi \cdot ID_o}{p} \rightarrow p = \frac{\pi \cdot ID_o}{\tan(\alpha)} \quad (2.1)$$

Where: (p) is the pitch (axial length for one helical fin turn).

The helical fin length " H_L " (details showed in figure 2.3 and 2.4) can be calculated by the Pythagorean theorem which depend on helix angles (α), the results are shown in the table 2.1.

$$(H_p)^2 = (p)^2 + (\pi \cdot ID_o)^2 \rightarrow H_p = \sqrt{p^2 + (\pi \cdot ID_o)^2} \quad (2.2)$$

$$H_L = \frac{L \times H_p}{p} \quad (2.3)$$

Where: (H_p) is the helical fin length in one turn and (H_L) is the helical fin length in all the tube distance.

With these dimensions we can calculate the external surface of fins (ES_f), which is equal to the external circumference (EC_f) multiply by the fin length (H_L) [$ES_f = EC_f \times H_L$], the external fin circumference without the base length is equal to $EC_f = 2.657 \text{ mm}$ (see Annex I). Moreover, we can also calculate the electrical resistance of each helical fin depending on its helix angle by this relation:

$$R_f = \frac{\rho_e \times H_L}{S_f} = \frac{2.82 \times 10^{-8}}{3.6 \times 10^{-7}} H_L = 0.0783 H_L (\Omega) \quad (2.4)$$

Where: (ρ_e) is the aluminum electrical resistivity equal to $2.82 \times 10^{-8} \Omega \cdot m$ and (S_f) is the cross-sectional area of the trapezoidal fin equal to $3.6 \times 10^{-7} \text{ m}^2$.

The physical principles governing this problem are accurately modelled by the following equations, along with their respective initial and boundary conditions. the dimensionless numbers of Reynolds ($Re = 399.02$) and Prandtl ($Pr = 8.201$) are evaluated at the fluid inlet temperature (see Annex II).

Table 2.1: finned tubes parameters for different helix angles

Finned annulus	smooth annulus	Fins number		One Fin length " H_L " (mm)	Fin electrical resistance " R_f " (Ω)	One Fin surface " ES_f " (mm^2)	Total fins surface (mm^2)	Internal surface without fins (mm^2)	Total internal surface of outer tube (mm^2)	Fin pitch " p " (mm)	Fin spacing (distance between two fins) ' T_s ' (mm)	Increased surface (%)
		4 fins	2 fins									
20°	-	1064	1064	1037	0.1645	2771.4	5543	29472.8	35015.9	82.862	14.7	16.1
		1037	1037									
		0.3290										
		2771.4										
		11086.1										
		28787										
		39897.8										
		82.862										
		7.2										
		32.3										

Longitudinal fins	45°		30°		8 fins	
	8 fins	8 fins	8 fins	8 fins	8 fins	8 fins
1000	1414	1154.5	1064	1037	0.6580	2771.4
1000	1249.8	1089.6	1037	1037	0.7028	2949
0.6264	0.8343	0.7028	0.6580	0.6580	0.7028	23592.1
2652.4	3450.6	2949	2771.4	2771.4	2771.4	22172.2
21219.2	27605.1	23592.1	22172.2	22172.2	22172.2	27414.7
27416.5	27414.7	27414.7	27414.7	27414.7	27414.7	49639.4
48635.8	55026.6	49660.8	49639.4	49639.4	49639.4	82.862
-	30.16	52.237	82.862	82.862	82.862	3.4
3.4	3.4	3.4	3.4	3.4	3.4	64.6
61.26	82.45	64.7	64.6	64.6	64.6	

2.3. Governing equations

The fundamental equations governing the system consist of the mass conservation equation, the Navier-Stokes equations, and the energy equation. Considering the cylindrical shape of the domain, we express these equations in cylindrical coordinates. Since the problem is inherently three-dimensional, we focus on solving the equations in cylindrical form. Moreover, to streamline our analysis and alleviate complexity, we introduce several assumptions. These assumptions aim to provide a reasonable physical representation of the problem while simplifying the application of boundary conditions. These hypotheses include:

- The thermal radiation, the viscous dissipation and the pressure force work are negligible.
- The fluid (distilled water) is Newtonian, while the flow is assumed to be laminar and incompressible.
- The physical properties of the fluid and of the wall are constant except the density who obeys the approximation of Boussinesq in the term of the Archimedes force.

2.3.1. Conservation of Mass

The rate of mass entering a specified volume ($drd\theta dz$) must be equal to the rate of mass leaving that same volume. To express this, we use the Continuity Equation for three-dimensional, incompressible fluids, which can be written as follows:

$$\frac{1}{r} \frac{\partial(ru)}{\partial r} + \frac{1}{r} \frac{\partial v}{\partial \theta} + \frac{\partial w}{\partial z} = 0 \quad (2.5)$$

Where: (u, v and w) are the velocity components in the r, θ and z directions, respectively.

2.3.2. Conservation of Momentum (Navier-Stokes Equations)

The principle of Conservation of Momentum, often represented by the Navier-Stokes equations, comprises three equations for each spatial direction. These equations are rooted in Newton's second law of motion, which posits that an object's momentum is directly proportional to the net force acting upon it in the same direction. This net force encompasses both body forces and surface forces acting on the element's surface.

In cylindrical coordinates, these three equations are formulated under the assumption of a Newtonian fluid with constant density and viscosity. They can be expressed as follows:

$$\rho \left(u \frac{\partial u}{\partial r} + \frac{v}{r} \frac{\partial u}{\partial \theta} + w \frac{\partial u}{\partial z} \right) = -\frac{\partial P}{\partial r} + \mu \left[\frac{1}{r} \frac{\partial}{\partial r} \left(r \frac{\partial u}{\partial r} \right) + \frac{1}{r^2} \frac{\partial^2 u}{\partial \theta^2} + \frac{\partial^2 u}{\partial z^2} \right] \quad (2.6)$$

$$\rho \left(u \frac{\partial v}{\partial r} + \frac{v}{r} \frac{\partial v}{\partial \theta} + w \frac{\partial v}{\partial z} + \frac{uv}{r} \right) = -\frac{1}{r} \frac{\partial P}{\partial \theta} + \mu \left[\frac{1}{r} \frac{\partial}{\partial r} \left(r \frac{\partial v}{\partial r} \right) + \frac{1}{r^2} \frac{\partial^2 v}{\partial \theta^2} + \frac{\partial^2 v}{\partial z^2} \right] \quad (2.7)$$

$$\rho \left(u \frac{\partial w}{\partial r} + \frac{v}{r} \frac{\partial w}{\partial \theta} + w \frac{\partial w}{\partial z} \right) = -\frac{\partial P}{\partial z} + \mu \left[\frac{1}{r} \frac{\partial}{\partial r} \left(r \frac{\partial w}{\partial r} \right) + \frac{1}{r^2} \frac{\partial^2 w}{\partial \theta^2} + \frac{\partial^2 w}{\partial z^2} \right] \quad (2.8)$$

Where: (ρ) is the fluid density, (μ) fluid viscosity and (P) static pressure.

2.3.3. Conservation of Energy

The fundamental principle of the first law of thermodynamics asserts that energy cannot be created or destroyed, but rather undergoes transformation from one form to another. In the realm of fluid dynamics, this law is interpreted as an equilibrium between the rate of change in internal energy and kinetic energy within a fluid element and the energy

transferred into that element through convection, conduction, and work performed by external forces.

$$\rho C_p \left(u \frac{\partial T}{\partial r} + \frac{v}{r} \frac{\partial T}{\partial \theta} + w \frac{\partial T}{\partial z} \right) = k \left[\frac{1}{r} \frac{\partial}{\partial r} \left(r \frac{\partial T}{\partial r} \right) + \frac{1}{r^2} \frac{\partial^2 T}{\partial \theta^2} + \frac{\partial^2 T}{\partial z^2} \right] + q \quad (2.9)$$

Where: (C_p) Specific heat, (T) temperature, (k) Thermal conductivity and (q) is the heat flux $q = -k \frac{\partial T}{\partial r}$.

2.3.4. Nusselt number

The Nusselt number represents the ratio of convective heat transfer to conductive heat transfer, increasing it enhances heat transfer efficiency, while decreasing it reduces heat transfer efficiency.

$$Nu = \frac{h D_h}{k_w} \quad (2.10)$$

$$D_h = \frac{4 * \text{Area of flow}}{\text{wetted perimeter}}$$

$$\text{finned tube case} \rightarrow D_h = \frac{4 \left[\frac{\pi}{4} (ID_o^2 - ED_i^2) - NS \right]}{N(2e + c) + \pi ED_i - Nb + \pi ID_o} \quad (2.11)$$

Where: (h) is the convective heat transfer coefficient, (k_w) water thermal conductivity, (D_h) hydraulic diameter, (ED_i) external diameter of inner tube, (ID_o) internal diameter of outer tube, (e) fin height, (b) fin base distance, (c) fin top distance, (N) fins number, (S) fin cross section area.

2.4. Important parameters

Understanding parameters such as pressure drop, friction coefficient, and head loss is crucial for comprehending the thermohydraulic behavior of fluids. These parameters provide valuable insights into the dynamics of fluid flow and heat transfer within a system. By analyzing these parameters, we can make informed decisions to enhance the efficiency and reliability of fluid systems in various applications.

2.4.1. Pressure drop

The pressure drop or pressure loss in pipe flow indicates the change in pressure along the flow path, offering insights into energy losses and system efficiency. It can be calculated using the known Darcy-Weisbach equation:

$$\Delta p = f \frac{L}{D_h} \frac{\rho V^2}{2} \quad (2.12)$$

Where: (f) is the Darcy friction factor and (V) average velocity.

2.4.2. Friction factor

In fluid dynamics, the friction factor is a unitless value employed in the Darcy–Weisbach equation to characterize friction losses in both pipe flow and open-channel flow. The choice of friction factor formula depends on the type of flow present [96], as indicated in Table 2.2.

Table 2.2: the friction factor in different flow regimes

Laminar flow $Re < 2320$	Transient region $2300 < Re < 4000$	Turbulent flow $Re > 4000$		Fanning friction factor (f_F)
		Blasius equation for Smooth pipe	Colebrook equation (depending on the pipe roughness)	
$f = \frac{64}{Re}$	<i>The value of the Darcy friction factor is subject to large uncertainties in this flow regime.</i>	$f = \frac{0.136}{Re^{\frac{1}{4}}}$	$\frac{1}{\sqrt{f}} = -2 \log \left[\frac{(\varepsilon/D_h)}{3.7} + \frac{2.51}{Re \sqrt{f}} \right]$	$f = 4f_F$

Where: (ε) is the tube roughness [m].

Wang et al. [97] determined the Friction factors for the internal helically-finned tube and the plain tube at $5300 < Re < 34,000$. They found an increase in the Friction factors of internal helically-finned tube with Re below 17,000, but it decreases above 17,000.

2.4.3. Head loss

The head loss in a pipe signifies the reduction in the fluid's total mechanical energy due to factors like friction and turbulence, aiding in the assessment of system performance

and design optimization. It is a result of the viscous shear stress on the wall, it involves energy per unit weight, we can write it's equation as follows:

$$HL = f \frac{L}{D} \frac{\rho V^2}{2g} \quad \rightarrow \quad \Delta p = f \frac{L}{D} \frac{\rho V^2}{2} \quad \rightarrow \quad HL = \frac{\Delta p}{g} \quad (2.13)$$

Where: (g) is the acceleration due to gravity [m/s^2].

2.4.4. Colburn J-factor

The Colburn J-factor, a dimensionless parameter, characterizes heat transfer and fluid friction in a system. Increasing the Colburn J-factor typically enhances thermohydraulic performance by improving heat transfer efficiency while minimizing pressure drop. Conversely, decreasing the Colburn J-factor often indicates reduced heat transfer effectiveness and increased energy losses due to higher fluid friction. Therefore, optimizing the Colburn J-factor is essential for maximizing system efficiency and performance in various engineering applications. It is defined as:

$$j = \frac{Nu}{Re Pr^{1/3}} \quad (2.14)$$

The j-factor for internal helically-finned tube in the study of **Wang et al. [97]** is about 3.5 times of that for the plain tube.

2.4.5. Performance evaluation criterion “PEC”

The Performance Evaluation Criterion (PEC) is a universal metric that represents the overall performance of a heat transfer unit [98]. It is defined as follows:

$$PEC = \frac{Nu/Nu_0}{(f/f_0)^{1/3}} \quad (2.16)$$

Where: (Nu_0) and (f_0) are the Nusselt number and friction factor for smooth tube respectively.

Huang et al. [61] discovered that the heat transfer enhancement coefficient (PEC) of helical finned tubes is generally lower than that of tubes with protrusions, particularly at lower Reynolds numbers (Re). However, as the Reynolds number increases, the PEC of tubes with protrusions decreases more noticeably compared to helical finned tubes.

Consequently, at higher Reynolds numbers, the PEC of tubes with protrusions is expected to be lower than that of helical finned tubes.

2.4.6. Fin effectiveness

Fin effectiveness is defined as the ratio of heat transfer rate with fin to the heat transfer rate without fin from the surface.

$$\epsilon_f = \frac{(Q_f/A_f)}{(h(T_b - T_\infty))} \quad (2.17)$$

Where: (Q_f) is the actual heat transfer rate from the fin, (A_f) total surface area of the fin, (T_b) the fin base temperature, (T_∞) the surrounding fluid temperature.

A value of 1 signifies that the fin is transferring heat as effectively as a plain surface with the entire base area at the base temperature.

2.4.7. Fin efficiency

Fin efficiency is the major parameter which is used to determine the fin performance, it shows how well the fin utilizes its own surface area for heat transfer compared to an ideal fin at a uniform base temperature, it is defined as the:

$$\eta_f = \frac{Q_f}{Q_b} \quad (2.18)$$

Where: (Q_b) is the heat transfer rate from the base area of the fin

A value of 1 indicates perfect efficiency, while values closer to 0 indicate a less effective fin due to heat loss through the fin itself. However, In the study of **Wang et al. [97]** the efficiency index " η ", which indicates the enhancement of the internal helically-finned tube, decreased from 1.8 to 1.55 as the Reynolds number increased from 10,000 to 32,000.

2.5. Geometrical characteristics

The main geometric parameters described the internal helically-finned tubes are:

- Fin height (e).
- Tube inside diameter (ID).

- Helix angle (α) or the pitch (p) of a helix which is the height of one complete helix turn, measured parallel to the axis of the helix.
- Number of fins or number of starts (N_s).

Pirbastami [99] investigated the heat transfer performance of internally grooved tubes under turbulent flow conditions using CFD software STAR-CCM+. He examined various pitch sizes (7.1 mm, 12.7 mm, 50 mm, and 130 mm) and found that the CFD results aligned well with theoretical and experimental findings in the literature. Pirbastami observed that grooved tubes exhibited higher Nusselt numbers and friction factors compared to smooth tubes. Reducing the groove pitch size from 130 mm to 7.1 mm resulted in increased Nusselt numbers. Additionally, increasing the Reynolds number led to higher turbulence, enhancing mixing and consequently increasing the Nusselt number. However, a higher Reynolds number also led to a greater pressure drop, resulting in decreased thermal performance. Pirbastami concluded that heat transfer augmentation is less efficient for Reynolds numbers exceeding 15,000 due to the substantial pressure drop. Furthermore, the thermal enhancement factor for grooved tubes tended to increase with the Reynolds number, with the highest thermal factor observed for a pitch size of 7.1 mm. Thus, selecting an appropriate pitch size is crucial for heat enhancement.

As previously discussed, **Deorah [68]** studied different fin patterns in the vertical direction, such as a single fin with a large number of turns like a coiled shape and a large number of fins (10 equally spaced fins) with a single turn, for three fin geometries: rectangular, concave parabolic, and trapezoidal.

Numerous researchers have explored the characteristics of internally helically-finned tubes, encompassing a wide range of geometric parameters ($0.31 \text{ mm} < e < 16 \text{ mm}$, $5.89 \text{ mm} < D_i < 100 \text{ mm}$, $10^\circ < \alpha < 48^\circ$, $10 < N_s < 60$, $0.15 \text{ mm} < s < 3 \text{ mm}$) as outlined in Table 2.3. Theoretical and experimental studies have consistently demonstrated that for Reynolds numbers (Re) below 3500, the friction factor of internally helically-finned tubes is generally higher than that of plain tubes. However, a divergence in findings emerges at higher Reynolds numbers. **Webb et al. [85]** observed that for $Re > 20,000$, the friction factors of internally helically-finned tubes did not plateau at a constant value. In contrast, **Wang et al. [97]** concluded that the friction factors in these tubes exhibited an earlier transition to a fully rough region for Reynolds numbers exceeding 10,000, where the friction factors became independent of the Reynolds number. This discrepancy suggests that the behavior of friction

factors in internally helically-finned tubes at high Reynolds numbers remains an area of ongoing research and requires further investigation to clarify the underlying mechanisms.

Table 2.3: different geometry parameters of helical fin tubes from the previous works

	[97] 2017	[100] 2012	[101] 2012	[85] 2014	[99] 2015	[70] 2008	[41] 2017
Tube length “L” (mm)	2640	-	-	970	120	2745	2000
Outside diameter (mm)	25.14	7	53	-	116	18.77 – 18.86	6.35 – 8
Inside diameter (mm)	22.48	6.41	50	-	100	15.57 – 15.65	5.89 – 7.56
Number of fins “ N_s ”	60	60	10	1	1	10 – 45	44 – 60
Teeth space “ T_s ” (mm)	0.57	-	-	-	-	-	0.35 – 0.4
fin base width or thickness (mm)	0.61	0.14	2 – 4	1	3	-	0.15 – 0.25
apex angle (°)	43.1	20	-	-	-	-	24.5 – 33
fin height “e” (mm)	0.5	0.25	5	16	-	0.31 – 0.51	0.17 – 0.23
helix angle “ α ” (°)	45	15	-	-	-	25 – 48	18 – 28
Pitch (mm)	-	-	-	17	19.8	-	-

2.6. Benefit

Fins serve as essential components for effectively managing high heat fluxes within constrained spaces, as evidenced by previous research findings. The utilization of internally enhanced surfaces, particularly those incorporating surface roughness, has emerged as economically advantageous for various commercial applications. In their study, **Muñoz et al. [95]** noted that while the fabrication costs associated with implementing internally helically finned tubes for parabolic trough collectors may escalate, the anticipated 2% enhancement in plant efficiency substantiates their inclusion in preliminary cost

assessments. This highlights the pragmatic approach of considering such systems despite potential cost implications, emphasizing their overall efficiency gains in thermal management.

2.7. Conclusion

Based on the comprehensive mathematical modeling presented in this chapter, our study addresses laminar forced convection, with a particular emphasis on conjugated heat transfer phenomena within a horizontal annulus subjected to uniform heat flux. By incorporating longitudinal and helical fins into our analysis, we delve into the intricate interplay between fin parameters, such as the number of starts and helix angle, and their impact on fluid thermodynamics. Our investigation not only encompasses the formulation of conservation equations for continuity, momentum, and energy but also integrates pertinent geometric considerations and key parameters, including pressure drop and friction factor. Through this meticulous modeling approach, we aim to provide a deeper understanding of the complex heat transfer processes occurring within the system, thereby laying a solid foundation for subsequent analyses and practical applications.

Chapter 3

Numerical resolution

3.1.Introduction

Prediction of heat transfer and fluid-flow processes can be obtained by two main methods according to **Patankar [36]** experimental investigation and theoretical calculation, the theoretical calculation has more advantages than the experimental investigation, as such as the low cost and speed which are the important factors, and also the complete information treatment as it provides the values of all the relevant variables throughout the domain of interest such as velocity, pressure, temperature ... etc. Also, the ability to simulate realistic conditions and the ideal conditions can be easily simulated too. For those reasons, in our investigation we choose to work with CFD simulation using ANSYS Fluent software, as the CFD offer a myriad of advantages over traditional programming methods employing Fortran and MATLAB, particularly in terms of efficiency and accuracy. One notable benefit lies in

their capability to significantly reduce calculation time, as CFD simulations leverage advanced algorithms and parallel computing techniques for swift data processing. Additionally, CFD software packages provide intuitive graphical user interfaces, streamlining the setup and execution process compared to the labour-intensive coding required in Fortran and MATLAB. Moreover, CFD simulations mitigate the inherent risk of human errors, such as forgetting brackets or commas, thereby enhancing reliability and reproducibility in results. Consequently, CFD simulations emerge as a superior tool for our research, enabling rapid prototyping, optimization, and analysis in fluid dynamics applications with heightened precision and efficiency.

3.2. FIRST TEST: the mesh

The governing equations were solved using the finite-volume method as described by **Patankar [36]**. This method involves dividing the physical domain into small control volumes, where the modeling equations are discretized within each volume using the SIMPLE algorithm. A second-order upwind scheme was utilized for the continuity, momentum, and energy equations, while a second-order scheme was applied for the pressure term.

The boundary conditions for the simulation were defined as follows:

- **Solid Walls:** No-slip and no-penetration conditions were applied to all solid walls, indicating that the fluid does not slip along the wall and cannot penetrate it.
- **Outer Tube Wall:** A heat flux of 1000 W was applied to the external wall of the outer tube, representing a constant heat input.
- **Annulus Inlets:** Velocity-inlet boundary conditions were specified at the inlets of the annulus, defining the fluid velocity entering the domain.
- **Annulus Outlets:** Pressure-outlet boundary conditions were applied at the outlets of the annulus. A pressure of zero was assumed at the outlets, ensuring that the pressure drop across the domain was equal to the inlet pressure.

This setup simulates a scenario where the fluid is driven through the annulus by a pressure gradient, with a constant heat flux applied to the outer tube wall. The combination of boundary conditions creates a realistic representation of the flow and heat transfer processes within the system.

Our study focused on a trapezoidal fin attached to a flat surface, the analysis of thermal energy balance incorporated certain assumptions: steady-state conditions, heat transfer occurring through convection and conduction, no heat generation within the fin,

constant thermal conductivity and negligible temperature difference across the fin thickness. In order to ensure high-quality results, we choose the unstructured tetrahedral mesh (figure 3.1), then we perform an element size mesh test, which was a comparison between 0.0001 m and 0.0005 m of mesh element size, as it detailed as follows.

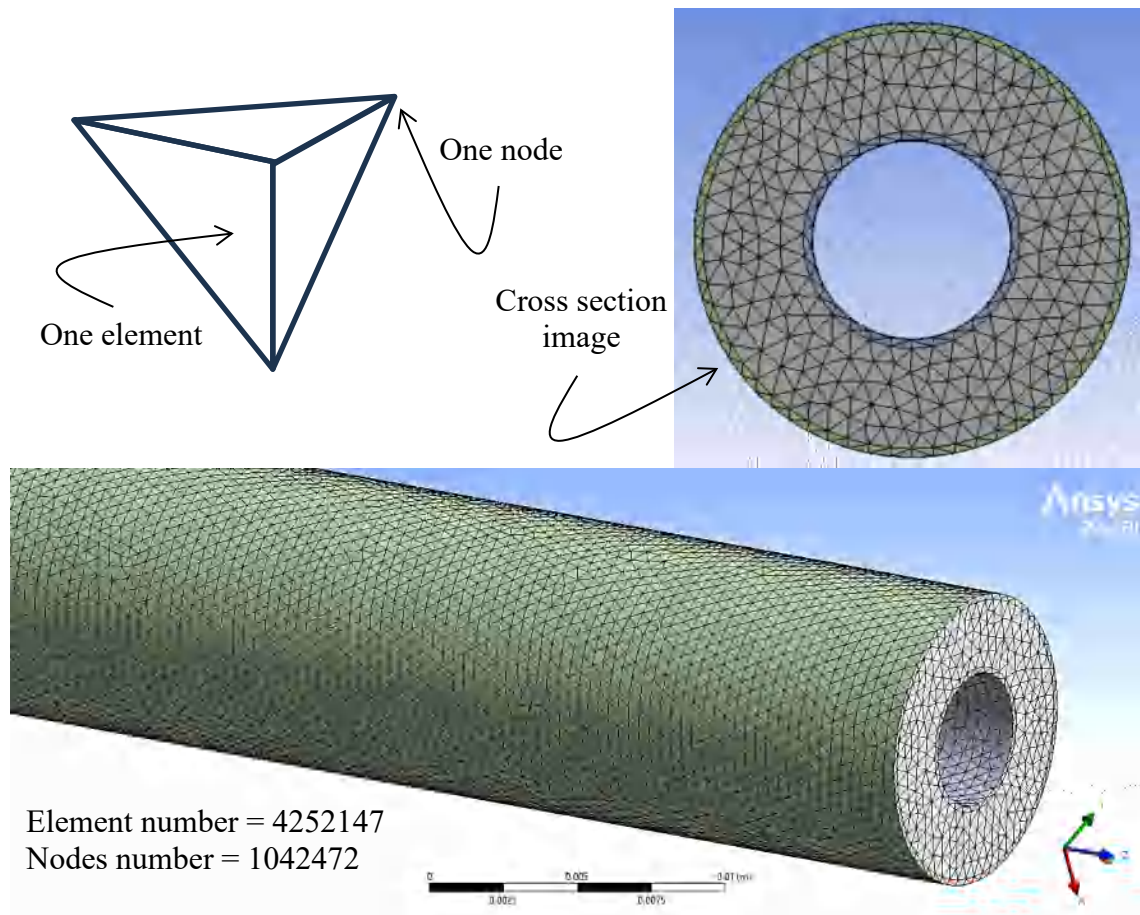


Figure 3.1: Tetrahedral mesh structure illustration

3.2.1. Mesh elements size test

Choosing an optimal mesh elements size is crucial in computational simulations to attain accurate solutions efficiently. To determine the most suitable mesh element size, we conducted a mesh test in a small annulus with 30.16 mm of length and two helical fins attached on the internal surface of the outer tube with 45° of helix angle, the test made with two different element sizes: 0.0001 m and 0.0005 m. These sizes represent the dimensions of the finite volume in the simulation, it means that all the tetrahedron lengths are equal to one of the mentioned values. It is evident that reducing the element size enhances accuracy and precision in the results (figure 3.6). However, this reduction in element size significantly

increases the computational time without yielding a substantial difference in the outcomes. Figures 3.3 demonstrate a similarity in outlet velocity and temperature values between the two cases, except for the maximum outlet temperature, where the smaller element size exhibits a slightly higher value.

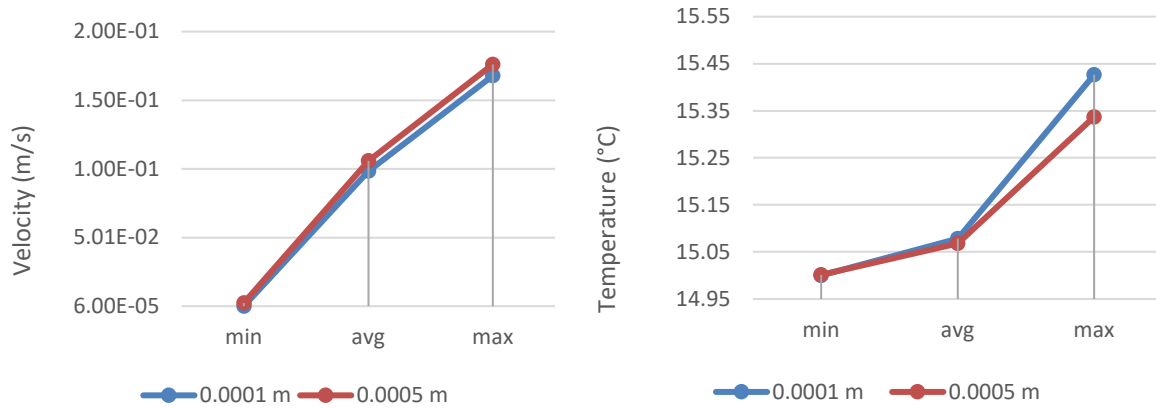


Figure 3.2: outlet velocity and temperature elements size comparison

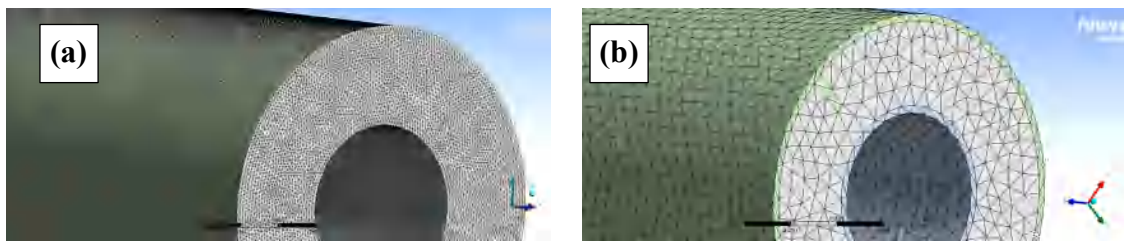


Figure 3.3: illustration of mesh element size difference between (a) 0.0001 m and (b) 0.0005 m

Considering the computational time, the convergence time for the case with a 0.0001 m element size is notably longer, approximately 1 hour and 17 minutes, compared to just about 2 minutes and 29 seconds for the case with a 0.0005 m element size (refer to Table 3.2). Given that our study involves a tube length of 1 meter, completing simulations with the finer mesh size would require an extensive amount of time, with marginal differences in velocity and temperature values (see figure 3.5).

Table 3.1: element size parameters comparison

		Element size 0.0001 m	Element size 0.0005 m
Outlet temperature (°C)	Min	15.000055	15.001337
	Avg	15.078189	15.068335
	Max	15.426477	15.337
Outlet velocity (m/s)	Min	8.6489243e-05	0.0024899591
	Avg	0.098516806	0.10602345

		Max	0.16793428	0.17618495
At the interface outer-fluid	Average wall shear stress	(Pa)	0.43523497	0.40884705
	Average skin friction coefficient	(Pa)	0.71058771	0.66750539
	Average total surface heat flux	(W/m^2)	832.1436	881.27135
	Average surface heat transfer coefficient	(W/m^2K)	2963.1408	3068.6471
	Average surface Nusselt number	-	4938.568	5114.4119
	Nodes number	-	106934	34290
	Element number	-	457284	138354
	Number of iterations	-	363	142
	Time to converge		1h 17m 55s	0h 02m 29s

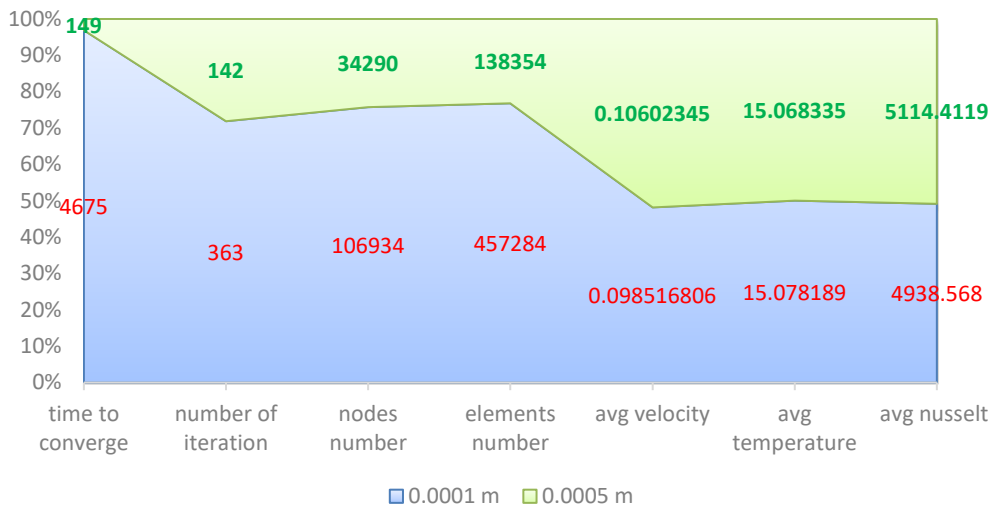
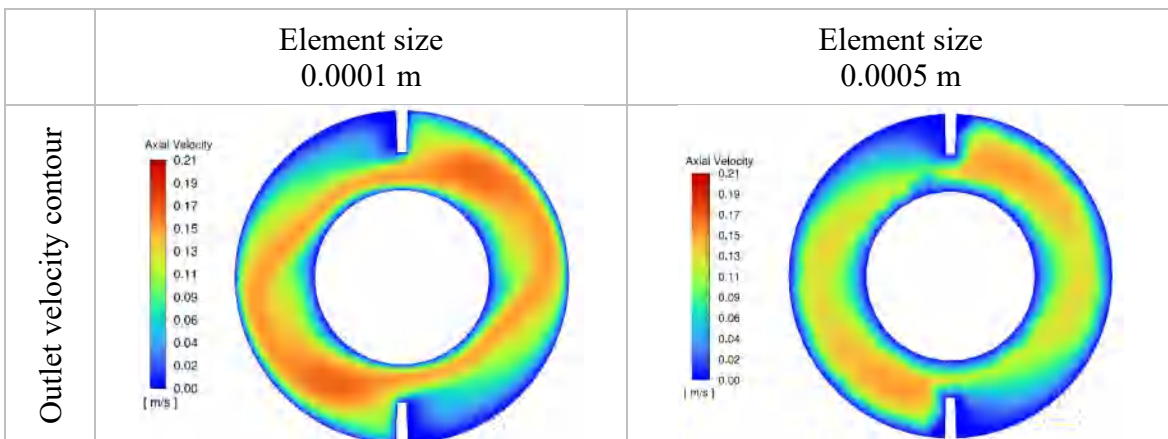


Figure 3.4: key parameters comparison between 0.0001 m and 0.0005 m cases

Figure 3.6 shows the outlet velocity and temperature contours for the two cases with a clearly seen that the smallest element size gives better accuracy contours, also it shows good element quality than the case of 0.0005 m.



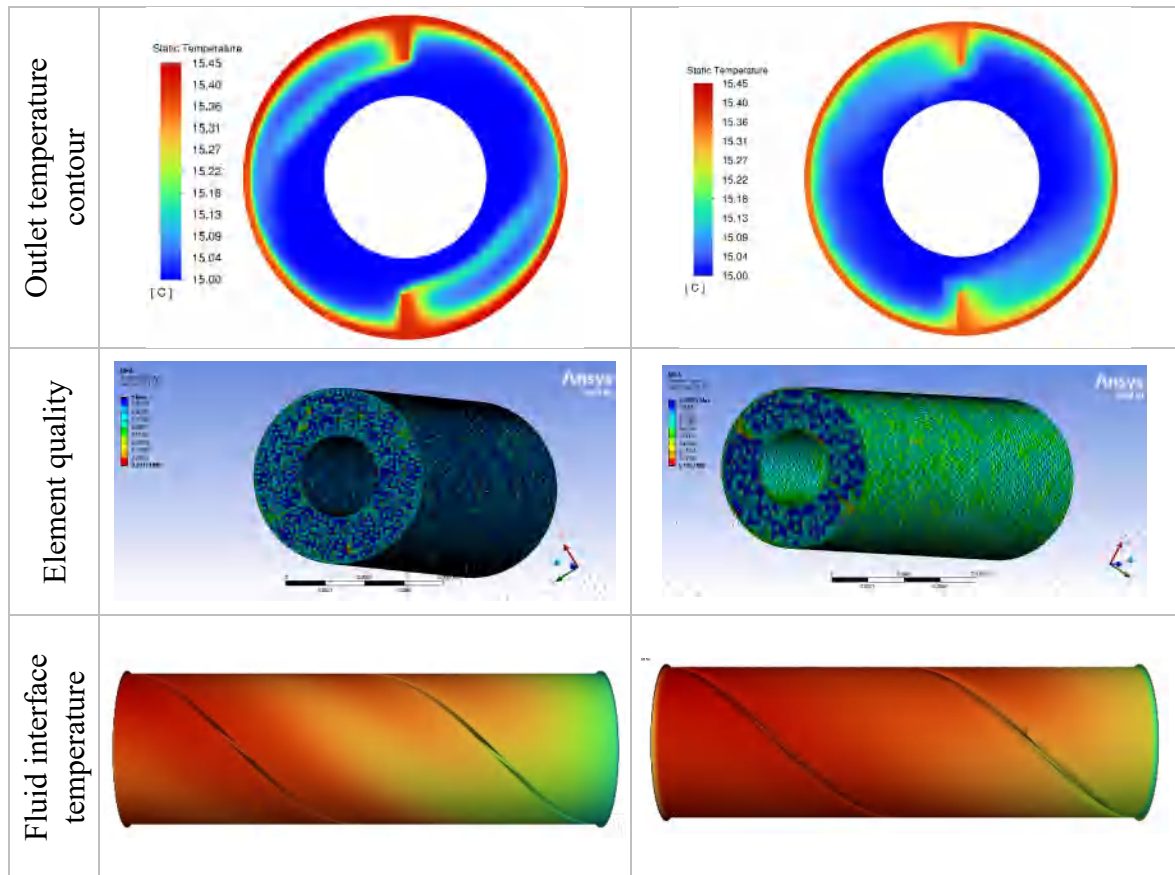


Figure 3.5: velocity and temperature contours, element quality and fluid interface temperature for the 0.0001 m and 0.0005 m element size cases

Consequently, we opt for the 0.0005 m element size in our study to achieve a balance between computational efficiency and solution accuracy. This decision underscores the importance of selecting an appropriate mesh structure to optimize computational resources while ensuring reliable results.

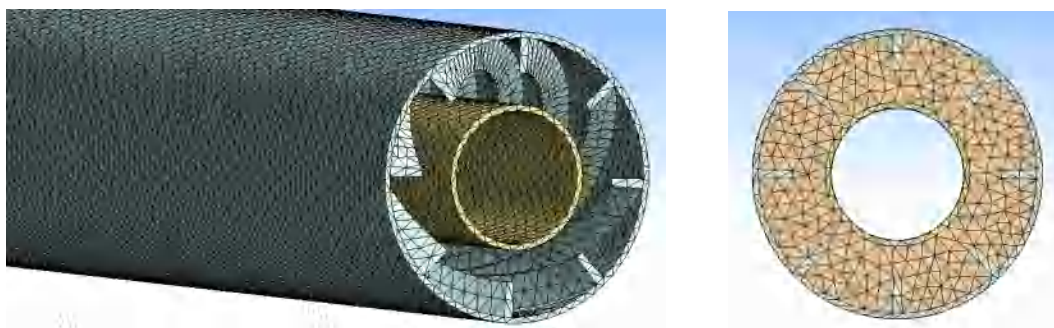


Figure 3.6: illustration of tetrahedral mesh with 0.0005 m element size for the case of 8 helical fins with 45° helix angle

3.3. Results validation

In Figure 3.7, the results regarding the axial Nusselt number at the interface between fluid and outer tube are compared with those obtained numerically by **Nazrul et al. [102]** for forced convection. The comparison shows a good agreement between the two sets of results. However, In the short entry zone, the axial Nusselt number experiences a sharp drop due to the rapid increase in the temperature difference between the outer cylinder wall and the average fluid temperature. This is followed by a slower decrease in the axial Nusselt number because the temperature difference stabilizes. At the exit of the annulus, the value of the axial Nusselt number is the same for both cases.

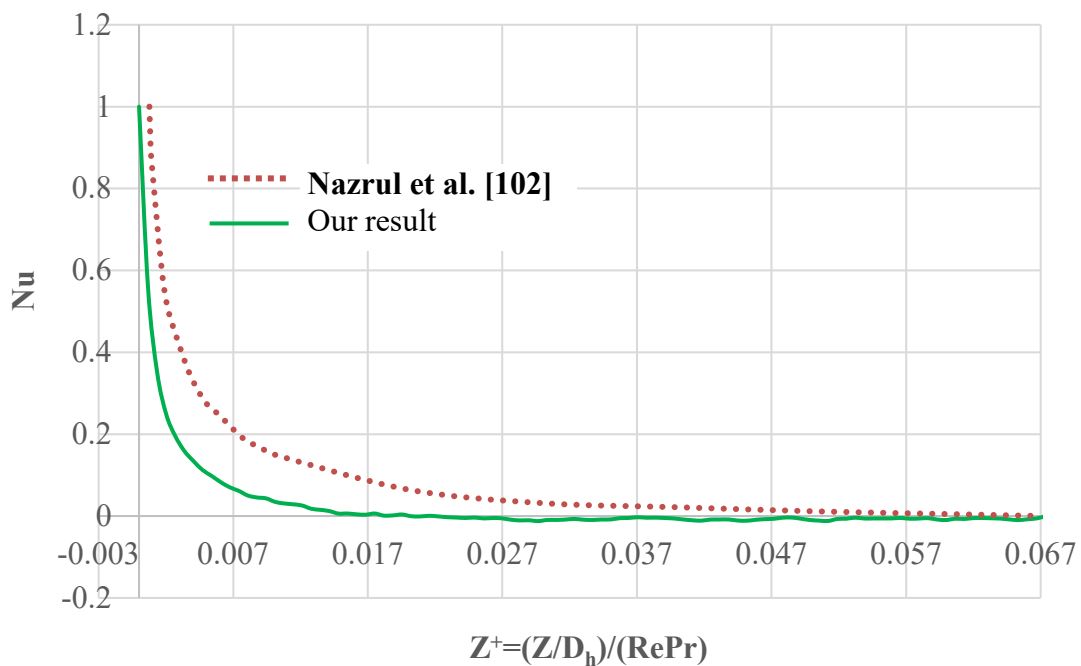


Figure 3.7: Validation of the calculation code for a horizontal pipe: a comparison with the values of the average circumferential Nusselt obtained by **Nazrul et al. [102]**

3.4. Conclusion

In conclusion, our investigation in this chapter has demonstrated the advantages of computational fluid dynamics (CFD) simulations over traditional methods. After choosing the tetrahedral mesh structure, to be adopted for our numerical analyses (figure 3.6). we found that while reducing the mesh element size improves accuracy, it significantly increases computational time without substantial gains in outcomes. Therefore, we have chosen a 0.0005 m element size to strike a balance between efficiency and accuracy in our study. This decision emphasizes the critical role of selecting optimal mesh parameters to maximize computational resources while ensuring dependable results in fluid dynamics applications.

Chapter 4

Results and discussion

4.1. Introduction

In this chapter, we present and analyze the results derived from CFD simulation using Ansys fluent software on laminar forced convection of water flowing inside an annulus with longitudinal and helical fins attached on the internal surface of the outer tube, The outer tube's external surface is subjected to a constant heat flux of 1000 W/m^2 . Our study encompasses multiple tests (figure 4.1). Initially, we performed a comparative examination of mesh element size as we saw in the previous chapter, after choosing the unstructured tetrahedral mesh, we evaluated how different mesh element sizes (0.0001 m and 0.0005 m) affected both the efficiency and accuracy of calculations. Moreover, the second test involved the influence of increasing fins number on the hydrothermal behavior of the fluid, with fin numbers set at 2, 4, and 8 helical fins, each with a fixed helix angle of 20° , those cases are compared with reference case of smooth annulus. Additionally, we explored the effect of altering the helix angle at the third test, keeping the fins number constant at 8 while adjusting the helix angle from 0° (longitudinal fins) to 20° , 30° , and 45° . Furthermore, we investigated in the fourth test the effects of varying the applied heat flux on the outer tube's surface. This entailed comparing a reference case with a smooth annulus of 1000 w/m^2 , to another smooth annulus with a heat flux of 3000 W/m^2 , and three cases with 2 helical fins, each with a 20° helix angle but differing heat fluxes of 500, 1000, and 3000 W/m^2 . Finally, we conducted an

examination of inlet velocity in the fifth test, studying its impact on the thermo-hydraulic behavior of the water fluid. Three cases featuring 8 helical fins and a 45° helix angle were examined, with velocities set at 0.06, 0.0988, and 0.3 m/s. Throughout all previous tests, the fluid's inlet temperature remained constant at 15°C , while the inlet velocity was fixed at 0.0988 m/s, except during the velocity test section, where it was varied. The tubes utilized in all of the investigation had a length of 1 m, an outer tube internal diameter of 9.6 mm, an outer tube external diameter of 10 mm, an inner tube internal diameter of 4.6 mm, and an inner tube external diameter of 5 mm. The tubes and fins are made with aluminum with a thermal conductivity equal to 202.4 W/m.K .

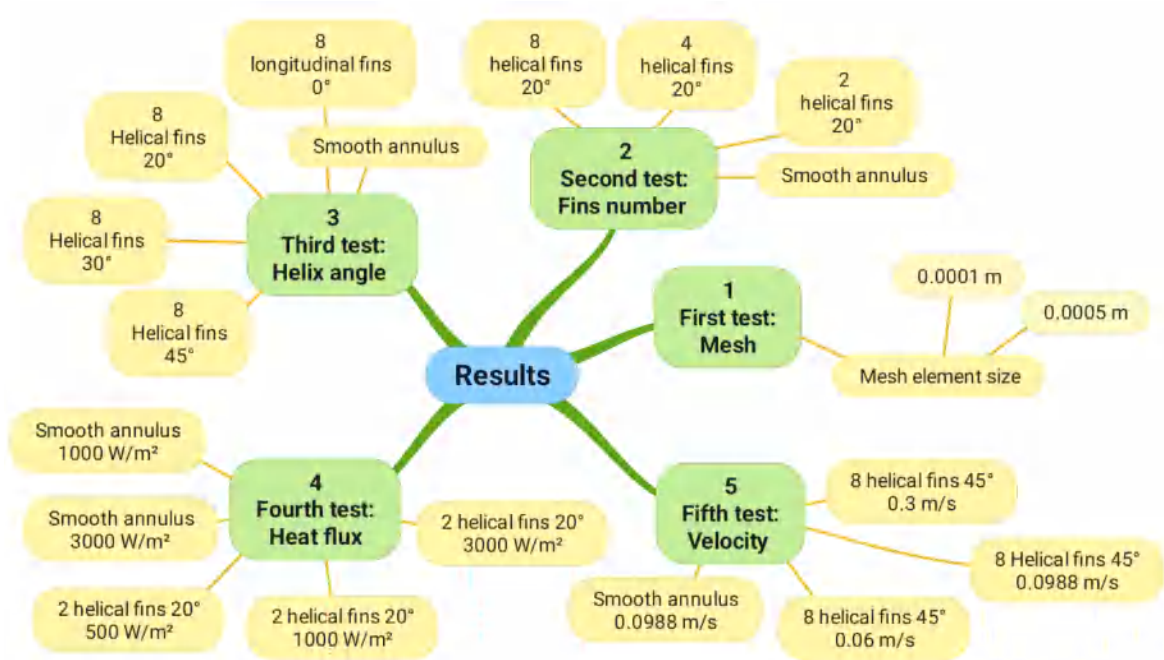


Figure 4.1: mind map of all tests done in the study

4.2. SECOND TEST: fins number

Using fins inside an annulus plays a significant role in enhancing the hydro-thermal behavior of fluids. In this segment of our investigation, we examine how increasing the number of fins affects fluid dynamics and heat transfer. Three cases are analyzed and compared against a reference case (smooth annulus). The helix angle is fixed at 20° , while the number of fins is varied. The first case involves two helical fins positioned at $(\theta = 0)$ and $(\theta = \pi)$, the second case has four helical fins at $(\theta = 0)$, $(\theta = \pi/2)$, $(\theta = \pi)$ and $(\theta = 3\pi/2)$, and the third case features eight helical fins at $(\theta = 0)$, $(\theta = \pi/4)$, $(\theta = \pi/2)$, $(\theta = 3\pi/4)$, $(\theta = \pi)$, $(\theta = 5\pi/4)$, $(\theta = 3\pi/2)$ and $(\theta = 7\pi/4)$ (refer to Figure 4.2).

Additionally, the introduction of helical fins significantly impacts the exchange surface area, as demonstrated in Table 4.1. Compared to the reference case, the outer tube's internal surface area increases by 16.1%, 31.9%, and 63.8% for the first, second, and third cases, respectively. However, a slight reduction in the cross-sectional area of the finned cases is observed due to the increased number of fins. This finding underscores the importance of using fins inside an annulus to enhance heat transfer while also taking into account the compromises associated with modifications in surface area (figure 4.3).

Table 4.1: Parameters of the cases studied in test 02

	N_s	α	Fin pitch "p" (mm)	Total fins surface (mm ²)	Total internal surface of outer tube (mm ²)	Increased surface (%)	Cross section area (mm ²)
Reference case 'Smooth annulus'	-	-	-	-	30159.3	0	52.74
2 helical fins 20°	2	20°	82.86	5543	35015.9	16.1	52.03
4 helical fins 20°	4	20°	82.86	11084	39783	31.9	51.3
8 helical fins 20°	8	20°	82.86	27605.1	55026.6	63.82	49.87

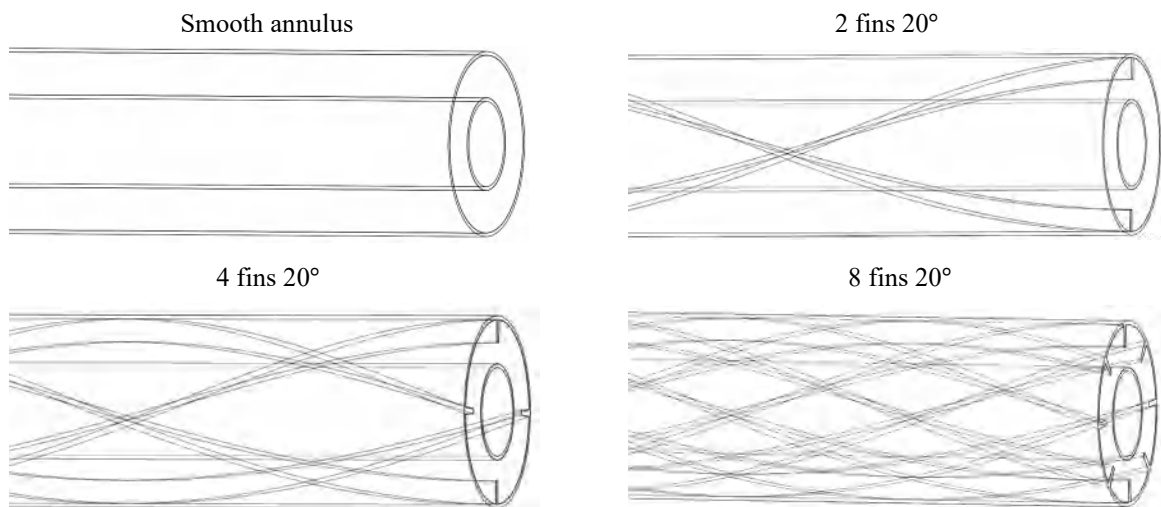


Figure 4.2: Cases studied geometries in test 02

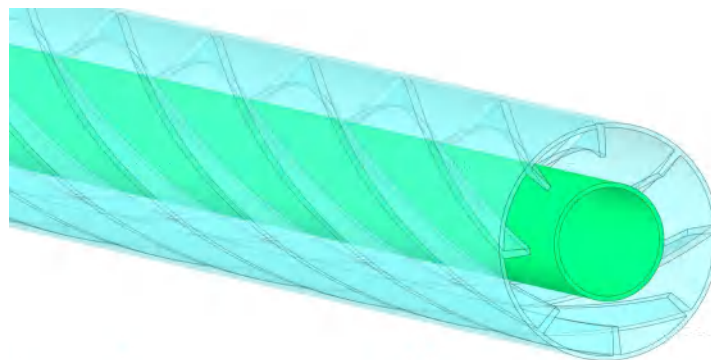
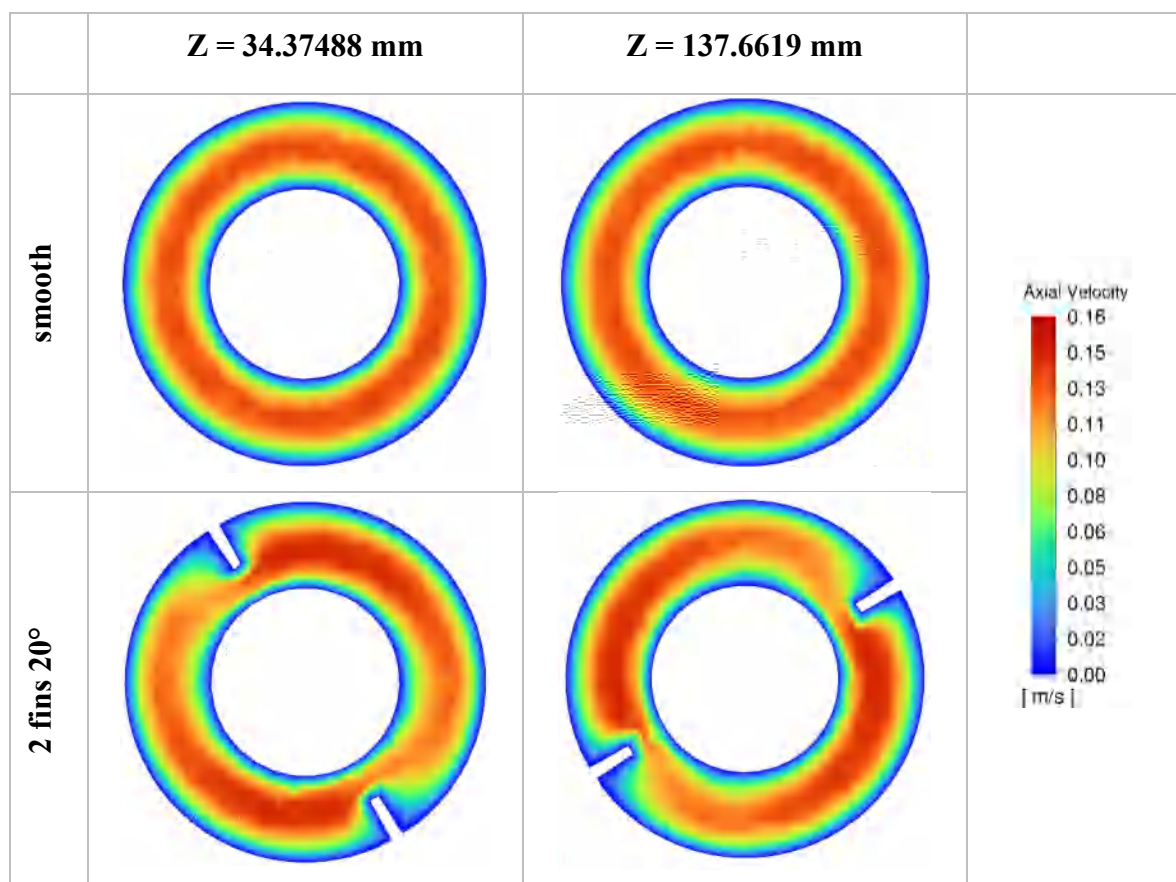


Figure 4.3: illustration of 8 fins 20° annulus geometry

4.2.1. Hydrodynamic

The examination of velocity contours within the annular domain offers valuable insights into the fluid flow behaviour and its hydrodynamic characteristics. The velocity contours depict the spatial distribution of fluid velocities throughout the annulus, shedding light on the flow patterns and velocity gradients present within the system. At the entrance, the flow exhibits a hydrodynamically developed profile. This profile represents a laminar flow condition characterized by a parabolic velocity distribution, where the axial velocity is maximum at the centreline between the tubes and decreases linearly towards the tube walls. In our study, this profile showcases the maximum axial velocity at the center of the distance between the two tubes, with minimum values observed on the inner wall of the outer tube and the outer wall of the inner tube. Furthermore, zero velocity components are maintained within the fin walls throughout the conduit. Upon introducing helical fins, the axial velocity distribution remains minimal near the tube and fin walls, with the maximum velocity occurring close to the center between two fins, albeit slightly closer to the left fin's wall. This observed trend is consistent in the contour of the first case featuring two helical fins (refer to Figure. 4.4).



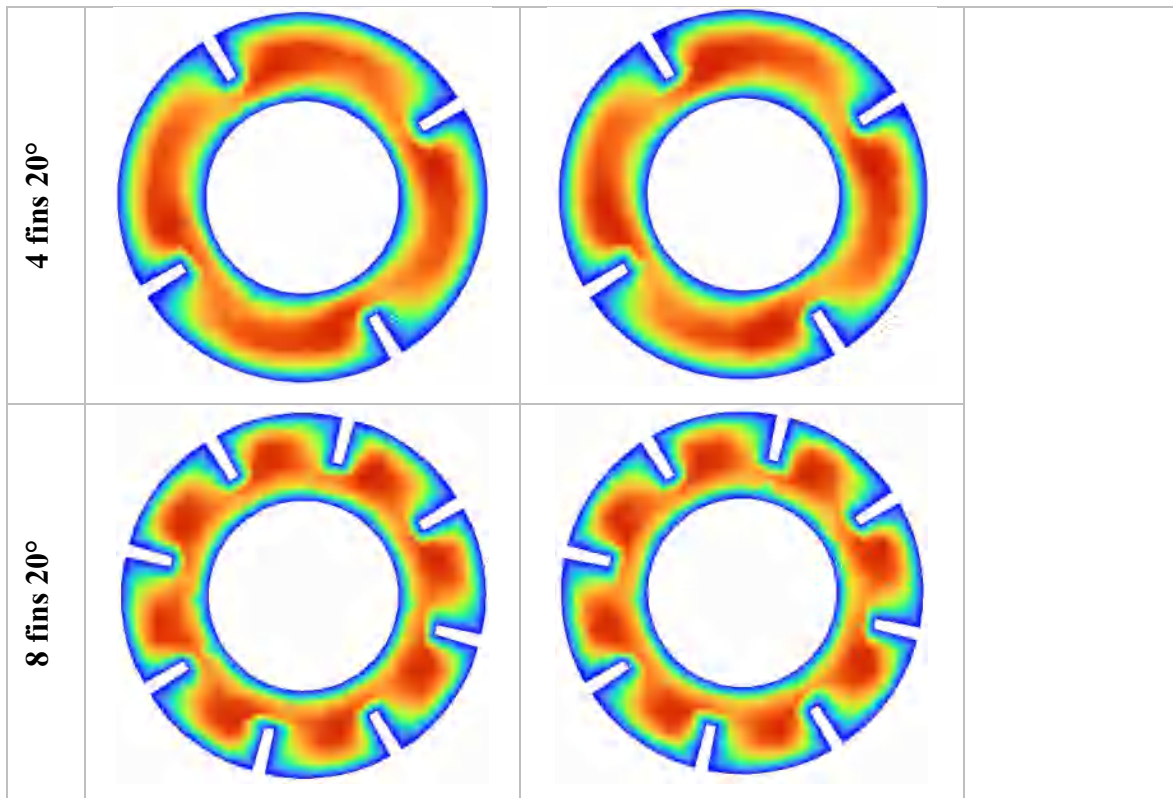


Figure 4.4: velocity contours of all cases in test 02

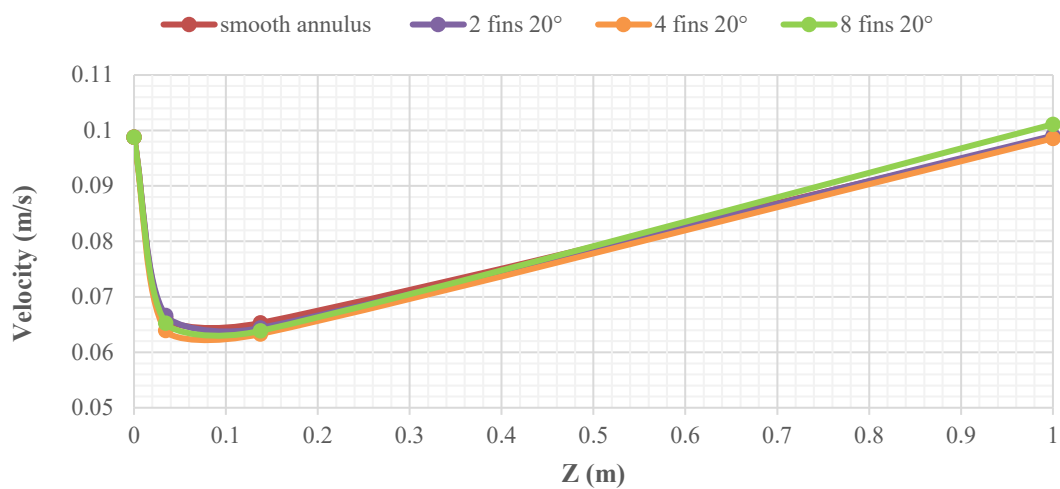


Figure 4.5: average axial velocity for all cases in test 02

It is clearly visible from **Figure 4.5** and **Table 4.2** that configurations featuring helical fins exhibit a slight increase in the rotational flow component, which is attributed to the increment in helical fin number. As a consequence, the cross-sectional area is reduced, adhering to Bernoulli's principle, which states that a decrease in cross-sectional area leads to an increase in velocity. This phenomenon is evident in our study, where the introduction of

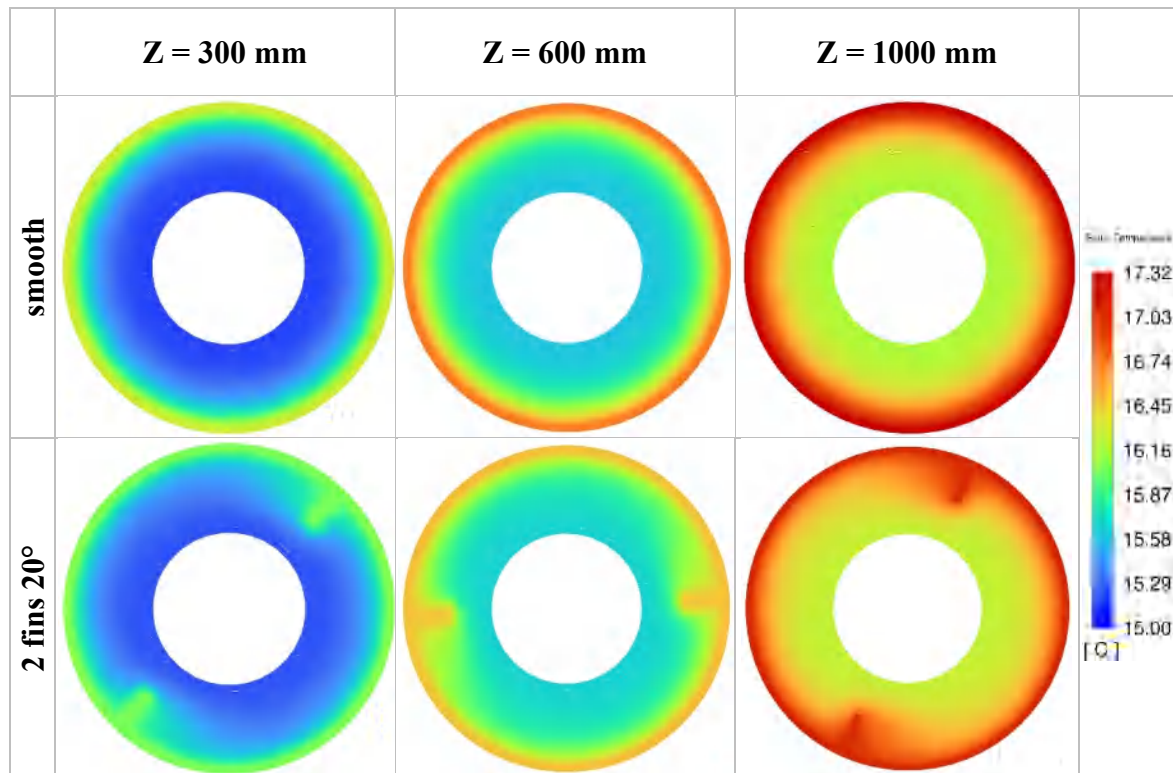
helical fins results in a reduction in cross-sectional area, consequently leading to an increase in fluid velocity.

Table 4.2: Average axial velocity values of the cases studied in test 02

Z (m)	Average axial velocity (m/s)			
	smooth annulus	2 helical fins 20°	4 helical fins 20°	8 helical fins 20°
0	0.0988	0.0988	0.0988	0.0988
0.03437488	0.06620	0.06662	0.06390	0.06527
0.1376619	0.06528	0.06438	0.06330	0.06386
1	0.09866	0.09904	0.09857	0.10111

4.2.2. Thermal

As it was described previously, a heat flux of 1000 W/m^2 was applied on the external surface of the outer tube produces uniform volumetric heat generation, the large portion of this heat being transferred to the fluid by radial flow at the solid-fluid interface, the rest will spread out to the outside air as heat losses.



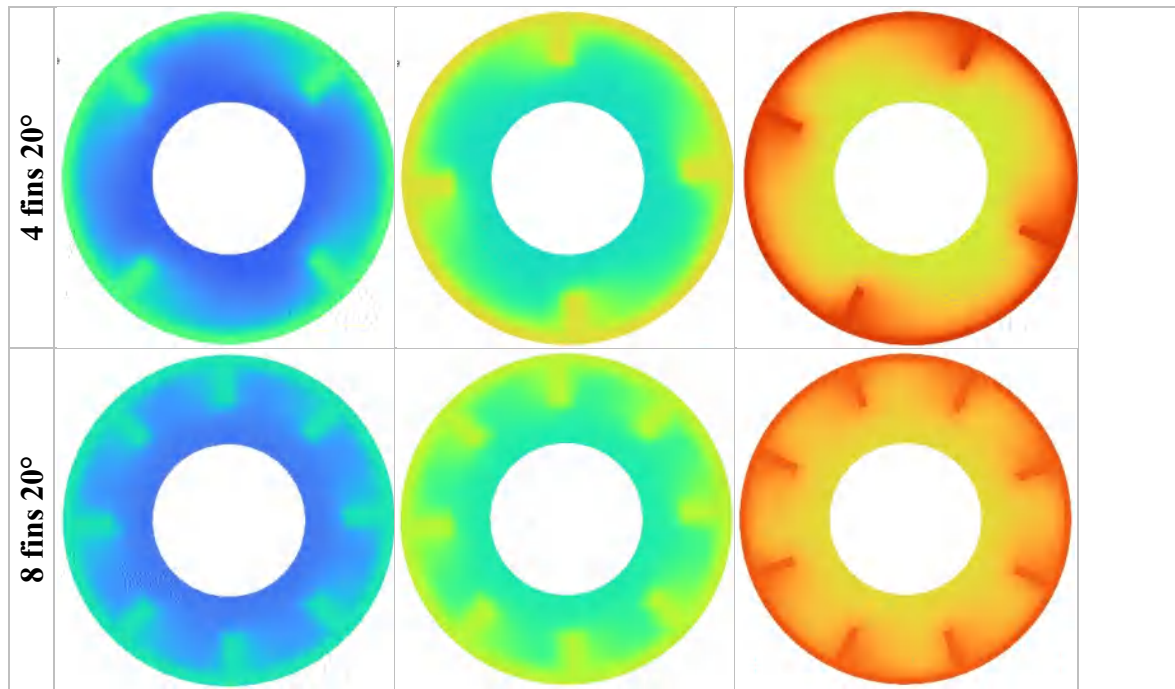


Figure 4.6: temperature contours of all cases in test 02

At the inlet, the fluid temperature is uniform. As the fluid moves through the tube and fins, heat is released, creating a temperature difference between the outer and inner tubes. This causes the temperature distribution to be symmetrical along the axial direction, with the zone near to the internal wall of outer tube having the highest temperature. This symmetry happens because there is no sideways flow, so the temperature changes only in the axial and radial directions (see Fig. 4.6).

Near the centre of each section of the tube, the fluid's temperature forms concentric circles, with the lowest temperature at the inner tube's surface. As the distance from the inner tube increases, the circular temperature pattern changes due to the heat released by the fins. The highest fluid temperature occurs at the outer tube's surface away from the fins. Additionally, the fluid's temperature at the fins' surface is lower than that at cylindrical interface because the fins release heat on both sides, reducing the temperature.

Analysing the flow and using Newton's law of cooling $Q = hA(T_w - T_\infty)$, it's expected that helical fins will increase heat transfer in two ways: by increasing the surface area because of their shape (number of fins and helix angle) and by increasing the heat transfer coefficient due to higher fluid velocities. However, higher velocities might also lead to increased pressure loss as the fluid moves through the annulus region.

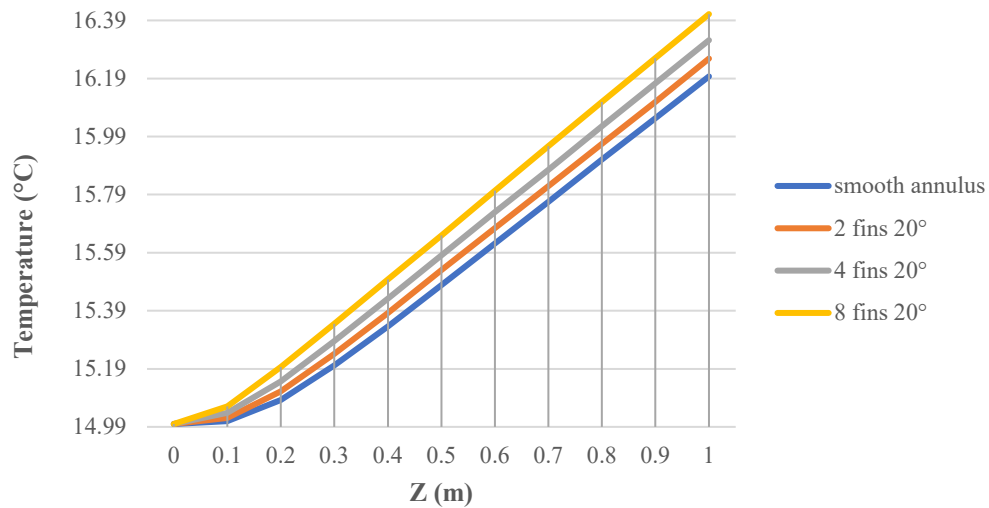


Figure 4.7: minimum fluid temperature along the axial direction of all cases in test 02

Fig. 4.7 illustrates how the minimum fluid temperature changes along the axial direction. It's evident from the graph that the helical fins design results in a higher minimum fluid temperature compared to the setup of smooth. Additionally, the case of two helical fins with 20° of helix angle gives results less than that of 4 helical fins and more less than that of 8 helical fins, but it steel better than smooth annulus.

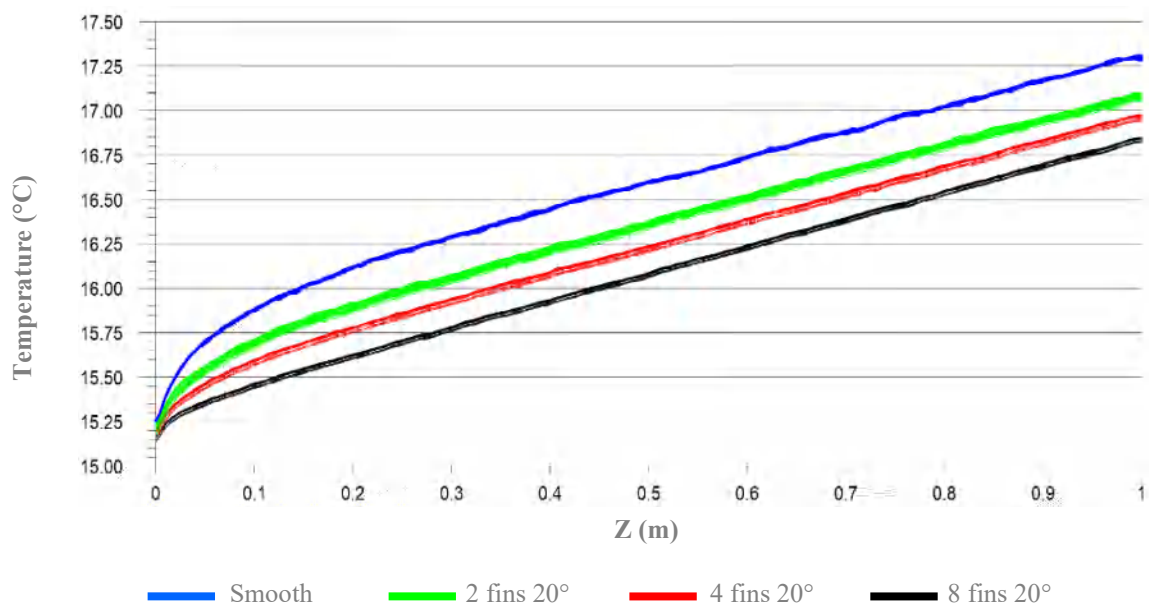


Figure 4.8: average interface fluid-outer tube temperature along the axial direction for test

02

Fig. 4.8 show's that the average internal wall temperature of the outer tube reached its highest value for the smooth tube configuration. This is because the smooth tube has the least amount of surface area for heat exchange compared to all other cases. In contrast, the case of eight helical fins at a 20° helix angle displayed the lowest temperature among the cases studied due to its larger surface area for heat exchange, which give high temperature dissipation to the fluid.

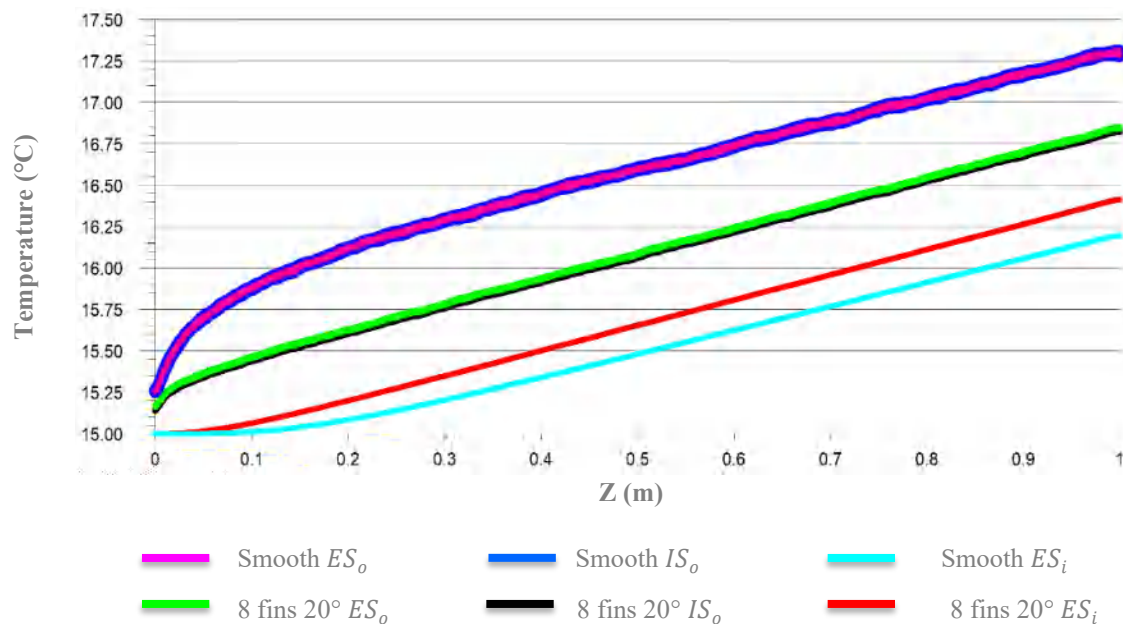


Figure 4.9: average tubes walls temperature for test 02

As depicted in Fig. 4.9, the main point previously discussed is evident. The smooth annulus configuration results in a higher temperature for the outer tube walls compared to the third case. However, it leads to a lower temperature for the external wall of the inner tube. This is attributed to the effective distribution of internal wall temperature in the helical finned tubes, which dissipate more heat release to the fluid. Consequently, this can elevate the temperature of the external wall of the inner tube which can be observed from the figure to surpass that of the smooth configuration. Moreover, the differential temperature between external and internal surfaces of outer tube is larger at the smooth case compared to third case, it is caused by good distribution of heat to the fluid by fins.

4.2.3. Pressure drop

Pressure drop plays a crucial role in heat transfer studies of tubes using Computational Fluid Dynamics (CFD). A high-pressure drop indicates increased resistance

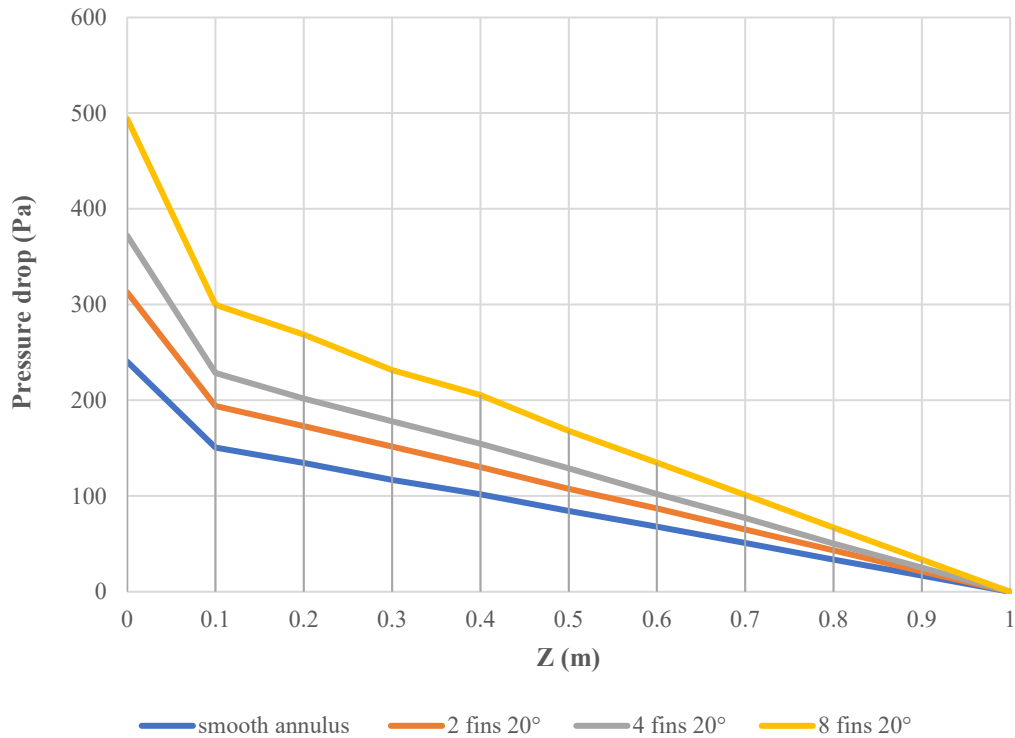


Figure 4.10: pressure drop variation along the axial direction for test 02

to fluid flow within the tube, which can lead to higher energy consumption and reduced system efficiency. For example, in HVAC systems, high pressure drop can result in decreased airflow and reduced heat transfer rates, leading to inefficient heating or cooling. Conversely, a low-pressure drop signifies minimal resistance and efficient fluid flow, which promotes enhanced heat transfer and lower energy consumption.

The relationship between pressure drop and the number of fins gives us important information about how heat transfer systems behave. Using helical fins makes the pressure drop increase noticeably compared to smooth tubes. with an average increase of 1.3, 1.5, and 2.0 times for cases 1, 2, and 3, respectively, compared to a smooth tube configuration. There are a few reasons for this. First, the shape of helical fins creates obstacles in the flow path, making it harder for the fluid to flow. Second, the sudden change in how the fluid moves, especially near the beginning, makes the pressure go up even more. Third, because there's more surface area for the fluid to flow along, the pressure increases even more, especially with higher number of fins. Figure 4.10 shows how pressure drop changes along the length of the flow path within the fins. Even though a few things cause pressure to increase, the biggest reason is the higher surface area created by fins.

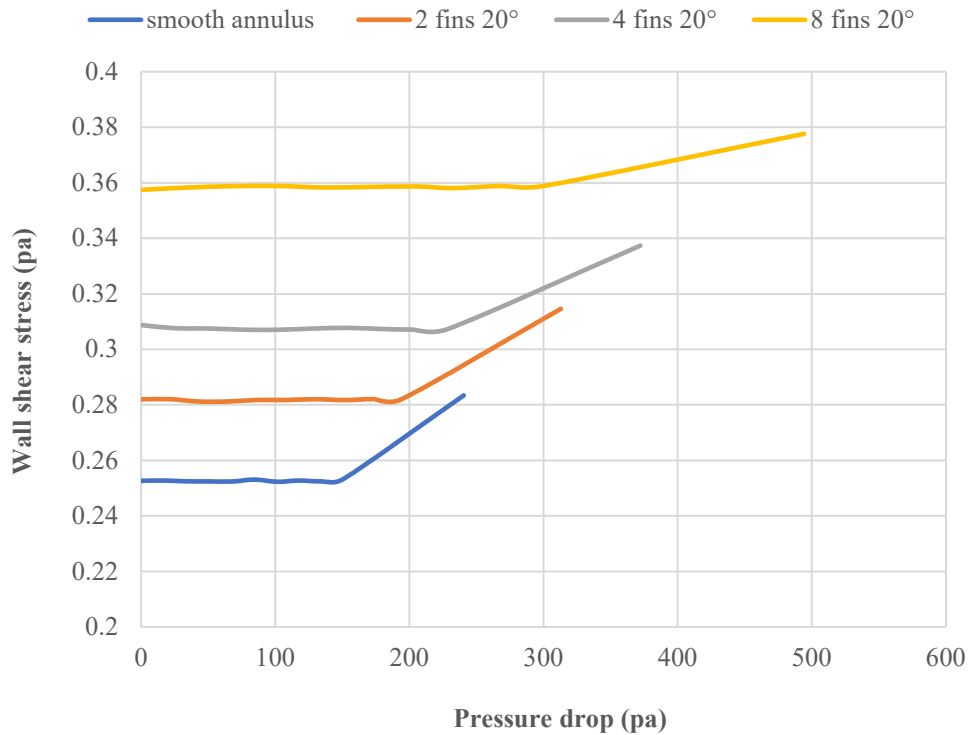


Figure 4.11: wall shear stress versus pressure drop for all cases in test 02

As Figure 4.11 shows, a proportional relationship between wall shear stress and pressure drop is clearly seen. As the wall shear stress increases, there is a corresponding increase in pressure drop. This shows that both pressure drop and wall shear stress increase with the augmentation of helical fins number.

4.2.4. Heat transfer

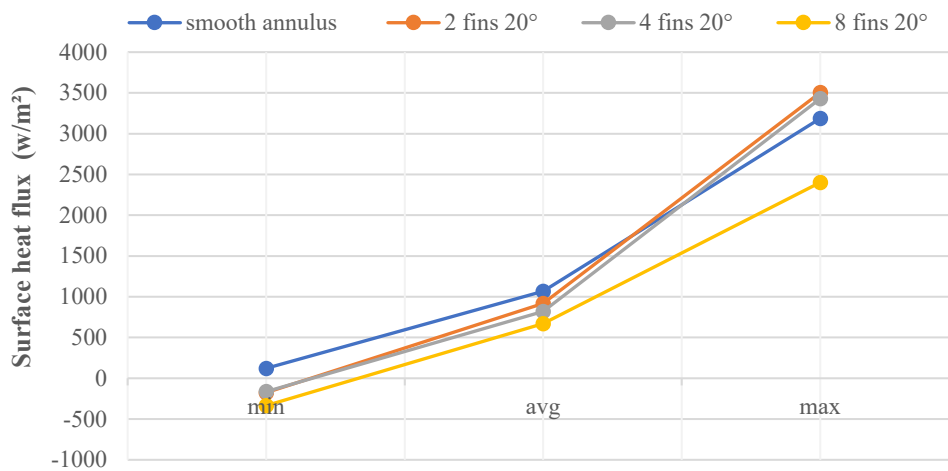


Figure 4.12: surface heat flux values of all cases in test 02

Based on the data presented in Figure 4.12, it is apparent that the average heat flux investigated by the internal surface of the outer tube exhibits variations depending on the tube configuration. Specifically, the smooth tube configuration yields the highest heat flux, whereas the introduction of 2 fins with a helix angle of 20° results in a reduction in heat flux. Furthermore, as the number of fins increases, particularly with 8 helical fins, there is a further decrease in surface heat flux. Interestingly, the configuration with 8 helical fins demonstrates the lowest heat flux. These observations persist even when considering a constant temperature difference between the outer tube walls, as represented in Figure 4.9, and assuming a uniform thermal conductivity, such as that of aluminum (202.4 w/m.K). By applying Fourier's law of conduction, which states that heat transfer Q is proportional to the negative thermal conductivity $-k$ multiplied by the temperature difference ($T_{ES} - T_{IS}$) and divided by the distance difference ($x_{EX} - x_{IS}$), it is evident that variations in the distance (Δx) directly impact the surface heat flux. Thus, an increase in distance results in a corresponding decrease in surface heat flux, consistent with the observed trends in our cases data.

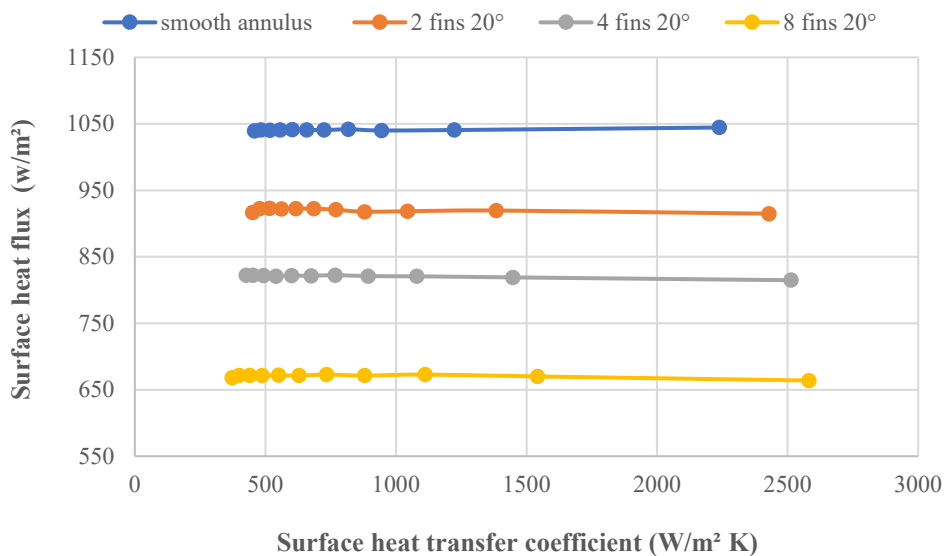


Figure 4.13: heat flux versus heat transfer coefficient for all cases of test 02

Utilizing helical finned tubes is widely recognised as a highly effective methods for increasing the heat transfer coefficient under a constant mass flow rate. Upon examination of Figure 4.13, it is evident that the maximum heat transfer coefficient was attained at the lowest surface heat flux (the third case). This phenomenon can be attributed to a remarkable dissipation of temperature from the solid to the fluid, which caused by an increase in the

exchange surface area. Therefore, the increase in the surface heat transfer coefficient directly results from this enhancement.

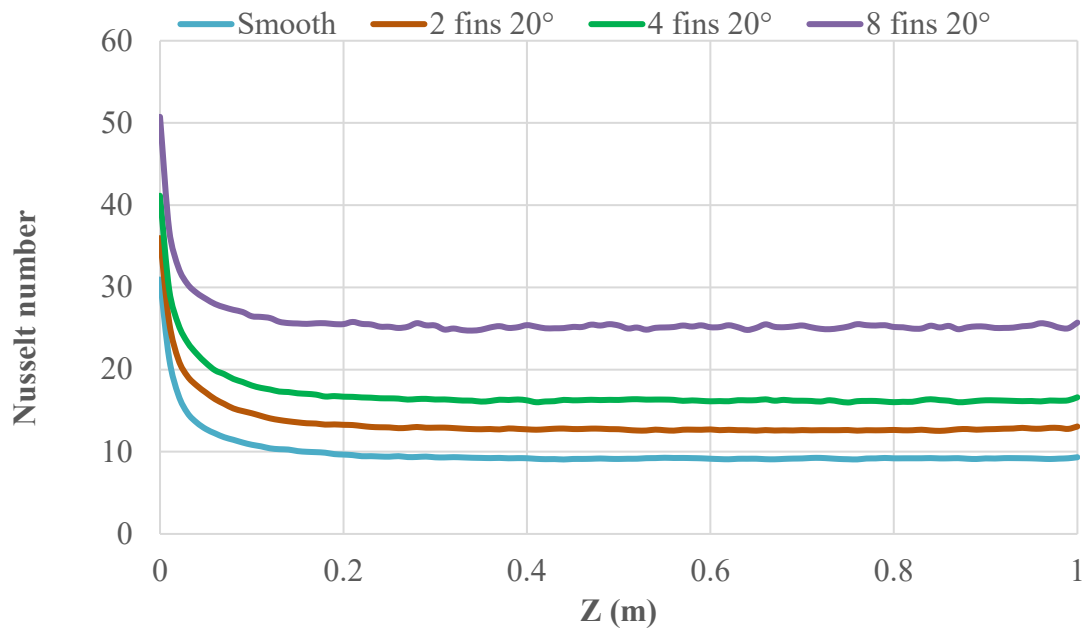


Figure 4.14: plot of Nusselt number along the axial direction for all cases of test 02

Figure 4.14 illustrates the variation of the Nusselt number. It is evident that the highest Nusselt number was recorded at the inlet for the case of 8 helical fins equal to 0.145. This increase is attributed to the higher heat transfer coefficient of the third case. Additionally, the axial Nusselt numbers at the inlet for the other cases were 0.102, 0.117, and 0.088 for the first, second, and reference cases, respectively. Figure 4.14 demonstrates that the axial Nusselt number starts with its maximum value at the inlet, followed by a rapid decrease in the entrance region and subsequent stabilization. At the outlet, all cases exhibit similar change due to the rapid increase in the temperature difference between the outer cylinder wall and the average fluid temperature, followed by a gradual decrease in the axial Nusselt number due to temperature difference stabilization.

4.2.5. Conclusion

This test examined the influence of increasing the number of helical fins within an annulus on fluid dynamics and heat transfer. Compared to a smooth annulus, configurations with 2, 4, and 8 fins significantly increased the exchange surface area, leading to notable changes in both hydrodynamic and thermal characteristics. While the presence of fins led to slightly higher fluid velocities, the most significant impact was observed in heat transfer.

The average internal wall temperature of the outer tube was considerably lower in configurations with fins, particularly in the 8-fin case, indicating enhanced heat dissipation to the fluid. However, this improvement came at the expense of increased pressure drop, which was proportionally related to the number of fins. This test demonstrates that increasing the number of helical fins can significantly enhance heat transfer, but careful consideration must be given to the associated pressure drop and its impact on energy consumption.

4.3. THIRD TEST: helix angle

The effect of increasing the helix angle on the surface exchange and hydrothermal behavior of water flowing inside an annulus is a critical aspect of our investigation. By varying the helix angle, we aim to elucidate its impact on heat transfer efficiency and fluid dynamics within the annular conduit. Previous tests have shown promising results with configurations featuring eight helical fins, suggesting that this arrangement offers optimal hydrothermal performance. Therefore, in this section, we explore the influence of different helix angles on heat transfer and flow characteristics, utilizing eight helical fins as the standard configuration. Additionally, we incorporate longitudinal fins, considered as helical fins with a helix angle of 0° as a first case, second, third and fourth cases has eight helical fins with helix angles of 20° , 30° , and 45° , respectively (see figure 4.15), with all fins positioned identically to the previously mentioned setups. Furthermore, the analysis reveals a significant alteration in the exchange surface area with increasing helix angle, as demonstrated in Table 4.3. Specifically, compared to the reference case, the outer tube's internal surface area increases by 61.2%, 63.8%, 67.3%, and 82.4% for the first, second, third, and fourth cases, respectively.

Table 4.3: Parameters of the cases studied in test 03

	N_s	α	Fin pitch "p" (mm)	Total fins surface (mm ²)	Total internal surface of outer tube (mm ²)	Increased surface (%)	Cross section area (mm ²)
Reference case 'Smooth annulus'	-	-	-	-	30159.3	0	52.74
8 longitudinal fins	8	0°	-	21219.2	48635.8	61.26	49.87
8 helical fins 20°	8	20°	82.86	22168	49407	63.82	49.87
8 helical fins 30°	8	30°	52.23	23560	50471	67.35	49.87
8 helical fins 45°	8	45°	30.16	27605.1	55026.6	82.45	49.87

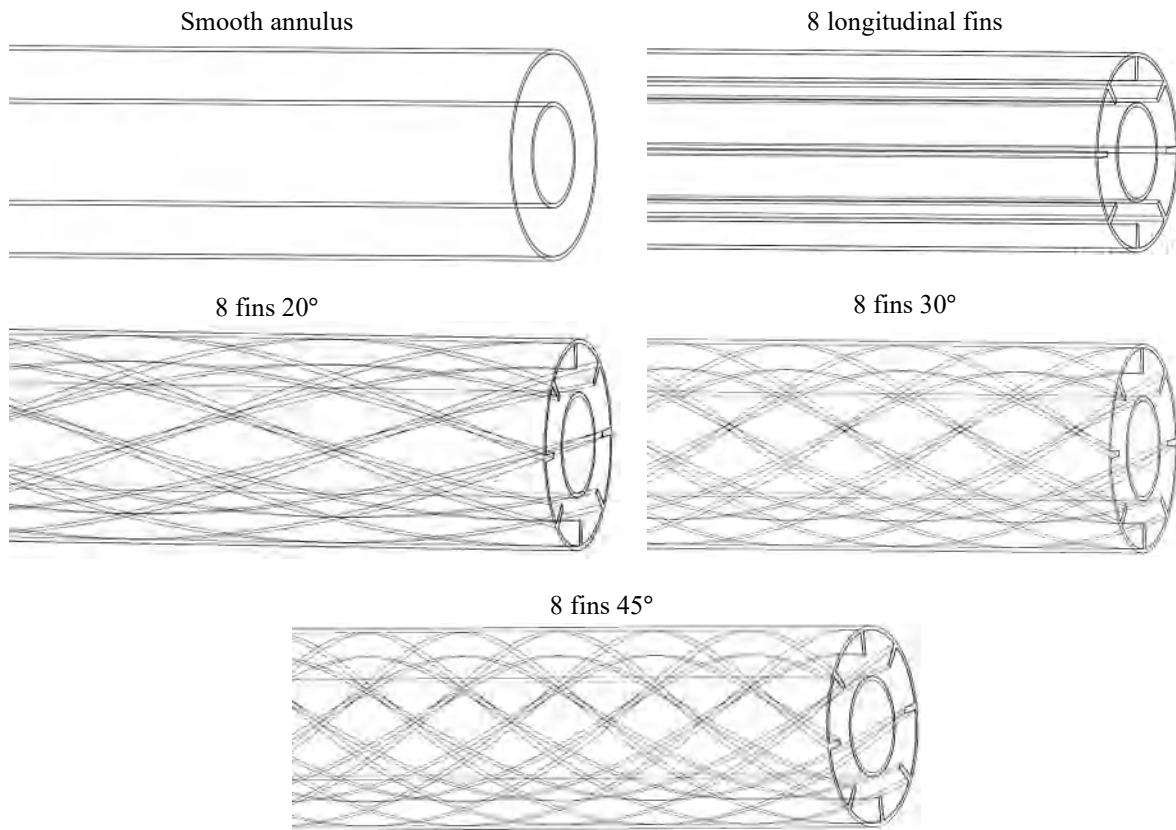
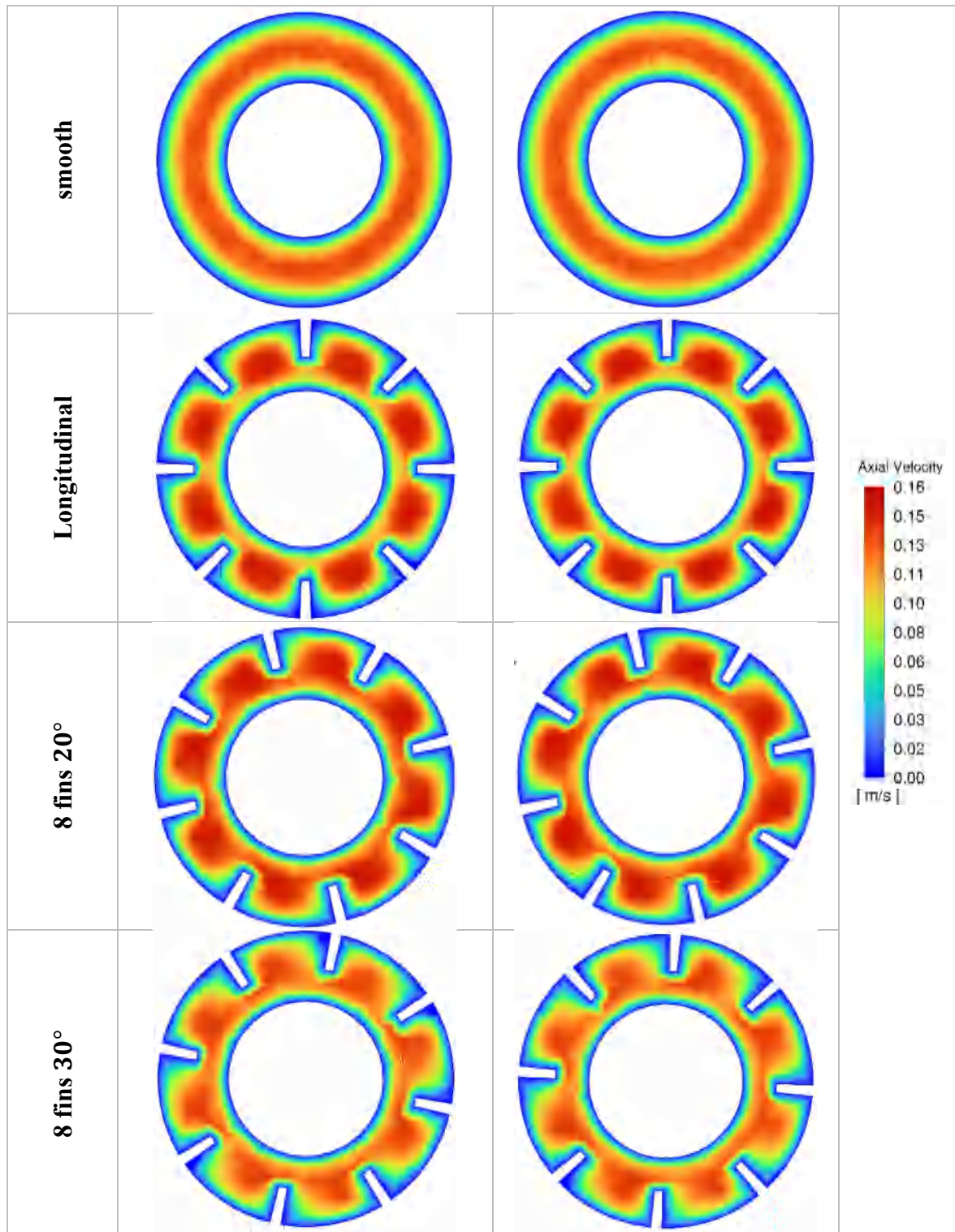


Figure 4.15: Cases studied geometries of test 03

4.3.1. Hydrodynamic

As it shown in figure 4.16, the velocity contours of the reference cases showed that the axial component takes a maximum value in the centre of the distance between the two tubes, and a minimum value on the internal wall of the outer tube and on the external wall of the inner tube. Furthermore, the axial velocity for the longitudinal and helical fins cases is consistently minimal near the tube and fins walls, with a maximum velocity occurring close to the centre between two fins but slightly closer to the left fins wall. When helix angle increased the velocity accrued to be reduced at the centre between two helical fins and concentrate close to the inner tube wall, but in general all cases have a quiet similar value (see figure 4.17 and table 4.4).

	Z = 34.37488 mm	Z = 137.6619 mm	
--	------------------------	------------------------	--



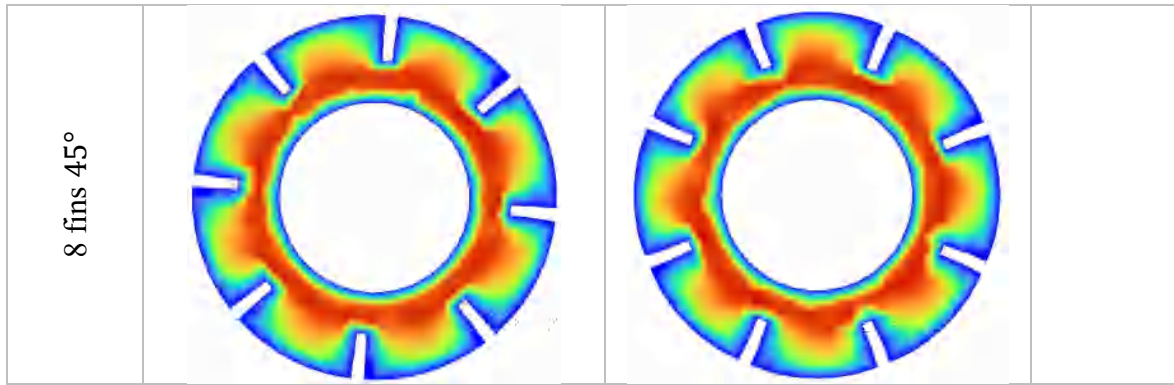


Figure 4.16: velocity contours of all cases in test 03

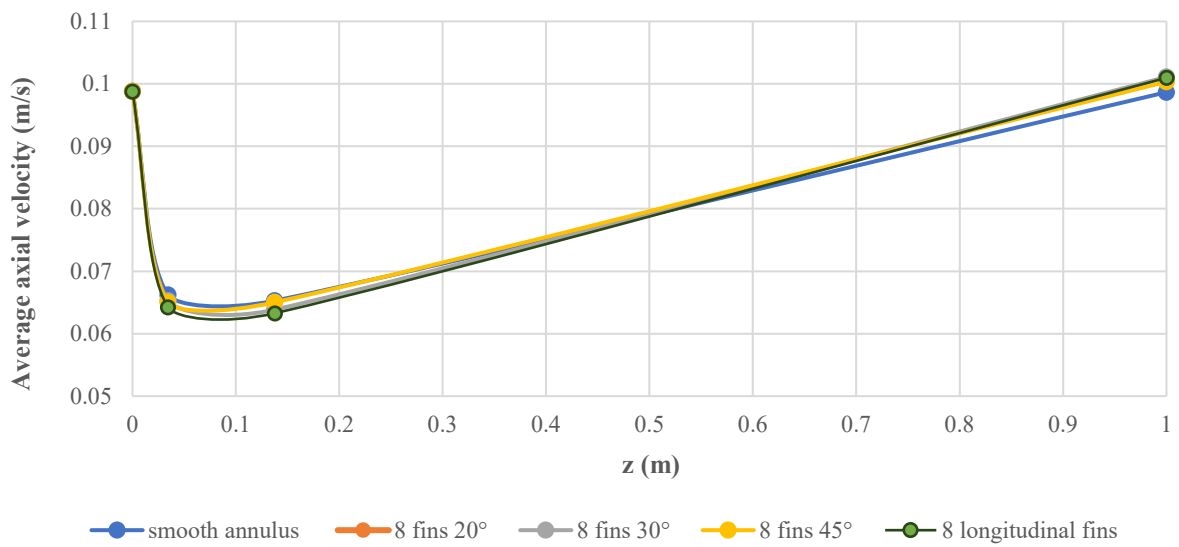


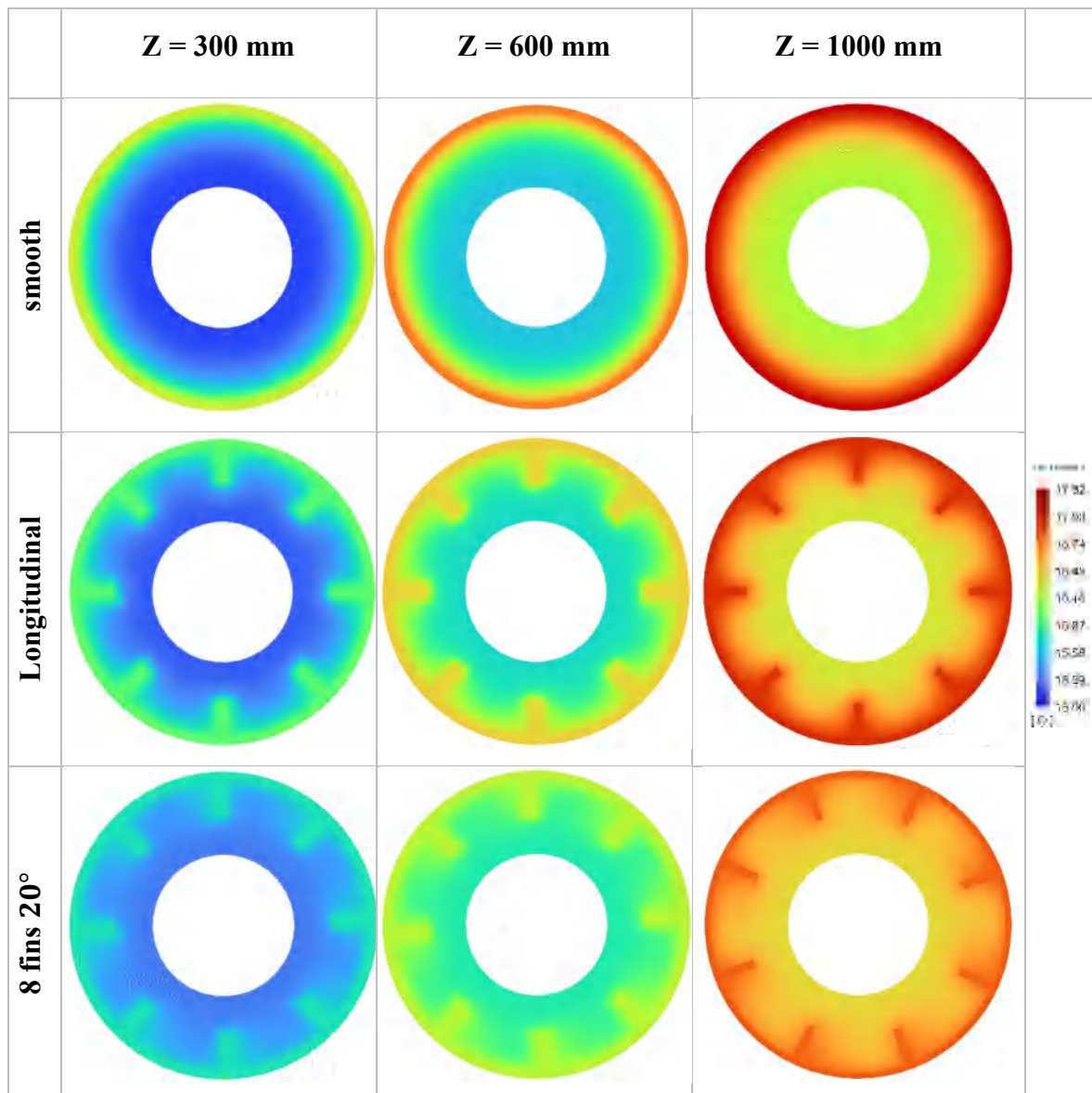
Figure 4.17: average velocity along the axial direction

Table 4.4: Average axial velocity of the cases studied in test 03

Z (m)	Average axial velocity (m/s)				
	smooth annulus	8 longitudinal fins	8 helical fins 20°	8 helical fins 30°	8 helical fins 45°
0	0.0988	0.0988	0.0988	0.0988	0.0988
0.03437488	0.06620	0.06424	0.06527	0.06540	0.06502
0.1376619	0.06528	0.06327	0.06386	0.06519	0.06502
1	0.09866	0.10096	0.10111	0.09914	0.10034

4.3.2. Thermal

As previously elucidated, a heat flux of 1000 W/m^2 was uniformly applied to the external surface of the outer tube, resulting in volumetric heat generation within the system. This heat flux initiates a complex heat transfer process, primarily characterized by radial flow at the solid-fluid interface, facilitating the transfer of a significant portion of thermal energy to the fluid. However, it is imperative to note that a fraction of this heat is dissipated to the surrounding air as heat losses. This phenomenon underscores the intricate interplay between heat generation, transfer mechanisms, and heat dissipation within the system, highlighting the multifaceted nature of thermal dynamics in the studied configuration (figure 4.18).



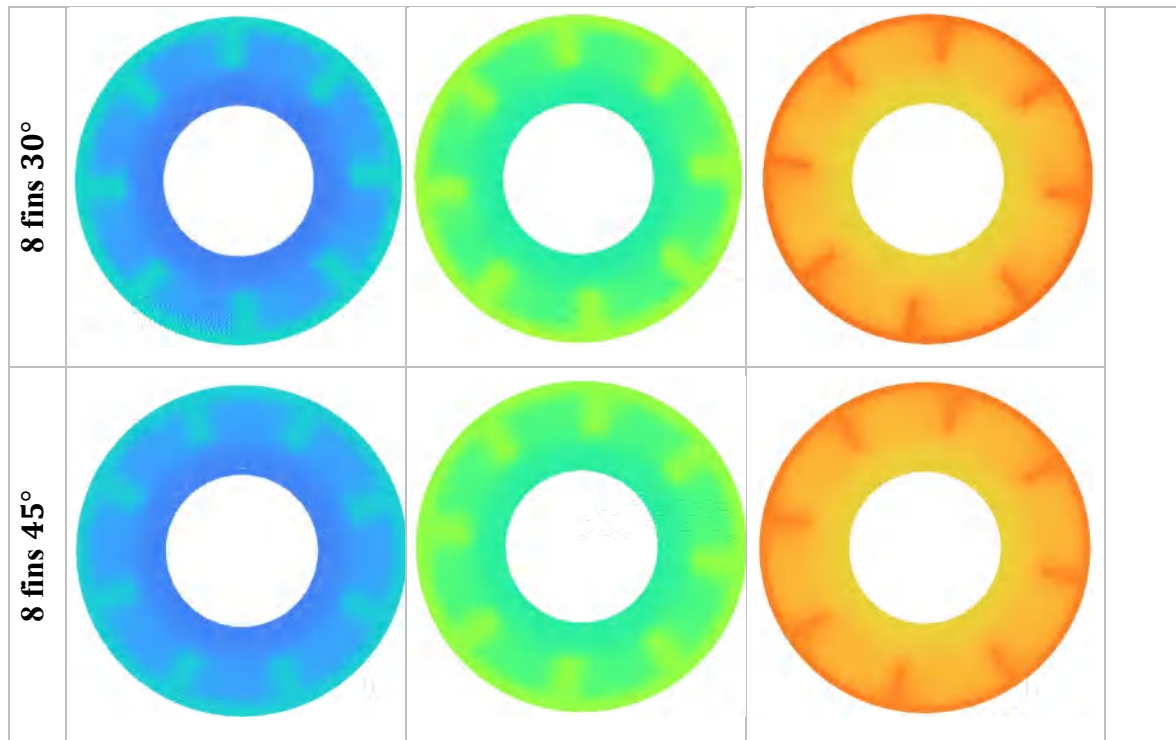


Figure 4.18: temperature contours for all cases in test 03

As the fluid enters the system, its temperature remains uniform, but as it progresses through the tube and fins, heat dissipation occurs, generating a temperature difference between the inner and outer tubes. This results in a symmetrical temperature distribution along the axial direction, with the highest temperature observed at the midpoint between the tubes. Concentric circles of temperature form near the center of each tube section, with the lowest temperature at the inner tube's surface. Moving away from the inner tube, the temperature pattern changes due to heat release from the fins, reaching its peak at the outer tube's surface. Additionally, the temperature at the fins' surface is lower than at the cylindrical interface due to heat dissipation on both sides. Analysing the flow dynamics using Newton's law of cooling, it's expected that increasing the helix angle of helical fins will enhance heat transfer by increasing surface area and heat transfer coefficient. However, higher velocities may lead to increased pressure loss in the annulus region.

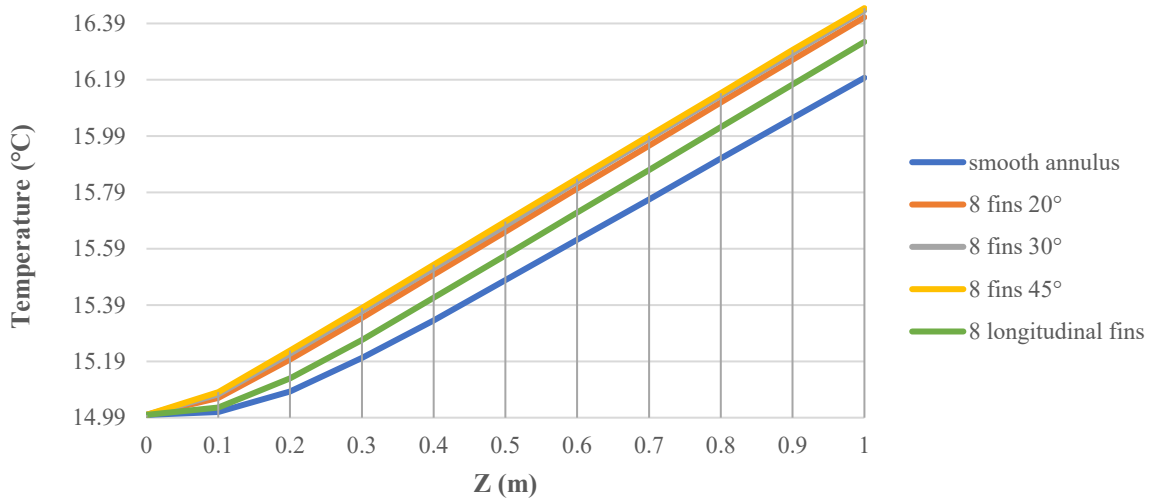


Figure 4.19: minimum fluid temperature along the axial direction of all cases in test 03

Figure 4.19 provides a comprehensive depiction of the minimum fluid temperature variation along the length of the tube. The graphical representation reveals notable trends, showcasing an increase in the minimum fluid temperature with rising helix angle. Specifically, for the configuration featuring eight helical fins with a helix angle of 45° , the minimum fluid outlet temperature peaks at 16.44°C . This observation contrasts with the reference case, where the minimum fluid temperature reaches only 16.19°C . The graph serves as a valuable tool for discerning the impact of different helix angles on fluid temperature dynamics within the annular conduit, highlighting the efficacy of varying helix angles in influencing heat transfer behavior.

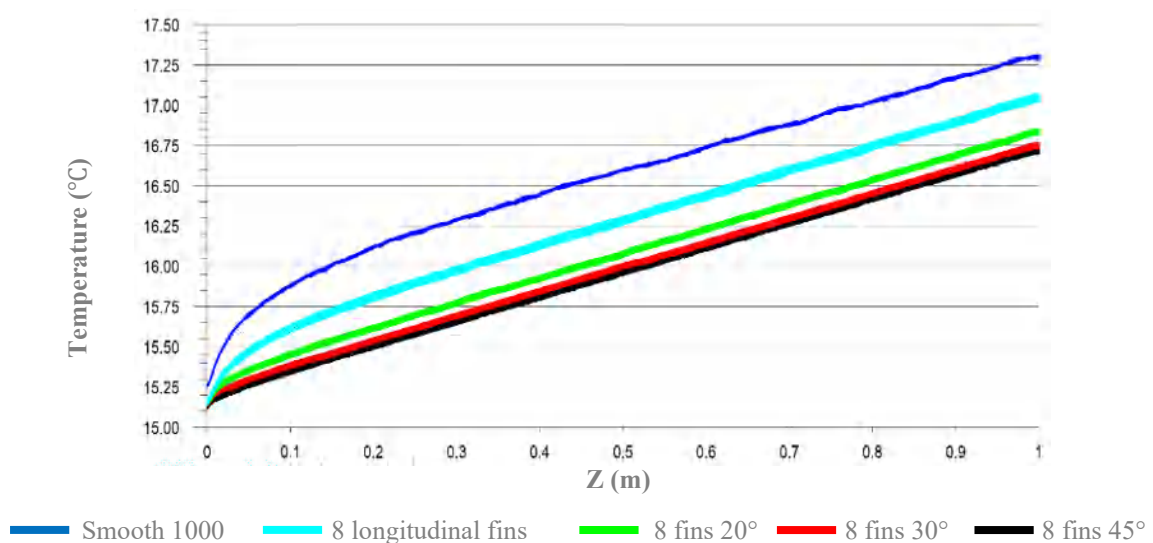


Figure 4.20: average interface fluid-outer tube temperature along the axial direction for test 03

Figure 4.20 provides insightful observations regarding the average internal wall temperature of the outer tube across different configurations. Notably, the smooth tube configuration attains its peak temperature, primarily attributed to its minimal surface area available for heat exchange compared to other cases. Conversely, the case featuring eight helical fins at a 45° helix angle exhibits the lowest temperature among the studied cases. This outcome is attributed to the larger surface area available for heat exchange, facilitating heightened temperature dissipation to the fluid. These findings underscore the pivotal role of surface area in influencing heat transfer dynamics within the annular conduit, emphasizing the significance of varying configurations in optimizing temperature control and fluid performance.

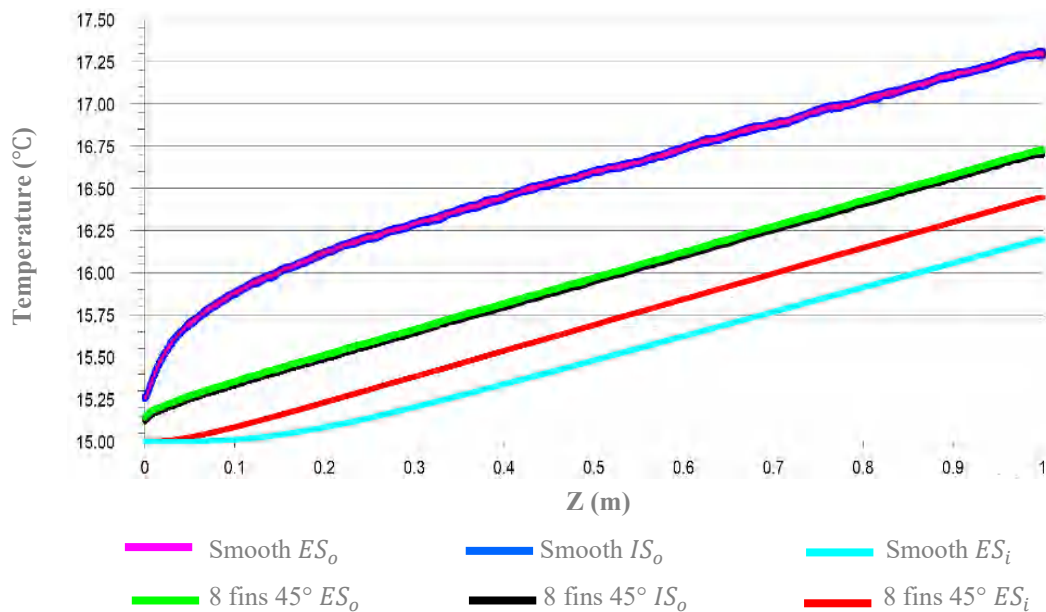


Figure 4.21: average tubes walls temperature for test 03

Figure 4.21 illustrates the key points previously discussed. The comparison between the smooth annulus configuration and the third case is particularly noteworthy. While the smooth configuration yields higher temperatures for the outer tube walls, it results in lower temperatures for the external wall of the inner tube. This discrepancy can be attributed to the efficient distribution of internal wall temperature in the helical finned tubes. These fins facilitate enhanced heat dissipation to the fluid, consequently elevating the temperature of the external wall of the inner tube. As depicted in the figure 4.21, this effect causes the temperature to surpass that of the smooth configuration. This observation underscores the

significance of considering heat distribution dynamics in optimizing thermal performance within the annular conduit.

4.3.3. Pressure drop

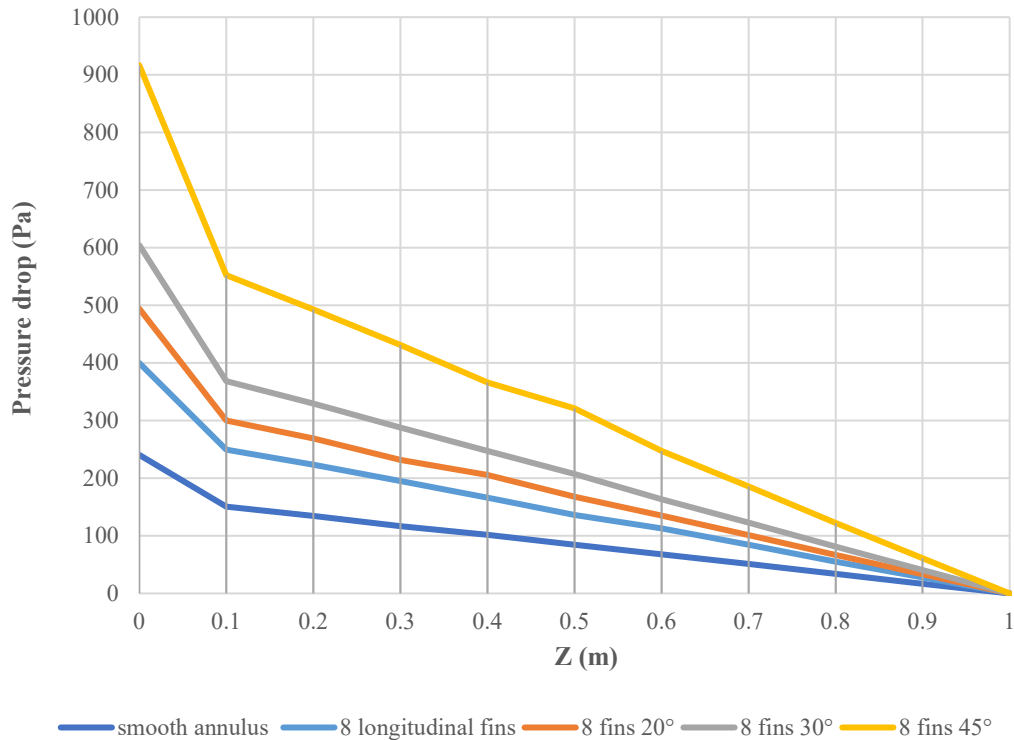


Figure 4.22: pressure drop variation along the axial direction for test 03

The relationship between pressure drop and the fins helix angle gives us important information about how heat transfer systems behave. Using helical fins makes the pressure drop increase noticeably compared to smooth tubes. with an average increase of 1.6, 2.0, 2.5, and 3.8 times for cases 1, 2, 3, and 4 respectively, compared to a smooth tube configuration. There are a few reasons for this. First, the shape of helical fins creates obstacles in the flow path, making it harder for the fluid to flow. Second, the sudden change in how the fluid moves, especially near the beginning, makes the pressure go up even more. Third, because there's more surface area for the fluid to flow along, the pressure increases even more, especially with higher helix angle. Figure 4.22 shows how pressure drop changes along the length of the flow path within the fins. Even though a few things cause pressure to increase, the biggest reason is the higher surface area created by fins.

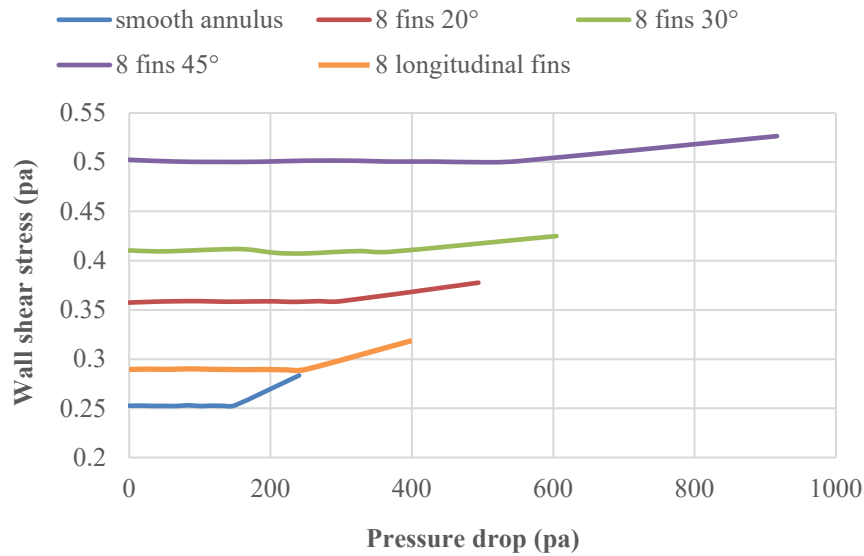


Figure 4.23: wall shear stress versus pressure drop for all cases in test 03

As Figure 4.23 shows, a proportional relationship between wall shear stress and pressure drop is clearly seen. As the wall shear stress increases, there is a corresponding increase in pressure drop. This shows that both pressure drop and wall shear stress increase with the augmentation of helical fins helix angle. Furthermore, it is noteworthy that longitudinal fins do not exhibit a comparable increase in wall shear stress and pressure drop as observed with two helical fins. The results suggest that the effect of longitudinal fins on wall shear stress and pressure drop aligns more closely with that of two helical fins rather than eight helical fins. This underscores that the primary factor contributing to the increase of pressure drop and wall shear stress is the augmentation of fins' helix angle.

4.3.4. Heat transfer

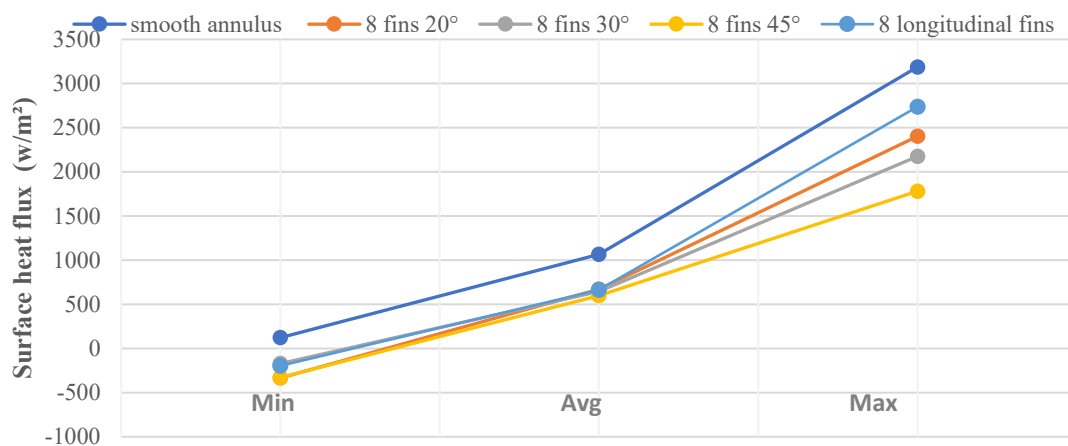


Figure 4.24: surface heat flux values of all cases in test 03

Based on the data presented in Figure 4.24, it is apparent that the average heat flux experienced by the internal surface of the outer tube exhibits variations depending on the tube configuration. Specifically, the smooth tube configuration yields the highest heat flux, whereas the introduction of 2 fins with a helix angle of 20° results in a reduction in heat flux. Furthermore, as the number of fins increases, particularly with 8 longitudinal fins, there is a further decrease in heat flux. Interestingly, the configuration with 8 helical fins at a helix angle of 45° demonstrates the lowest heat flux. These observations persist even when considering a constant temperature difference between the outer tube walls, as represented in Figure 4.21, and assuming a uniform thermal conductivity, such as that of aluminum ($202.4 \text{ W/m}\cdot\text{K}$). By applying Fourier's law of conduction, which states that heat transfer Q is proportional to the negative thermal conductivity $-k$ multiplied by the temperature difference $(T_{ES} - T_{IS})$ and divided by the distance difference $(x_{EX} - x_{IS})$, it is evident that variations in the distance (Δx) directly impact the surface heat flux. Thus, an increase in distance results in a corresponding decrease in surface heat flux, consistent with the observed trends in our cases data.

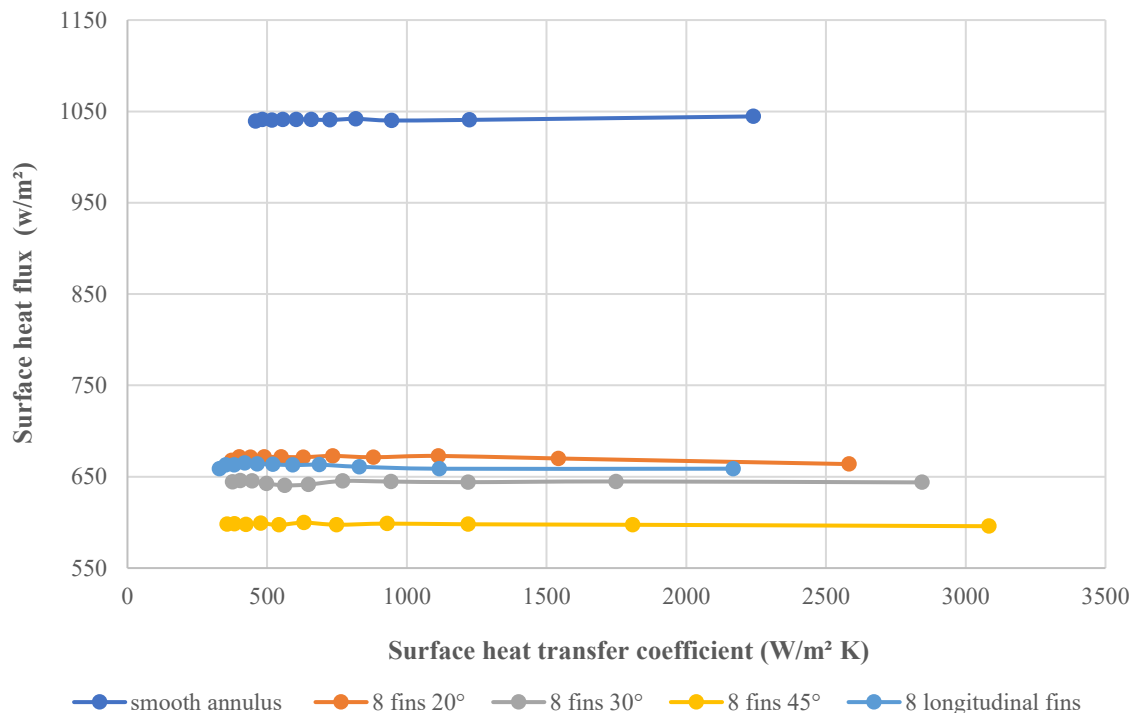


Figure 4.25: heat flux versus heat transfer coefficient for all cases of test 03

In heat transfer processes, the heat transfer coefficient represents the effectiveness of heat transfer between a solid surface and a fluid, indicating the rate at which heat energy is

transferred per unit area and per unit temperature difference. On the other hand, the heat flux refers to the amount of heat energy transferred through a given surface area per unit time. The relationship between the heat transfer coefficient and heat flux is intrinsic to understanding heat transfer mechanisms, where an increase in the heat transfer coefficient with decrease heat flux for a given temperature difference, this relationship signifies enhanced thermal performance, indicating that larger quantities of heat are effectively delivered to the fluid. Furthermore, upon analysis of Figure 4.25, it becomes apparent that the highest heat transfer coefficient was achieved at the lowest surface heat flux (the fourth case). This observation can be explained by the significant dispersion of temperature from the solid to the fluid, facilitated by the increased exchange surface area resulting from an elevated helix angle of the fins. Consequently, the augmentation in the surface heat transfer coefficient is directly attributable to this enhancement in surface area for heat transfer.

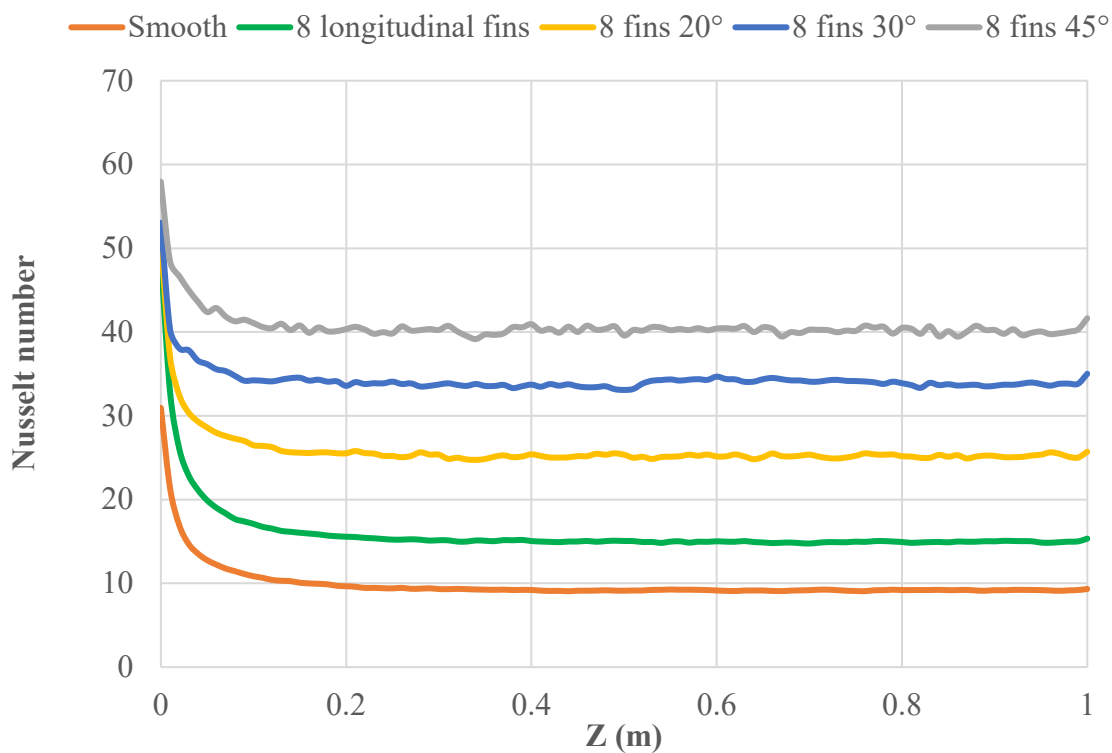


Figure 4.26: plot of Nusselt number along the axial direction for all cases of test 03

The Nusselt number in an annulus provides crucial insights into heat transfer characteristics. It signifies the ratio of convective to conductive heat transfer across the fluid boundary, aiding in assessing the efficiency of heat transfer processes. A higher Nusselt number indicates more efficient heat transfer, while a lower value suggests less effective heat transfer.

Figure 4.26 illustrates the variation of the Nusselt number along the annulus. It is notable that the highest Nusselt number was observed at the inlet for the case of 8 helical fins 45° , amounting to 0.165. This increase is attributed to the elevated heat transfer coefficient observed in the fourth case. Conversely, the axial Nusselt numbers for the other cases were 0.139, 0.145, 0.151 and 0.088 for the first, second, third and reference cases, respectively. Figure 4.26 further demonstrates the dynamics of the axial Nusselt number, showcasing its peak value at the inlet, followed by a rapid decline in the entrance region and subsequent stabilization to the outlet.

4.3.5. Conclusion

This test investigated the impact of varying the helix angle of eight helical fins within an annulus on fluid dynamics and heat transfer. Increasing the helix angle led to enhanced heat transfer, evidenced by a higher minimum fluid temperature and lower average internal wall temperature of the outer tube. This improvement is attributed to the increased exchange surface area associated with higher helix angles. Notably, the 45° helix angle configuration exhibited the highest heat transfer coefficient and Nusselt number, indicating superior heat transfer efficiency. However, this enhancement came at the cost of increased pressure drop, which was most evident in the 45° case. This test highlights the trade-off between heat transfer efficiency and energy consumption when utilizing helical fins in an annulus.

4.4. FOURTH TEST: heat flux

In this section of our investigation, we delve into the intricate relationship between heat flux variations applied to the external surface of the outer tube and the ensuing hydrothermal behavior of the fluid flowing within the tubes. Understanding the impact of heat flux on heat transfer processes is paramount in optimizing thermal performance and efficiency. Furthermore, Heat flux, represented by the amount of heat energy transferred per unit area per unit time, plays a pivotal role in dictating the rate and effectiveness of heat transfer. By varying the magnitude of heat flux applied to the external surface of the outer tube, we can discern its direct influence on the convective heat transfer process within the annulus. For our experimental setup, we selected three distinct values of heat flux: 500, 1000, and 3000 W/m². These values encompass a range of heat flux intensities commonly encountered in practical engineering applications. The reference case, characterized by a smooth tube, maintains a heat flux of 1000 W/m². This serves as a benchmark against which the effects of higher and lower heat flux values can be compared.

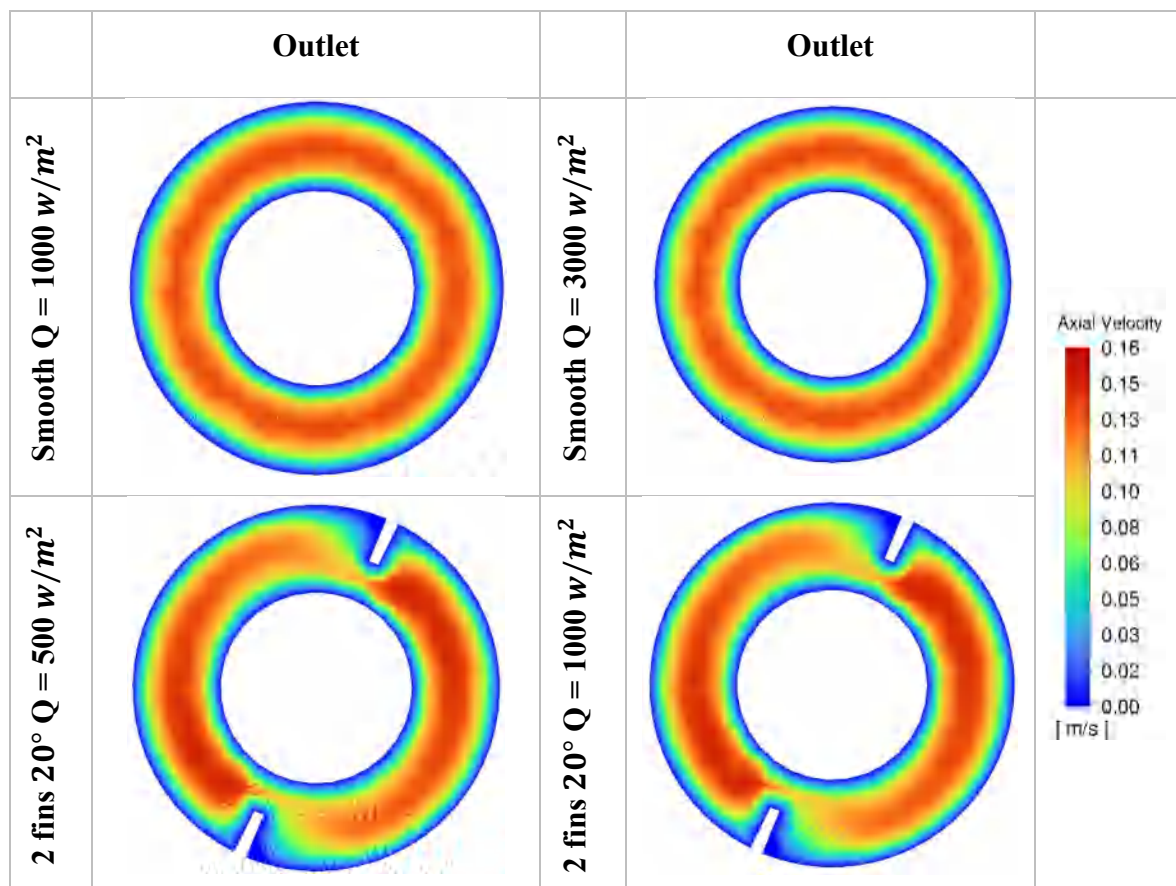
In the first case, we investigate the impact of a higher heat flux of 3000 W/m² applied to a smooth tube configuration. This elevated heat flux presents an opportunity to assess the thermal response and heat transfer characteristics under more intense heat transfer conditions. Moving on to the second case, we introduce a configuration featuring two helical fins with a helix angle of 20 degrees. This case adopts a lower heat flux of 500 W/m², allowing us to explore the interplay between heat flux intensity and the presence of helical fins on heat transfer efficiency. The third case, although previously studied, is revisited here to facilitate comparison with other configurations. This case involves two helical fins with a helix angle of 20 degrees and a heat flux of 1000 W/m². By maintaining the same heat flux value as the reference case but introducing helical fins, we can investigate the effects of fin geometry on heat transfer performance. Lastly, in the fourth case, we examine the combined influence of helical fins and a higher heat flux of 3000 W/m². This configuration enables us to investigate the synergistic effects of increased heat flux intensity and fin geometry on heat transfer efficiency within the annulus.

All cases maintain uniform fluid inlet velocity and temperature conditions, set at 0.0988 m/s and 15°C, respectively. By systematically varying heat flux values and configurations, we aim to gain comprehensive insights into the complex interplay between

heat flux intensity, fin geometry, and fluid dynamics on heat transfer performance within the annulus.

4.4.1. Hydrodynamic

Understanding the distribution and behavior of parameters such as velocity is crucial in heat transfer research. Visualizing contours, as depicted in Figure 4.27 and 4.28, allows for a comprehensive assessment of fluid dynamics within the system. Despite the lack of discernible differences in axial velocity across the studied cases, further investigation into other parameters, such as temperature and heat flux contours, may provide additional insights into the effects of varying heat flux on heat transfer processes. Moreover, from Figure 4.27 and 4.28 and Table 4.5, it is evident that there is no remarkable difference in the axial velocity among the cases examined in this chapter. Varying the heat flux does not exert a significant effect on the fluid velocity.



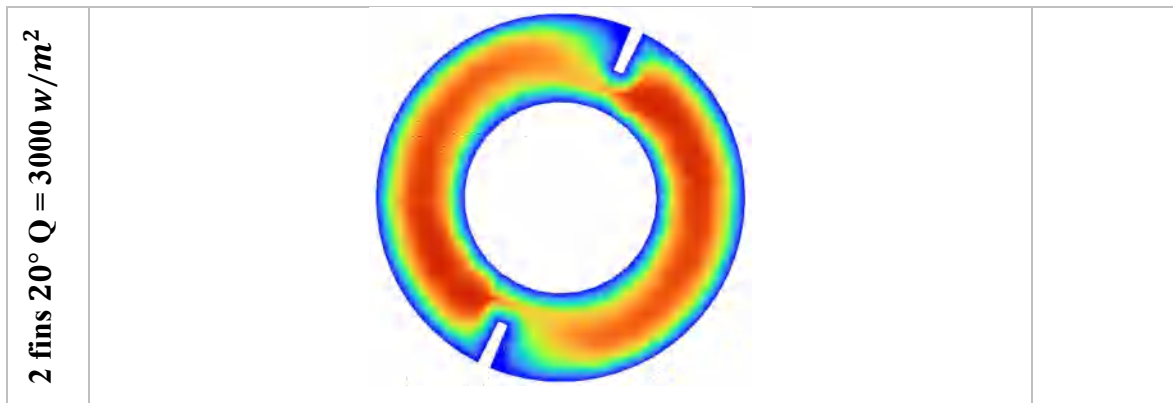


Figure 4.27: velocity contours for all cases in test 04

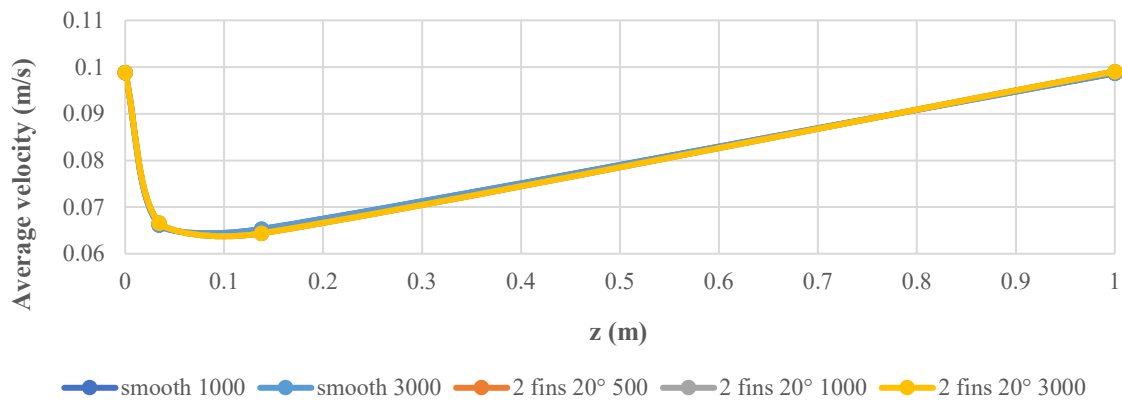


Figure 4.28: average velocity along the axial direction, test 04

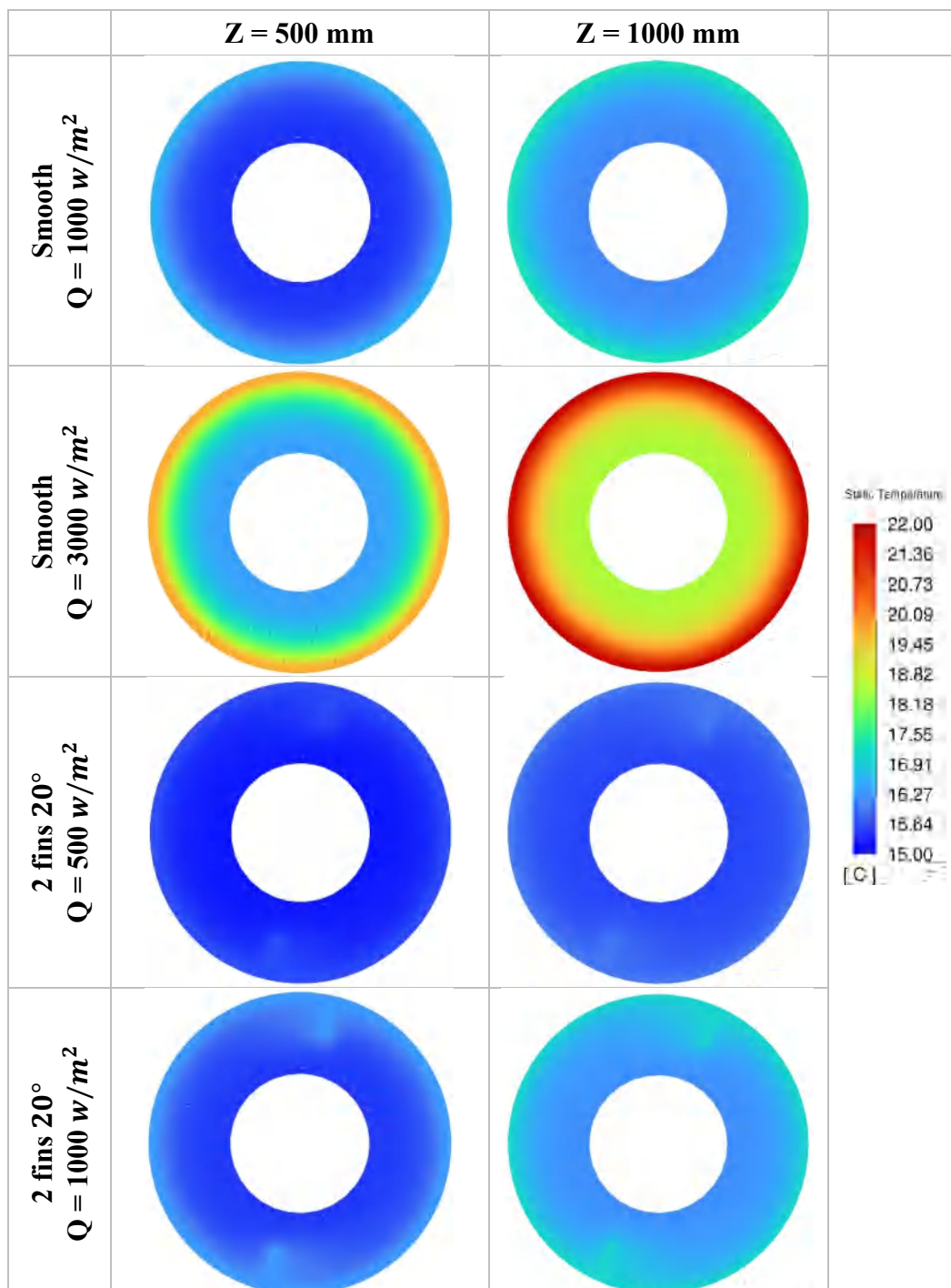
Table 4.5: Average axial velocity of the cases studied in test 04

Z (m)	Average axial velocity (m/s)				
	smooth 1000	smooth 3000	2 fins 20° 500	2 fins 20° 1000	2 fins 20° 3000
0	0.0988	0.0988	0.0988	0.0988	0.0988
0.03437488	0.06620	0.06620	0.06662	0.06662	0.06662
0.1376619	0.06528	0.06528	0.06437	0.06438	0.06437
1	0.09866	0.09866	0.09904	0.09904	0.09904

4.4.2. Thermal

The heat flux applied to the external surface of the outer annulus plays a pivotal role in shaping the thermal behavior of the fluid within the annulus. When the heat flux is increased or decreased, it directly impacts the temperature distribution and heat transfer processes within the annular space. Understanding these effects is crucial for optimizing thermal performance and efficiency in various engineering applications, ranging from heat exchangers to thermal management systems.

As we can observe from the contours, it's evident that increasing the heat flux directly influences the thermal behavior of the fluid within the annulus. The temperature contours depicted in Figure 4.29 clearly illustrate this phenomenon. Upon closer examination of the temperature contours, it becomes apparent that higher heat flux values result in elevated fluid temperatures within the annulus. This observation aligns with fundamental principles of heat transfer, where increased heat flux leads to greater heat input into the system, subsequently raising the fluid temperature. Conversely, lower heat flux values correspond to relatively lower fluid temperatures within the annulus.



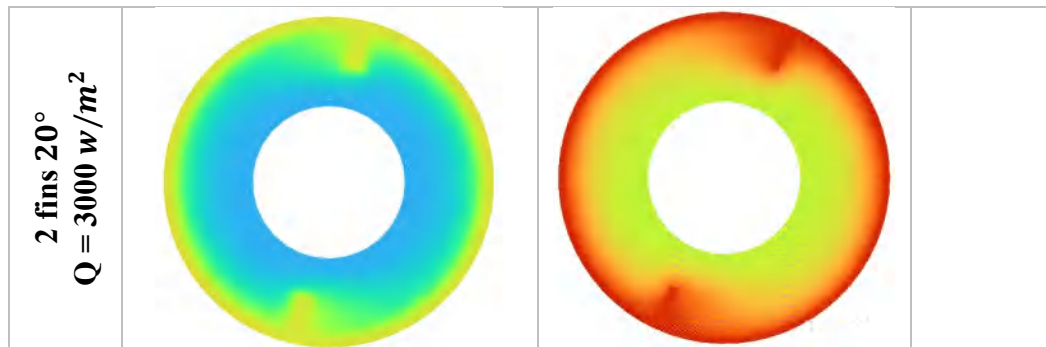


Figure 4.29: temperature contours for all cases in test 04

Understanding the impact of heat flux variations on thermal behavior is essential for optimizing heat transfer processes. The temperature contours provide valuable insights into how changes in heat flux affect the distribution of temperature within the annular space. By analyzing these contours, researchers can discern patterns and trends that elucidate the intricate dynamics of heat transfer processes. Moreover, the thermal behavior of the fluid within the annulus directly affects the overall performance and efficiency of heat transfer systems. Therefore, investigating the effects of increasing or decreasing heat flux is crucial for designing and operating thermal systems with optimal efficiency and performance. Further exploration of these effects can lead to advancements in engineering practices and the development of more efficient heat transfer technologies.

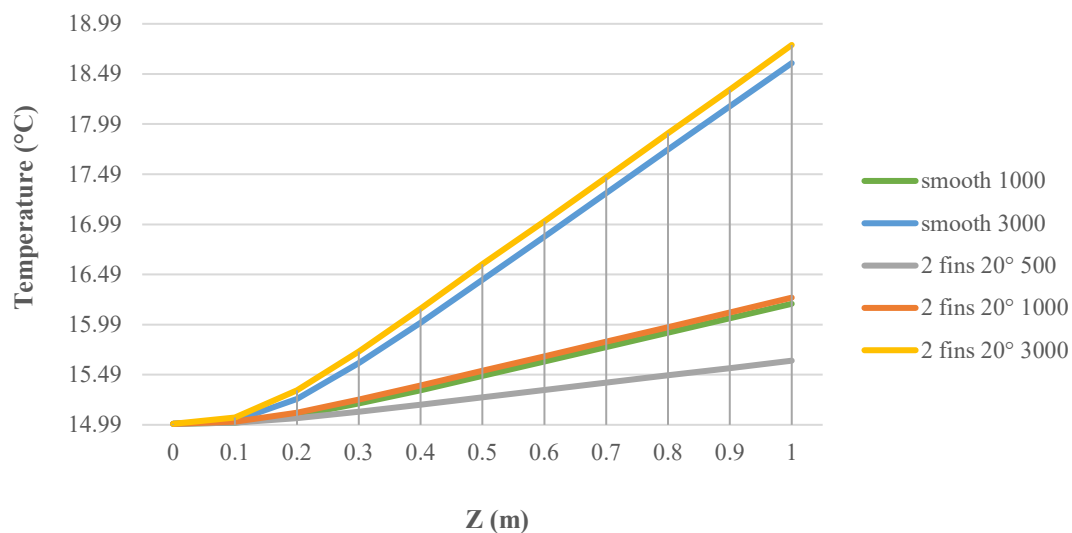


Figure 4.30: Minimum fluid temperature along the axial direction for all cases in test 04

Analyzing minimum fluid temperatures is essential in evaluating the thermal performance of a system. The minimum fluid temperature indicates the lowest temperature reached by the fluid within the system, providing insights into heat transfer efficiency and overall system effectiveness. By comparing minimum fluid temperatures across different

cases, we can assess the relative performance of each configuration and identify opportunities for improvement.

In the analysis of minimum fluid temperatures showed in figure 4.30, noteworthy differences among the cases studied were observed. The second case exhibited the lowest minimum fluid temperature, indicating relatively poorer performance compared to other configurations. Conversely, the fourth case demonstrated the best performance, as evidenced by its minimum outlet temperature of 18.78°C. In contrast, the first case recorded a minimum outlet temperature of just 16.19°C.

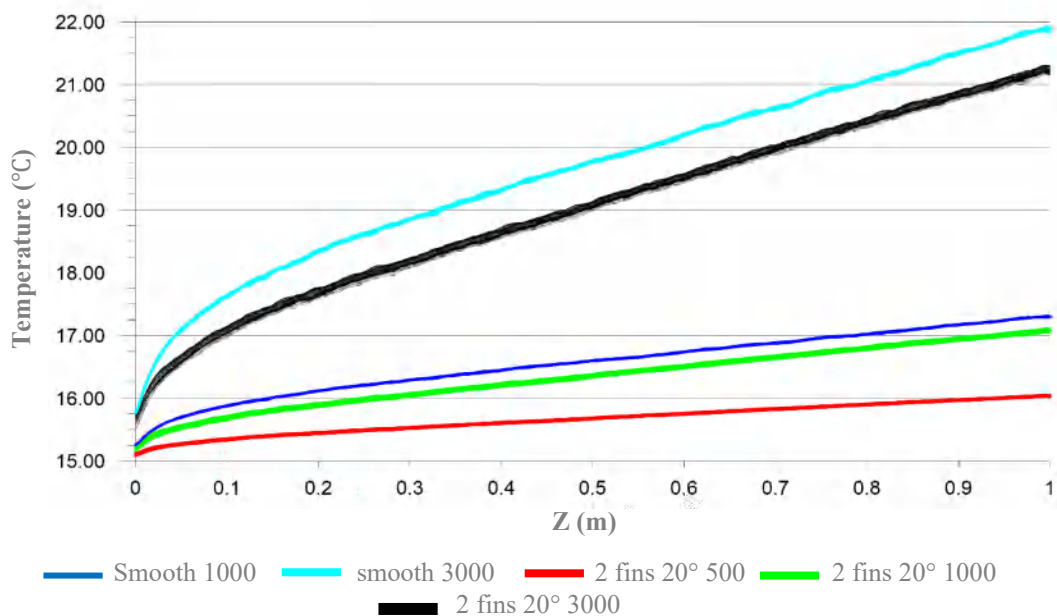


Figure 4.31: average interface fluid-outer tube temperature along the axial direction for test 04

As depicted in Fig. 4.31, a key observation emerges from the comparison of temperature differentials among various configurations. The smooth annulus configuration with a heat flux of 3000 W/m² exhibits higher temperatures for the outer tube walls compared to the other cases. However, a notable finding is the larger temperature differential between the smooth 3000 and the 2 fins 20° 3000 configurations, compared to the differential between the smooth 1000 and 2 fins 20° 1000 configurations. Furthermore, examining temperature variations offers useful insights into how heat is transferred within various system designs. A greater temperature difference observed between the smooth annulus and the finned annulus configurations suggests disparities in heat transfer effectiveness or thermal properties between these arrangements. Conversely, a smaller temperature gap between the

smooth and finned annulus configurations indicates more similar thermal behaviors in those scenarios. To sum up, understanding these variations in temperature differentials enables us to pinpoint factors influencing thermal performance and optimize system configurations for improved efficiency.

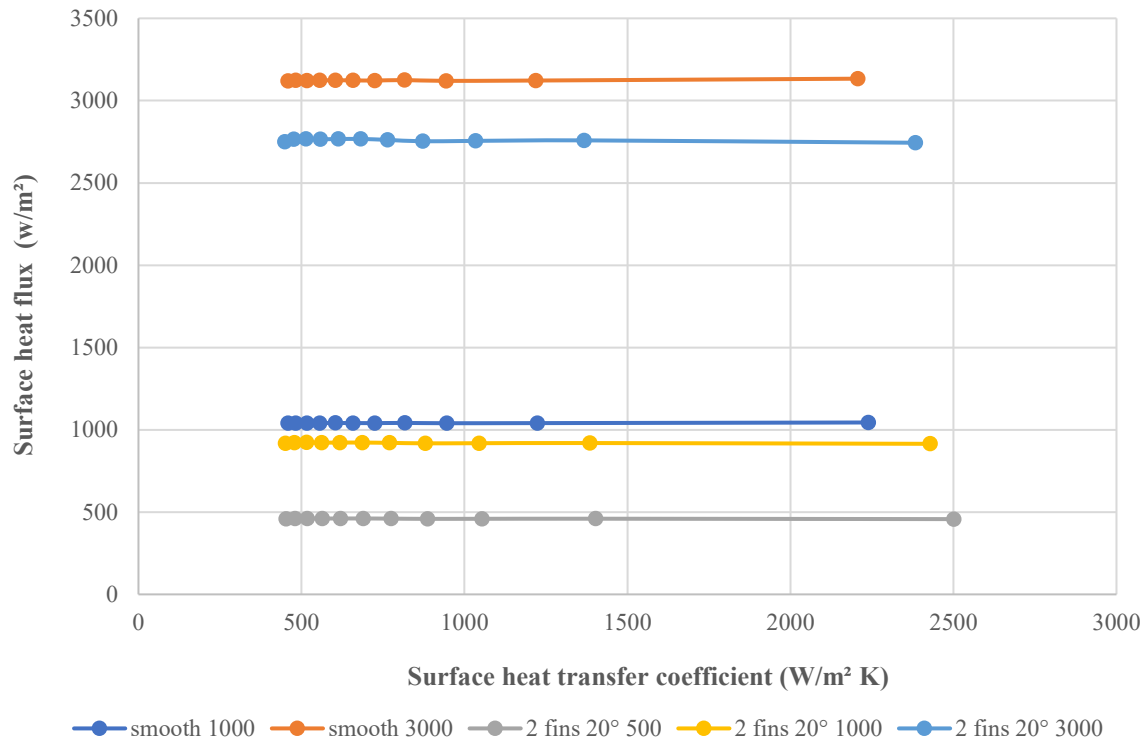


Figure 4.32: heat flux versus heat transfer coefficient for all cases of test 04

The surface heat transfer coefficient, represents the thermal conductivity between a solid surface and the surrounding fluid, typically in convection processes. As illustrated in Figure 4.32, an increase in heat flux leads to a decrease in the surface heat transfer coefficient. This phenomenon occurs due to the boundary layer forming around the solid surface, which thickens as heat flux increases, hindering heat transfer. Conversely, a decrease in heat flux tends to enhance the surface heat transfer coefficient by reducing the thickness of the boundary layer, thereby promoting convective heat transfer. In the case of a finned annulus, where higher heat flux is applied, the diffusion of a large amount of heat flux to the surrounding fluid is observed, indicating enhanced heat dissipation. The difference in average heat flux at the fluid-outer tube interface between different cases further highlights the effect of increasing heat flux on heat dissipation to the fluid. For instance, the comparison between the reference case and the third case reveals a difference of 121 W/m², while the difference between the second and fourth cases is recorded as 363

W/m^2 . This underscores that an increase in heat flux amplifies the heat dissipated to the fluid in finned annulus configurations, demonstrating the critical role of heat flux in determining the effectiveness of heat transfer in such systems.

In this case, it's clear that the pressure drop and wall shear stress remain constant without any noticeable changes. Consequently, we opted not to display graphs illustrating these parameters. It's apparent that an increase in heat flux does not have any discernible impact on either the pressure drop or the wall shear stress.

4.4.3. Nusselt number

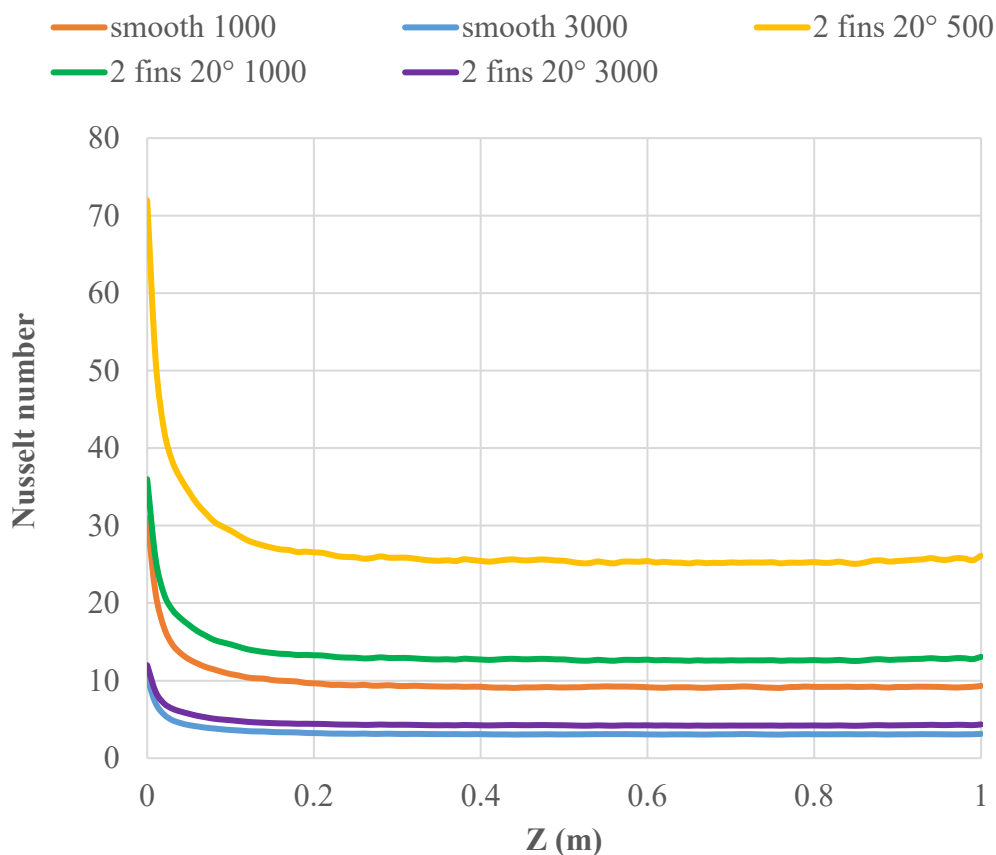


Figure 4.33: plot of Nusselt number along the axial direction for all cases of test 04

As we saw in figure 4.33 that increasing the heat flux applied on the external surface of outer tube will decrease the Nusselt number which leads to conduction dominating. In contrast with the first case when heat flux decreased which recorded the highest Nusselt number showing the domination of heat transfer by convection, table 4.6 resumes the inlet and outlet values of Nusselt number for each case.

Table 4.6: inlet and outlet values of Nusselt number for all case for the test 04

	Heat flux (W/m ²)	Nusselt number	
		Inlet	Outlet
Smooth	1000	0.0882	0.0265
	3000	0.0294	0.0089
2 fins 20°	500	0.2051	0.0744
	1000	0.1025	0.0372
	3000	0.0341	0.0124

4.4.4. Conclusion

This test investigated the impact of varying heat flux on the hydro-thermal behavior of fluid flowing within an annulus. While fluid velocity remained largely unaffected by changes in heat flux, higher heat flux values led to increased fluid temperatures, as expected. Notably, the configuration with two helical fins and a heat flux of 3000 W/m² exhibited the highest minimum fluid temperature, indicating superior heat transfer performance. However, an inverse relationship was observed between heat flux and the surface heat transfer coefficient, meaning higher heat flux resulted in a lower heat transfer coefficient due to boundary layer thickening.

4.5. FIFTH TEST: fluid velocity

This section of our thesis focuses on dynamic analysis, particularly emphasizing the significance of increasing velocity and its influence on the thermo-hydraulic behavior of water circulating within the finned annulus. Understanding the variations in fluid inlet velocity is crucial for grasping the fluid's hydro-thermal dynamics. Notably, fluid velocity plays a pivotal role in determining the time required to fill a tank within solar thermal collectors. Table 4.7 provides a detailed overview of the filling time for a tank with a capacity of 1 cubic meter. Within this section, we investigate three distinct cases, each compared to a reference case. All scenarios involve the presence of 8 helical fins with a helix angle of 45 degrees. The first case examines an inlet velocity of 0.006 m/s, followed by a revisit to a previously studied velocity of 0.0988 m/s in the second case, and finally, an exploration of a velocity of 0.3 m/s in the third case.

Table 4.7: cases parameters for the test 05

	Fluid velocity (m/s)	Volume of water flowing (m³/s)	Cross section area (mm²)	Time to fill a tank of 1 m³ by 10 tubes
Smooth	0.0988	5.21 E-06	52.74	5h 19m 51s
8 fins 45°	0.006	2.99 E-06	49.87	9h 17m 0s
	0.0988	4.92 E-06	49.87	5h 38m 15s
	0.3	1.49 E-05	49.87	1h 51m 24s

From Table 4.7, it is evident that decreasing the fluid velocity results in an extended filling time for the tank. The disparity between the first and third cases exceeds 7 hours. Although reducing the velocity may elevate the fluid temperature, the prolonged duration negatively impacts the efficiency of our system.

4.5.1. Hydrodynamic

The velocity contours depicted in Figure 4.34 and figure 4.35 indicate that increasing the velocity does not significantly alter the contours profile, aside from the velocity values. The minimum velocity is consistently observed at the walls of the tubes and fins, while the maximum velocity occurs at the midpoint between the two tubes and two fins.

	Z = 34.37488 mm	Z = 137.6619 mm	
--	------------------------	------------------------	--

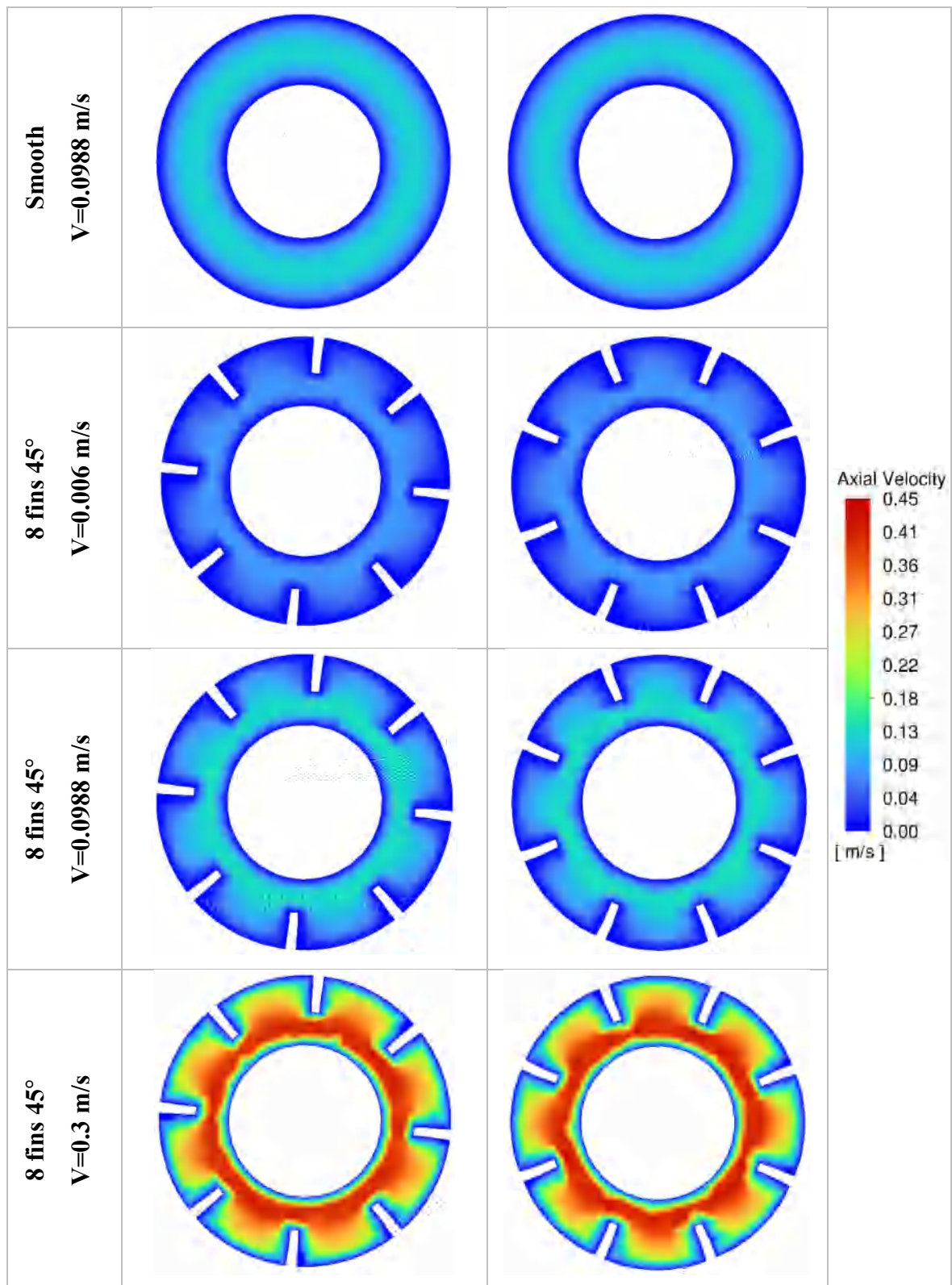


Figure 4.34: velocity contours for all cases of test 05

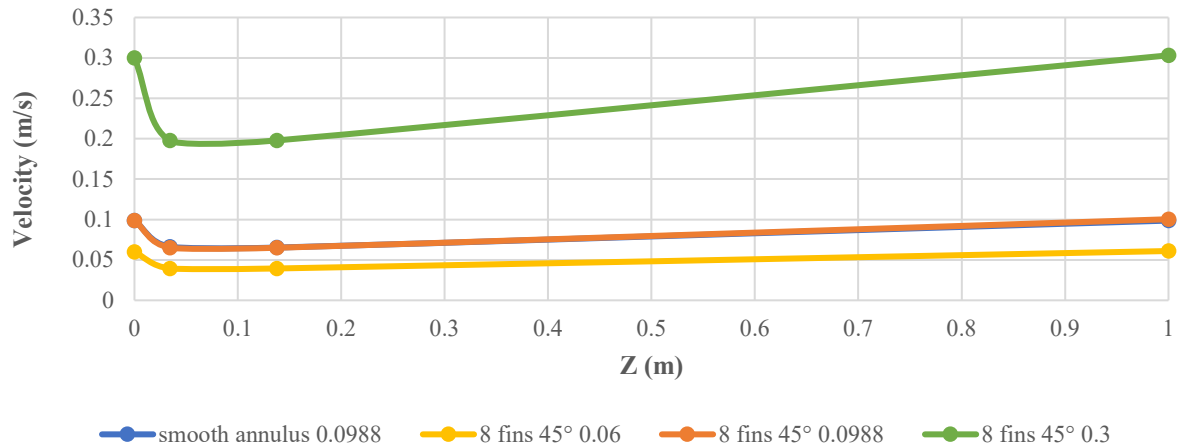


Figure 4.35: average velocity along the axial direction, test 05

Table 4.8: Average axial velocity of the cases studied in test 05

Z (m)	Average axial velocity (m/s)			
	Smooth annulus $v = 0.0988 \text{ m/s}$	8 fins 45° $v = 0.06 \text{ m/s}$	8 fins 45° $v = 0.0988 \text{ m/s}$	8 fins 45° $v = 0.3 \text{ m/s}$
0	0.0988	0.06	0.0988	0.3
0.03437488	0.06620	0.03941	0.06502	0.19756
0.1376619	0.06528	0.03940	0.06502	0.19787
1	0.09866	0.06100	0.10034	0.30315

In laminar flow, altering the velocity does not produce a distinct change in the velocity profile. However, a transition to turbulent flow regime may induce a significant alteration in the profile.

4.5.2. Thermal

Understanding how fast the fluid moves in a finned annulus is really important for making heat transfer work well. When the fluid moves faster or slower, it changes how heat spreads out in the system. We can see this by looking at temperature maps, like the one in Figure 4.36. For example, when the fluid slows down to 0.006 meters per second, the temperature at the outlet goes up by 1.9 degrees Celsius compared to when it's moving faster at 0.3 meters per second. This shows us that when we slow down the fluid, it gets hotter. Knowing this helps us make systems with fins work better at transferring heat. So, studying

how changing fluid speed affects heat is really important for making these systems work well.

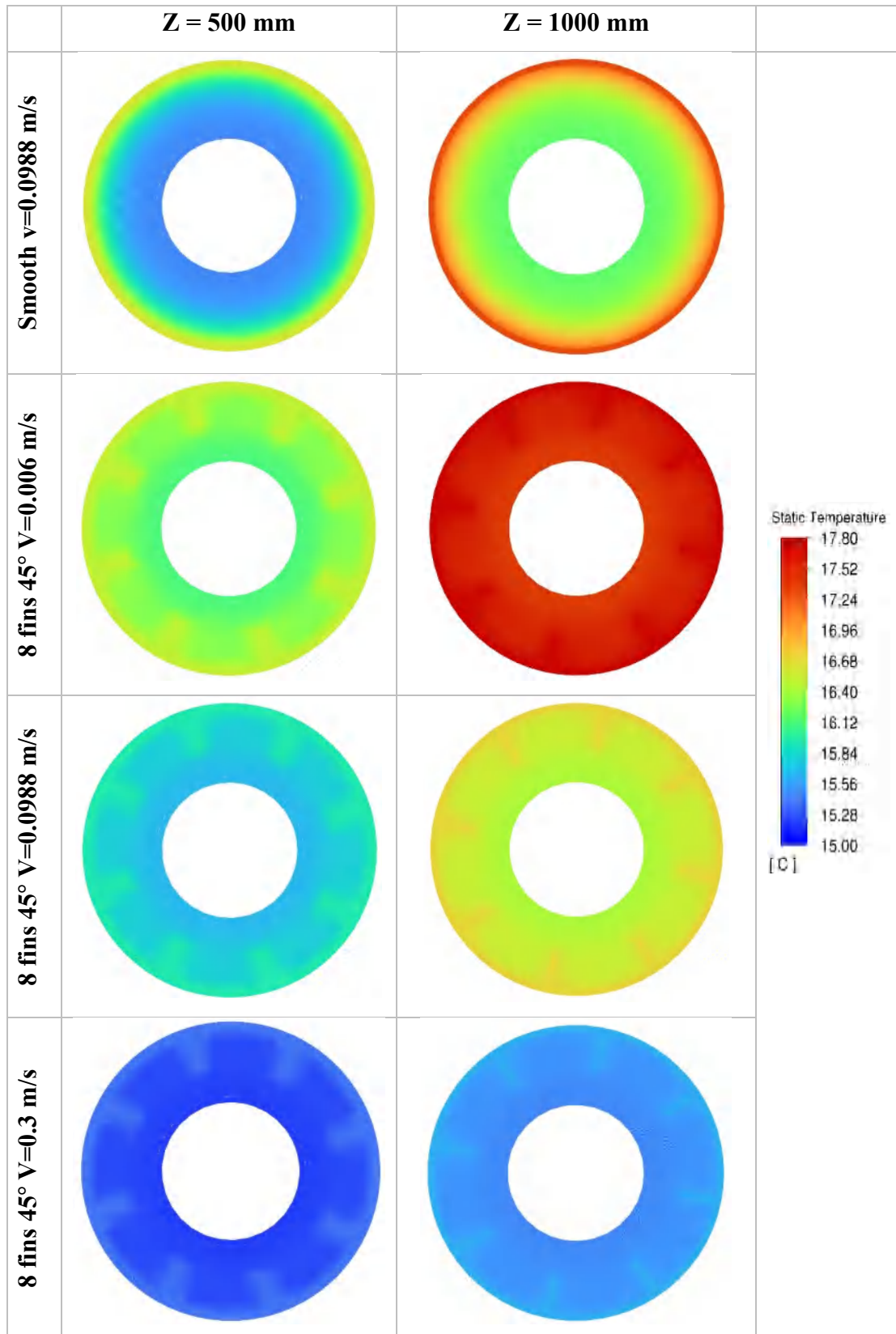


Figure 4.36: temperature contours for all cases in test 05

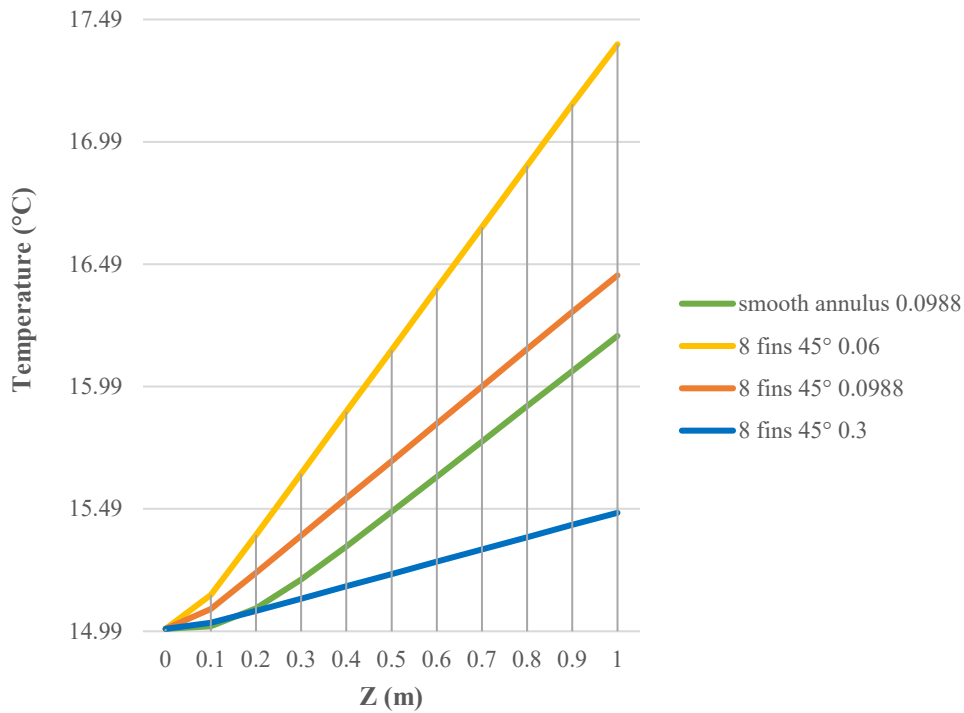


Figure 4.37: minimum fluid temperature along the axial direction for all cases in test 05

Figure 4.37 provides a visual representation of how the minimum fluid temperature changes over the axial direction. The minimum fluid temperature refers to the lowest temperature reached by the fluid within the system. Understanding this parameter is essential for assessing heat transfer efficiency and system performance. Upon examination of the graph, it becomes evident that decreasing the fluid velocity leads to an increase in the minimum fluid temperature along the axial direction. This observation indicates that lower fluid velocities result in higher fluid temperatures, which can have implications for heat transfer processes within the system. Furthermore, when comparing different velocity setups, it is observed that the third case with a velocity of 0.3 m/s yields minimum fluid temperatures that are lower than those observed in the cases of smooth and helical configurations with a velocity of 0.0988 m/s. Additionally, the minimum fluid temperatures in the third case are higher than those recorded in the case with a velocity of 0.06 m/s. Moreover, the increase in minimum fluid temperature at lower velocities is attributed to the extended duration the fluid spends in the system, allowing it to get more time to absorb heat from the heated outer tube. These findings highlight the complex interplay between fluid velocity and minimum fluid temperature, underscoring the importance of carefully optimizing velocity parameters to enhance system performance and efficiency.

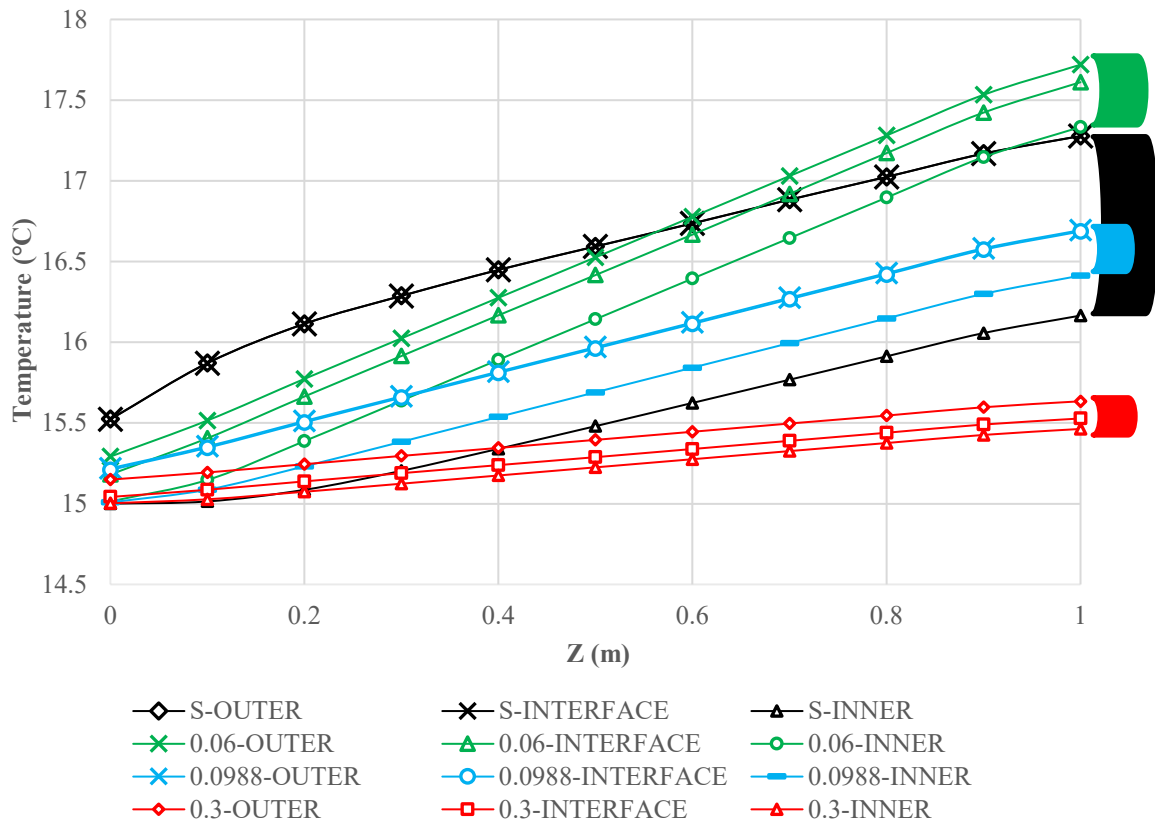


Figure 4.38: average tubes walls temperature for test 05

The diagram presented in Figure 4.37 depicts the changes in temperature along the axial direction of three walls: the outer tube external surface (OES), the outer tube internal surface (OIS) (fluid-outer tube interface), and the inner tube external surface (IES).

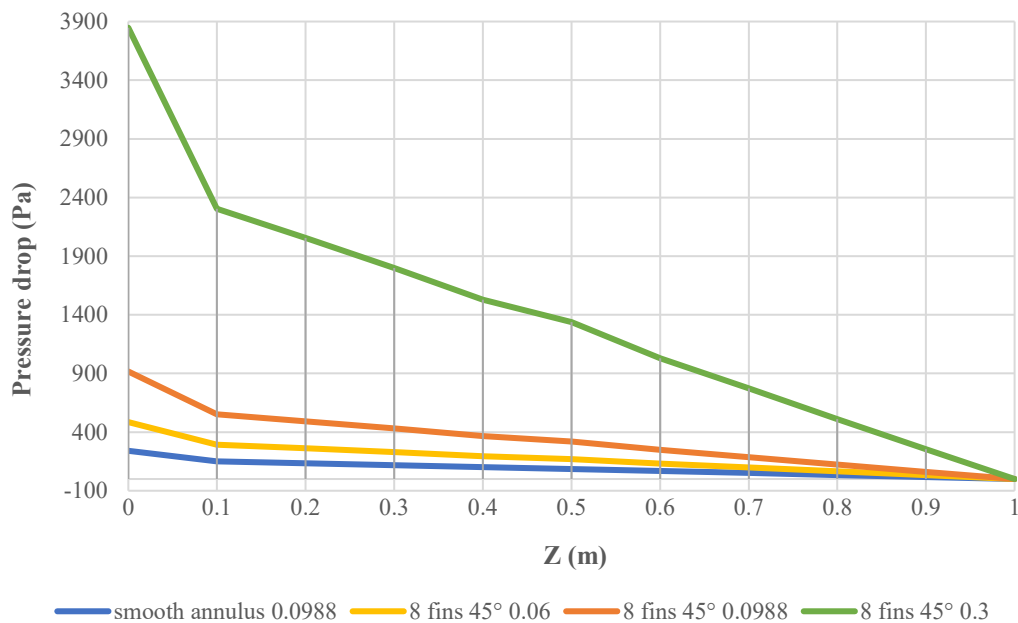
Examination of the figure 4.38 and Table 4.8 unveils a noteworthy trend: a decrease in fluid velocity correlates with an increase in the temperature differential (ΔT) between the (OES) and the (IES). Notably, the reference case exhibits a larger temperature differential between its outer and inner tubes, signifying a deficiency of extended surfaces in facilitating effective heat dissipation to the fluid. Conversely, the finned cases demonstrate superior heat dissipation to the fluid, resulting in smaller gaps between the temperatures of the outer tube and inner tube.

Table 4.9: different temperatures walls at the outlet in test 05

	Fluid velocity (m/s)	Average outlet temperature (°C)			ΔT Outer - fluid	ΔT Fluid - inner	ΔT Outer - inner
		External surface outer tube	Interface outer tube-fluid	External surface inner tube			
Smooth	0.0988	17.2782	17.2773	16.1655	0.0008	1.2203	1.2211
8 fins 45°	0.06	17.7195	17.6111	17.3334	0.1084	0.2777	0.3861
	0.0988	16.6950	16.6865	16.4130	0.0084	0.2819	0.2734
	0.3	15.6345	15.5280	15.4632	0.1064	0.0647	0.1712

Additionally, the examination of the temperature differentials between the outer tube's internal and external surfaces reveals pertinent insights. In the second case, the differential registers the lowest value among the cases at 0.008 °C, whereas the first and third cases exhibit closely averaged values around 0.107 °C. Furthermore, the third case exhibits the lowest temperature differential between the outer tube's internal surface and the inner tube's external surface, measuring at 0.06 °C. This observation underscores the dominance of convection as fluid velocity increases, contrasting with the scenario in the lowest velocity case where a larger temperature differential is evident.

4.5.3. Pressure drop

**Figure 4.39:** pressure drop variation along the axial direction for test 05

The relationship between pressure drop and the fluid velocity gives us important information about how heat transfer systems behave. Increasing the velocity makes the pressure drop increase noticeably compared to lower velocities. with an average increase of 2, 3.8, and 16 times for cases 1, 2, and 3 respectively, compared to a smooth tube configuration. When fluid velocity increases, it leads to greater frictional forces between the fluid and tube walls (see figure 4.39), this increased friction results in more energy being dissipated, causing a higher pressure drop along the flow path, moreover, higher fluid velocity typically correlates with a higher pressure drop and higher wall shear stress.

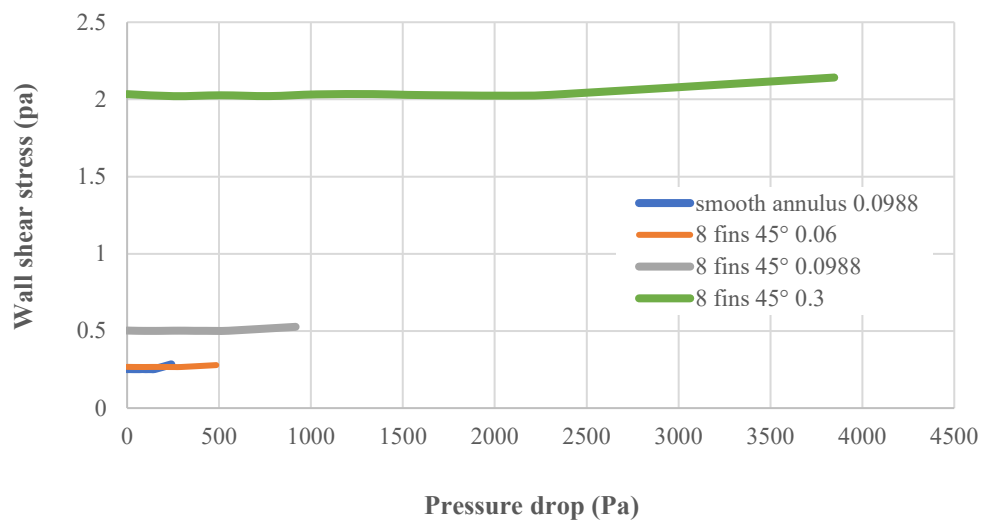


Figure 4.40: wall shear stress versus pressure drop for all cases in test 05

Figure 4.40 illustrates a clear connection between wall shear stress and pressure drop. As wall shear stress rises, so does pressure drop, indicating that both increase with higher fluid velocity. Notably, the first and second cases do not show a similar rise in wall shear stress and pressure drop compared to the third case. These findings imply that the impact of increasing velocity on wall shear stress and pressure drop is more similar to the third case than the first and second cases. This emphasizes that the main factor driving the increase in pressure drop and wall shear stress is the rise in fluid velocity.

4.5.4. Heat transfer

In our study, fins were identified as the primary factor contributing to a decrease in surface heat flux. This observation is supported by the figure 4.41, which demonstrates a slight reduction in surface heat flux with an increase in fluid velocity.

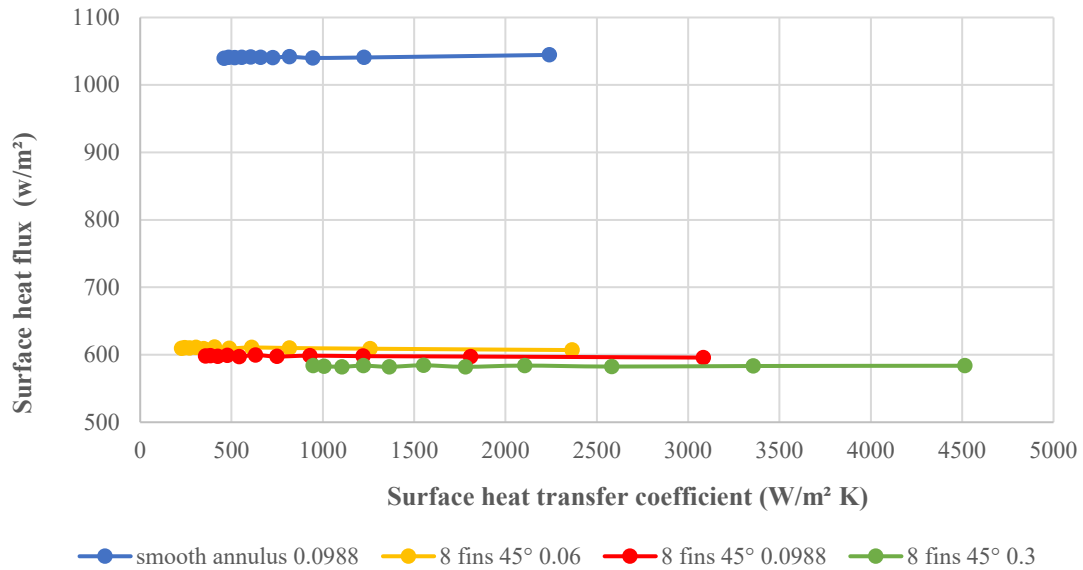


Figure 4.41: heat flux versus heat transfer coefficient for all cases of test 05

Furthermore, an increase in fluid velocity corresponds to a rise in the surface heat transfer coefficient, indicating a direct correlation between these two variables. As fluid velocity increases, so does the heat transfer coefficient. This can be attributed to the enhanced fluid mixing and increased convective heat transfer rate between the fluid and the tube surface at higher velocities. However, it is important to note that while increasing fluid velocity leads to a decrease in surface heat flux, as shown in figure 4.41, it also results in more heat being transferred per unit area.

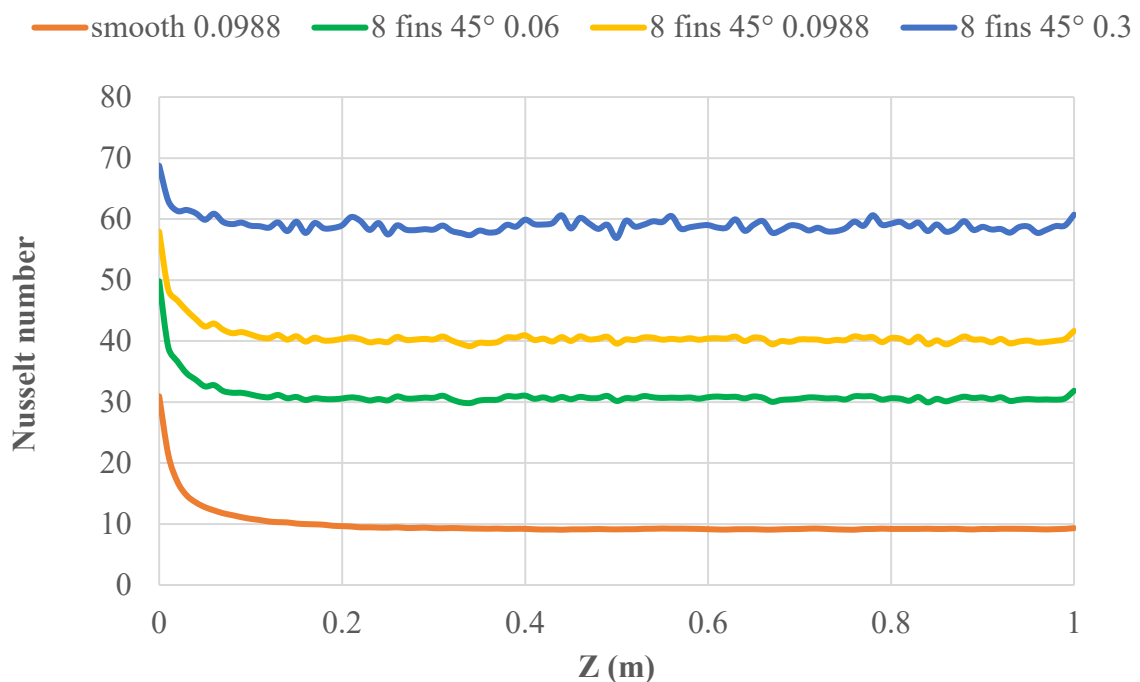


Figure 4.42: plot of Nusselt number along the axial direction for all cases of test 05

The Nusselt number (Nu) measures the effectiveness of convective heat transfer compared to conductive heat transfer in a fluid system. Higher fluid velocities typically result in higher Nusselt numbers due to increased mixing and turbulence, which enhance heat exchange. However, in the observed scenario, the Nusselt numbers varied across different cases. Specifically, in the third case, the average Nusselt number at the inlet reached 0.196. This notable increase is attributed to the elevated heat transfer coefficient observed in this case. In contrast, lower Nusselt numbers of 0.165, 0.142, and 0.088 were recorded for the second, first, and reference cases respectively. These variations highlight the direct relationship between fluid velocity, heat transfer coefficient, and Nusselt number, underscoring the significance of fluid dynamics in heat transfer processes. Additionally, a small perturbation in Nusselt plot was observed when increasing fluid inlet velocity and it was clear at the third case. Furthermore, the observed trends suggest that increasing velocity tends to dominate convective heat transfer, while decreasing velocity favors conductive heat transfer mechanisms.

4.5.5. Conclusion

This test investigated the influence of fluid velocity on heat transfer within a finned annulus. Three velocities (0.006, 0.0988, and 0.3 m/s) were examined in an annulus equipped with eight helical fins at a 45° helix angle. The results revealed a clear trend: increasing fluid velocity led to improved heat transfer, evidenced by lower minimum fluid temperatures. This is because faster-moving fluid has less time to absorb heat from the heated outer tube. Notably, the highest velocity case (0.3 m/s) exhibited the lowest minimum fluid temperatures, with an outlet temperature of 15.46°C compared to 17.33°C for the lowest velocity case (0.006 m/s). Additionally, the highest velocity case demonstrated the highest Nusselt number (0.196 at the inlet), signifying superior heat transfer efficiency. However, this enhancement in heat transfer came at the cost of increased pressure drop and wall shear stress. The pressure drop in the highest velocity case was 16 times higher than that in the smooth tube configuration, highlighting the trade-off between heat transfer and energy consumption.

General conclusion

This thesis delves into the intricate world of heat transfer and fluid dynamics within solar thermal collectors, specifically focusing on the tubes that transport the heat-carrying fluid. We conducted a comprehensive investigation, employing both theoretical analysis and advanced computer simulations, to understand how different tube designs and configurations impact the efficiency and performance of these crucial components.

Our journey began with a thorough review of existing research on solar thermal collectors, paying particular attention to studies on enhancing heat transfer within the tubes. We explored various methods, including the use of nanofluids, innovative tube geometries, and the integration of fins. Our focus ultimately landed on internal helical fins, a promising technology with the potential to significantly improve heat transfer efficiency.

To accurately model the complex physical processes at play, we developed a robust mathematical framework. This framework incorporated essential equations governing fluid flow and heat transfer, along with relevant parameters such as pressure drop, friction factor, and the Nusselt number. We carefully considered the geometry of the annulus and the helical fins, meticulously defining their dimensions and properties.

With the theoretical foundation laid, we turned to computational fluid dynamics (CFD) simulations to bring our model to life. We meticulously constructed the simulation environment, paying close attention to the mesh structure and element size to ensure accurate and reliable results. We then conducted a series of tests to investigate the impact of various factors on the system's thermo-hydraulic behavior.

We carefully designed each test and investigation for this PhD thesis to answer our research questions. By examining these results closely, we aim to contribute new knowledge to our field. We can conclude that all the results lead to the following points:

- Choosing the unstructured tetrahedral mesh, and by using a small mesh element size which found preferable for obtaining more accurate and precise results. However, it may require more time. Saving calculation time is one of the important factors to consider, especially when the differences in results are minimal. In our case, element sizes of 0.0001 and 0.0005 meters yield almost identical results, except for the visualization of velocity and temperature contours, where the finer mesh (0.0001 meters) provides clearer visuals. Nevertheless, due to the significantly longer calculation time associated with the finer mesh, we have opted for the 0.0005-meter element size for all our simulations.
- Several parameters are tested in our study with the aim of enhancing heat performance. We began by increasing the number of fins from 2 and 4 to 8 helical fins with a 20° helix angle. We then proceeded to increase the helix angle from 0° to 20°, 30°, and 45°. We also varied the heat flux, which was raised from 500 to 1000 to 3000 W/m² in the case of 2 helical fins with a 20° helix angle. Additionally, we examined fluid velocity, which yielded good results when decreased from 0.3 to 0.0988 to 0.06 m/s. Each variation underwent rigorous testing to improve the system's thermo-hydraulic performance, resulting in significant enhancement across all parameters and configurations. We found that increasing the number of fins, helix angle, and heat flux raises the fluid temperature and improves heat transfer performance, with similar results observed when decreasing fluid velocity.
- Using helical fins and increasing their helix angle leads to a decrease in the fluid-outer tube interface temperature, attributed to the increase in exchange surface area, which enhances temperature dissipation to the fluid, consequently raising fluid and inner tube temperatures compared to the reference case.
- The pressure drop increases with the number of fins, helix angle, and velocity due to increased surface area, frictional resistance, and greater turbulence encountered by the fluid flow. In contrast, when heat flux rises, the pressure drop remains constant.

- The wall shear stress has a proportional relationship with pressure drop, which also increases with the aforementioned parameters.
- The heat flux of the fluid-outer tube interface decreases with increasing fins number, helix angle, and fluid velocity, attributed to the enhanced temperature dissipation when these parameters are raised.
- The Nusselt number increases with elevating fins number, helix angle, and fluid velocity due to its relationship with heat transfer coefficient, except for the scenario of rising heat flux, which maintains an equal value due to constant heat transfer coefficient values in that case.
- In the test of increased velocity, we observed that a decrease in fluid velocity corresponds to an increase in temperature differential between outer and inner tube surfaces. Fins enhance heat dissipation to the fluid, resulting in smaller temperature gaps between the outer and inner tube surfaces compared to the reference case.
- Increasing fluid velocity leads to a dominance of convection, reducing temperature differentials between the outer tube's internal and external surfaces, emphasizing the relationship between fluid flow rate and heat transfer efficiency.

Finally, our comprehensive analysis and experimentation have shed light on crucial aspects of thermal-fluid dynamics within our system. Through meticulous testing and comparison, we have identified the tetrahedral mesh structures, the optimal mesh element size for balancing accuracy and computational efficiency, and the nuanced effects of varying parameters such as fins number, helix angle, heat flux, and fluid velocity on heat transfer performance and pressure drop. These findings not only deepen our understanding of the system's thermo-hydraulic behavior but also offer valuable insights for optimizing similar systems in practical applications.

Future studies

In future studies, it would be beneficial to explore additional avenues for enhancing the performance of solar thermal collector tubes beyond the parameters investigated in this research. One promising area for further investigation is the variation of fins height and width, as well as the geometry of the fins themselves. By altering these dimensions, we can potentially optimize heat transfer efficiency and pressure drop characteristics. Additionally, exploring the impact of tube thickness on thermal performance could provide valuable insights into the trade-offs between structural integrity and heat transfer capability. Furthermore, there are numerous other aspects of solar thermal collectors that warrant attention, such as the design of absorber plates, insulation materials, and overall system configuration. By systematically studying these factors, we can work towards achieving the perfect performance of solar thermal collector systems, as envisioned in the literature review. It is important to recognize that while our study focused specifically on solar thermal collector tubes, the principles and methodologies employed can be extended to other components of solar thermal systems, paving the way for comprehensive optimization and innovation in the field.

References

- [1] Student energy, energy systems map, <https://www.studentenergy.org/map>.
- [2] S. Mekhilef, r. Saidur, a. Safari, 2011, A review on solar energy use in industries, *Renewable and Sustainable Energy Reviews* 15 1777–1790.
- [3] Mirunalini thirugnanasambandam, s. Iniyan, ranko goic, 2010, A review of solar thermal technologies, *Renewable and Sustainable Energy Reviews* 14 312–322.
- [4] Cesare S. Survey of energy resources 2001 — solar energy. London, UK: World Energy Council, 2001.
- [5] California solar center, <http://californiasolarcenter.org/history-solarthermal/>.
- [6] National renewable energy laboratory, http://www.nrel.gov/pv/assets/images/efficiency_chart.jpg.
- [7] Us. Energy information administration, office of energy analysis, U.S. department of energy, Washington, DC 20585, International energy outlook 2016 – with projections to 2040.
- [8] The Regional Center for Renewable Energy and Energy Efficiency (RCREEE), Country Profile - Renewable Energy - Algeria 2012.
- [9] T. Boufendi, M. Afrid, Three-dimensional Conjugate Conduction-Mixed Convection with Variable Fluid Properties in a Heated Horizontal Pipe, *Rev. Energies Renouvelables*, Vol. 8, pp.1-18, (2005).
- [10] T. Boufendi, Contribution à l'étude théorique des transferts thermiques dans un conduit cylindrique horizontal soumis à un phénomène de convection mixte, Thèse de Doctorat d'Etat, Université Mentouri Constantine (2005).
- [11] M. Benkhadda, Transferts Thermiques dans un Conduit Cylindrique Annulaire Muni d'Ailettes, Mémoire de Magistère en physique Energétique, Département de physique, Université Mentouri Constantine (2010).
- [12] K. Chahboub, Influence de la conduction pariétale sur les transferts thermiques conjugués dans un conduit horizontal, Mémoire de Magistère en Physique Energétique, Département de physique, Université Mentouri Constantine (Dec.2011).
- [13] S. Touahri, phenomenes de convection mixte a proprietes variables dans les conduits cylindriques à ailettes et sans ailettes, Thèse de Doctorat d'Etat, Université Mentouri Constantine (2012).
- [14] J. H. Lienhard IV, J. H. Lienhard V, 2016, A heat transfer textbook, 4rd ed, Cambridge, MA, Phlogiston Press.

- [15] Abdeslam omara, 2007, numerical study of transient laminar mixed convection in vertical thick cylindrical duct, Ph.D. thesis, university of Mentouri Constantine.
- [16] Cours de transfert de chaleur de l'université de technologie de Compiègne.
- [17] S. A. Klein, 1975, Calculation of flat-plate collector loss coefficients, *Solar Energy*. Vol 17, pp. 79-8.
- [18] K. G. T. HOLLANDS, J. L. WRIGHT, 1983, heat loss coefficients and effective $\tau\alpha$ products for flat-plate collectors with diathermanous covers, *Solar Energy*. Vol 17, pp. 79-8.
- [19] N. E. WIJEYSUNDERA, M. IQBAL, 1991, effect of plastic cover thickness on top loss coefficient of flat-plate collectors, *Solar Energy* Vol. 46, No. 2, pp. 83-87.
- [20] A. Oliva, m. Costa, and c. D. Perez segarra, 1991, Numerical simulation of solar collectors: The effect of nonuniform and nonsteady State of the boundary conditions, *Solar Energy* Vol. 47. No. 5, pp. 359-373.
- [21] I.m. michaelides, s.a. kalogirou, i. Chrysis, g. Roditis, a. Hadjiyianni, h.d. kambezidis, m. Petrakis, s. Lykoudis, a.d. adamopoulos, 1999, Comparison of performance and cost effectiveness of solar Water heaters at different collector tracking modes in Cyprus and Greece, *Energy conversion & management* 40 1287–1303.
- [22] A. J. De Ron, 1980, Dynamic modelling and verification of a Flat-plate solar collector, *Solar Energy*, Vol 24, pp. 117–128.
- [23] F. Hilmer, k. Vajen, a. Ratka, h. Ackermann, w. Fuhs and o. Melsheimer, 1999, Numerical solution and validation of a dynamic model of Solar collectors working with varying fluid flow rate, *Solar Energy* Vol. 65, No. 5, pp. 305–321.
- [24] S.a. kalogirou, y. Tripanagnostopoulos, 2006, Hybrid PV/T solar systems for domestic hot Water and electricity production, *Energy Conversion and Management* 47 3368–3382.
- [25] G. A. Florides, s. A. Kalogirou, s. A. Tassou and l. C. Wrobel, 2002, Modelling and simulation of an absorption solar cooling System for Cyprus, *Solar Energy* Vol. 72, No. 1, pp. 43–51.
- [26] Z.s. lu, r.z. wang, z.z. xia, x.r. lu, c.b. yang, y.c. ma, g.b. ma, 2013, Study of a novel solar adsorption cooling system and a solar absorption cooling System with new CPC collectors, *Renewable energy* 50 299–306.
- [27] M. Balghouthi, m.h. chahbani, a. Guizani, 2012, Investigation of a solar cooling installation in Tunisia, *Applied energy* 98 138–148.

- [28] G. A. Florides, s. A. Kalogirou, s. A. Tassou and I. C. Wrobel, 2002, Modelling, simulation and warming impact assessment of a domestic-size absorption solar cooling system, *Applied thermal engineering* 22 1313–1325.
- [29] S.U.S. Choi, 1995, Enhancing thermal conductivity of fluids with nanoparticles *Developments and applications of Non-Newtonian Flows*, D.A. Siginer and H.P. Wang (Eds.), FED-vol. 231/MD-vol. 66, ASME, New York, pp. 99-105.
- [30] J.A. Eastman, S.U.S. Choi, S. Li, W. Yu, and L.J. Thompson, 2001, Anomalously increased effective thermal conductivities of ethylene glycol based nanofluids containing copper nanoparticles, *Applied Physics Letters*, 78(6): 718-720.
- [31] S.U.S. Choi, Z.G. Zhang, W. Yu, F.E. Lockwood, and E.A Grulke, 2001, Anomalous thermal conductivity enhancement in nanotube suspension, *Applied Physics Letters*, 79(14), pp. 2252-2254.
- [32] Hui Zhang, Hui-Jiuan Chen, Xiaoze Du, Dongsheng Wen, 2014, Photothermal conversion characteristics of gold nanoparticle dispersions, *Vol 100*, pp 141–147.
- [33] R. C. Martinelli, L. M. K. Boelter, *The Analytical Prediction of Superposed Free and forced Viscous Convection in a Vertical Pipe*, University of California, Publications in Engineering, Vol. 5, N°2, pp. 23-58, (1942).
- [34] J. Orfi, N. Galanis, Bifurcation in Steady Laminar Mixed Convection Flow in Uniformly Heated Inclined Tubes, *International Journal of Numerical Methods for Heat and Fluid Flow*, Vol. 09, N°5, pp. 543-567, (1999).
- [35] M. Wang, T. Tsuji, Y. Nagano, Mixed Convection with Flow Reversal in The Thermal Entrance Region of Horizontal and Vertical Pipes, *Int. Journal of Heat and Mass Transfer*, Vol. 37, N°15, pp. 2305-2319, (1994).
- [36] Patankar, Suhas. *Numerical heat transfer and fluid flow*. CRC press, 2018.
- [37] T. Boufendi, M. Afrid, the physical Aspect of Three-Dimensional Mixed Convection in a Uniformly Heated Horizontal Pipe, *Sciences et Technologie A*, N°22, pp. 39-52, (2004).
- [38] S. Touahri, T. Boufendi, Numerical Study of the Conjugate Heat Transfer in a Horizontal Pipe Heated by Joulean Effect, *Thermal Science*, Vol. 16, pp. 53-67, (2012).
- [39] S. Abboudi, F. Papini, Approche Numérique et Expérimentale du Transfert Thermique Métal-Fluide dans un Conduit Rectangulaire en Régime Instationnaire Laminaire, *Int. J. Heat and Mass Transfer*, Vol. 33, N°09, pp. 1909-1919, (1990).

- [40] N. Mokrane, Corrélation Du Transfert De Chaleur Par Convection Mixte Dans Un Conduit Cylindrique, Mémoire de Magistère en physique Energétique, Département de physique, Université Mentouri Constantine (Oct.2010).
- [41] Qingpu Li, Leren Tao, Lei Li, Yongpan Hu, Shengli Wu, experimental investigation of the condensation heat transfer coefficient of R134a inside horizontal smooth and micro-fin tubes, *energies*, 2017.
- [42] K. Chahboub, T. Boufendi, Computational Study of the Conjugate Heat Transfer and the Wall Conduction Effects in a Horizontal Pipe with Temperature Dependent Properties, *International Review of Mechanical Engineering (IREME)*, Vol. 5, N°2, pp. 361-368, (Feb. 2011).
- [43] Chen, X., Zhang, L., Wang, X., & Zhang, H. (2021). Numerical study of laminar flow and heat transfer in concentric annular pipes. *International Journal of Heat and Mass Transfer*, 170, 120734.
- [44] Kim, J. H., & Park, S. D. (2022). Experimental investigation on turbulent heat transfer in annular channels with twisted tape inserts. *International Journal of Thermal Sciences*, 179, 106576.
- [45] Mojtabi, Abdelkader, and J-P. Caltagirone. "Analyse du transfert de chaleur en convection mixte laminaire entre deux cylindres coaxiaux horizontaux." *International Journal of Heat and Mass Transfer* 23.10 (1980): 1369-1375.
- [46] S. Kotake, N. Hattori, Combined forced and free convection heat transfer for fully-developed laminar flow in horizontal annuli, *International Journal of Heat and Mass Transfer*, Volume 28, Issue 11, Pages 2113-2120, 1985.
- [47] Habib, M. A., and A. A. A. Negm. "Laminar mixed convection in horizontal concentric annuli with non-uniform circumferential heating." *Heat and Mass Transfer* 37.4 (2001): 427-435.
- [48] Teamah, Mohamed A. "Numerical simulation of double diffusive natural convection in rectangular enclosure in the presences of magnetic field and heat source." *International Journal of Thermal Sciences* 47.3 (2008): 237-248.
- [49] Padilla, Ricardo Vasquez, et al. "Heat transfer analysis of parabolic trough solar receiver." *Applied energy* 88.12 (2011): 5097-5110.
- [50] Richard L. Shilling, Patrick M. Bernhagen, Victor M. Goldschmidt, Predrag S. Hrnjak, David Johnson, Klaus D. Timmerhaus, 2008, Perry's chemical engineers handbook '8th edition' - Section 11 - Heat-Transfer Equipment.
- [51] Yves jannot, 2012, transferts thermiques, Ecole des Mines Nancy 2ème année.

- [52] M. Ouzzane, Développement simultané en convection mixte laminaire dans une conduite avec un flux de chaleur non uniforme sur sa surface externe : cas avec et sans ailettes Thèse de doctorats, Sherbrooke (2000).
- [53] E.N. Pis'mennyi, 2014, Heat transfer enhancement at tubular transversely finned heating surfaces, *International Journal of Heat and Mass Transfer* 70 1050–1063.
- [54] Abhishek Priyam, Prabha Chand, 2016, Thermal and thermo-hydraulic performance of wavy finned absorber solar air heater, *Solar Energy* 130, 250–259.
- [55] S.V. Patankar, M. Ivanovic, E.M. Sparrow, (1979), Analysis of turbulent flow and heat transfer in internally finned tubes and annuli, *Journal of Heat Transfer* 101:29-37.
- [56] Peng H, Liu L, Ling X, Li Y, (2016), Thermo-hydraulic performances of internally finned tube with a new type wave fin arrays. *Appl Therm Eng* 98:1174–1188.
- [57] M. Lin, L. Tian, Q-W. Wang, (2011), Laminar Heat Transfer Characteristic of Internally Finned Tube with Sinusoidal Wavy Fins, *Heat and Mass Transfer*, 47, 641-653.
- [58] Q-W. Wang, M. Lin, M. Zeng and L. Tian, (2008), Computational Analysis of Heat Transfer and Pressure Drop Performance for Internally Finned Tubes with Three Different Longitudinal Wavy Fins, *Heat and Mass Transfer*, 45, 147-156.,
- [59] I. Dağtekin, H. F. Öztop and A. Z. Şahin, (2005), An Analysis of Entropy Generation Through a Circular Duct with Different Shaped Longitudinal Fins Laminar Flow, *International Journal of Heat and Mass Transfer*, 48, 171–181.
- [60] Wang QW, Lin M, Zeng M, (2009), Effect of lateral fin profiles on turbulent flow and heat transfer performance of internally finned tubes, *Appl Therm Eng*, 29, 3006–3013.
- [61] Huang S, Wana Z, Tang Y, (2019), Manufacturing and single-phase thermal performance of an arc-shaped inner finned tube for heat exchanger, *Appl Therm Eng*, 159, 113817.
- [62] Liao Q, Zhu X, Xin MD, (2000), Augmentation of turbulent convective heat transfer in tubes with three-dimensional internal extended surfaces, *J Enhanc Heat Transf*, 7(3), 139–151.
- [63] Kim NH, (2015), Single-phase pressure drop and heat transfer measurements of turbulent flow inside helically dimpled tubes, *J Enhanc Heat Transf*, 22(4), 345–363.
- [64] Kim DK, (2016), Thermal optimization of internally finned tube with variable fin thickness, *Appl Therm Eng*, 102, 1250–1261.

- [65] Duan L, Ling X, Peng H, (2018), Flow and heat transfer characteristics of a double-tube structure internal finned tube with blossom shape internal fins, *Appl Therm Eng*, 128, 1102–1115.
- [66] Yampolsky JS, (1983), Spirally fluted tubing for enhanced heat transfer. In: Taborek J, Hewitt GF, Afgan N (eds) *Heat exchangers-theory and practice*. Hemisphere Publishing Corp, Washington, DC, pp 945–952.
- [67] Bilen K, Cetin M, Gul H, Balta T, (2009), The investigation of groove geometry effect on heat transfer for internally grooved tubes, *Appl Therm Engg*, 29(4), 753–761.
- [68] S. Deorah, (2012), CFD Analysis of a vertical tube having internal fins for the natural convection, thesis in Bachelor of Technology, Department of Mechanical Engineering National Institute of Technology, Rourkela.
- [69] Fujie K, Itoh N, Innami T, Kimura H, Nakayama N, Yanugidi T, (1977), Heat transfer pipe. U. S. Patent 4,044,797, assigned to Hitachi Ltd.
- [70] Gregory J. Zdaniuk, Louay M. Chamra, Pedro J. Mago, Experimental determination of heat transfer and friction in helically-finned tubes, *Experimental Thermal and Fluid Science* 32 (2008) 761–775.
- [71] Soliman, H.M., Chau, T.S. et Trupp, A.C., “Analysis of laminar heat transfer in internally finned tubes with uniform outside wall temperature”, *Journal of Heat Transfer*, vol. 102, November, pp. 598-604. 1980.
- [72] L.M. Schlager, M.B. Pate, A.E. Bergles, (1990), Evaporation and condensation heat transfer and pressure drop in horizontal, 12.7-mm microfin tubes with refrigerant 22, *J. Heat Transfer*, 112, 1041–1047.
- [73] Webb, R. L., & Li, W. (2000). Fouling in enhanced tubes using cooling tower water: Part I: long-term fouling data. *International journal of heat and mass transfer*, 43(19), 3567-3578.
- [74] Jamshed, S., Qureshi, s. R., Shah, A., & Hussain, A. "Investigation of entropy generation rate and its minimization in helical grooved tubes." *Journal of Mechanical Science and Technology* 32 (2018): 4983-4991.
- [75] Al-Fahed S, Chamra LM, Chakroun W, (1998), Pressure drop and heat transfer comparison for both microfin tube and twisted-tape inserts in laminar flow, *Exp Thermal Fluid Sci*, 18(4), 323–333.
- [76] Jensen MK, Vlakancic A, (1999), Technical note experimental investigation of turbulent heat transfer and fluid flow in internally finned tubes, *Int J Heat Mass Transf*, 42(7), 1343–1351.

- [77] Afroz HM, Miyara A, (2007), Friction factor correlation and pressure loss of single-phase flow inside herringbone microfin tubes, *Int J Refrig*, 30(7), 1187–1194.
- [78] Raj R, Lakshman NS, Mukkamala Y, (2015), Single phase flow heat transfer and pressure drop measurements in doubly enhanced tubes, *Int J Therm Sci*, 88, 215–227.
- [79] Wang C C, Chen P Y, Jang J Y, (1996), Heat transfer and friction characteristics of convex-louver fin-and-tube heat exchangers, *Exp Heat Transf*, 9, 61–78.
- [80] Copetti JB, Macagnan MH, de Souza D, Oliveski RDC, (2004), Experiments with micro-fin tube in single phase, *Int J Refrig*, 27(8), 876–883.
- [81] Li XW, Meng JA, Li ZX, (2007), Experimental study of single-phase pressure drop and heat transfer in a micro-fin tube, *Exp Thermal Fluid Sci*, 32(2), 641–648.
- [82] Mukkamala Y, Sundaresan R, (2009), Single-phase flow pressure drop and heat transfer measurements in a horizontal microfin tube in the transition regime, *J Enhanc Heat Transf*, 16 (2), 141–159.
- [83] Celen A, Dalkilic AS, Wongwises S, (2013), Experimental analysis of the single-phase pressure drop characteristics of smooth and micro-fin tubes, *Int Commun Heat Mass Transf*, 46, 58–66.
- [84] Ravigururajan TS, Bergles AE, (1995), Prandtl number influence on heat transfer enhancement in turbulent flow of water at low temperatures, *J Heat Transf*, 117(2), 276–282.
- [85] Webb RL, Narayanamurthy R, Thors P (2000) Heat transfer and friction characteristics of internal helical-rib roughness. *J Heat Transf* 122(1):134–142.
- [86] Han DH, Lee KJ, (2005), Single-phase heat transfer and flow characteristics of micro-fin tubes, *Appl Therm Engg*, 25(11–12), 1657–1669.
- [87] Zdaniuk GJ, Luck R, Chamra LM, (2008), Linear correlation of heat transfer and friction in helically finned tubes using five simple groups of parameters, *Int J Heat Mass Transf*, 51 (13–14), 3548–3555.
- [88] Aroonrat K, Jumpholkul C, Leelaprachakul R, Dalkilic AS, Mahian O, Wongwises S, (2013), Heat transfer and single-phase flow in internally grooved tubes, *Int Commun Heat Mass Transf*, 42, 62–68.
- [89] Solanki, A. K., & Kumar, R. (2018). Condensation of R-134a inside dimpled helically coiled tube-in-shell type heat exchanger. *Applied Thermal Engineering*, 129, 535-548.
- [90] A E Maakoul, M E Metoui, A B Abdallah, S Saadeddine, M Meziane, (2017), Numerical investigation of thermohydraulic performance of air to water double-pipe

- heat exchanger with helical fins, *Applied Thermal Engineering*, Volume 127, Pages 127-139.
- [91] M. Ito, H. Kimura, Boiling heat transfer and pressure drop in internal spiral grooved tubes, *JSME* 22 (1979) 1251–1257.
- [92] C M Yang, P Hrnjak, (2019), Effect of helical micro-fins on two-phase flow behavior of R410A evaporating in horizontal round tubes obtained through visualization, *Int. J. Heat Mass Transf*, 144, 118654.
- [93] G W Mann, S Eckels, (2019), multi-objective heat transfer optimization of 2D helical micro-fins using NSGA-II, *Int. J. Heat Mass Transf*, 132, 1250–1261.
- [94] G J Zdaniuk, L M Chamra, P J Mago, (2008), Experimental determination of heat transfer and friction in helically-finned tubes, *Exp Thermal Fluid Sci*, 32, 761–775.
- [95] J Muñoz, A Abánades, (2011), analysis of internal helically finned tubes for parabolic trough design by CFD tools, *A*
- [96] Darcy friction factor formulae. In Wikipedia. retrieved November 15, 2017, from https://en.wikipedia.org/wiki/Darcy_friction_factor_formulae.
- [97] Y-H Wang, J-L Zhang, Z-X Ma, Experimental determination of single-phase pressure drop and heat transfer in a horizontal internal helically-finned tube, *International Journal of Heat and Mass Transfer* 104 (2017) 240–246.
- [98] Munson, Bruce R., Young, Donald F., Okiishi, Theodore H., Huebsch, Wade W., *Fundamentals of Fluid Mechanics*, sixth edition, John Wiley & Sons, Inc., 2009.
- [99] S. Pirbastami, "CFD Simulation of Heat Enhancement in Internally Helical Grooved Tubes" (2015). UNLV Theses, Dissertations, Professional Papers, and Capstones. 2496.
- [100] Kaji, R., Yoshioka, S., Fujino, H., the effect of inner grooved tubes on the heat transfer performance of air-cooled heat exchangers of co2 heat pump system at international refrigeration and air conditioning conference, Purdue e-pubs, (2012).
- [101] Donalson I.G., Free convection in a vertical tube with linear wall temperature gradient, 1961.
- [102] I. Nazrul, U.N. Gaitonde, G.K. Sharma, Mixed convection heat transfer in the entrance region of horizontal annuli, *Int. J. Heat and Mass Transfer*, Vol. 44, N°11, pp. 2107-2120, (2001).

Annex I

How to calculate the trapeze external circumference, trapeze cross section, fin helical length?

$$b - a = a'' + b'' = 2a'' = 2b''$$

$$c^2 = b''^2 + h^2$$

$$c = \sqrt{b''^2 + h^2}$$

$$c = \sqrt{\left(\frac{b-a}{2}\right)^2 + h^2}$$

$$a = 0.257 \text{ mm}$$

$$b = 0.343 \text{ mm}$$

$$h = 1.2 \text{ mm}$$

$$c = \sqrt{\left(\frac{0.343 - 0.257}{2}\right)^2 + 1.2^2}$$

$$c = \sqrt{0.001849 + 1.44}$$

$$c = 1.2007 \text{ mm}$$

The trapeze external circumference (A) is equal to the sum

$$A = c + a + c$$

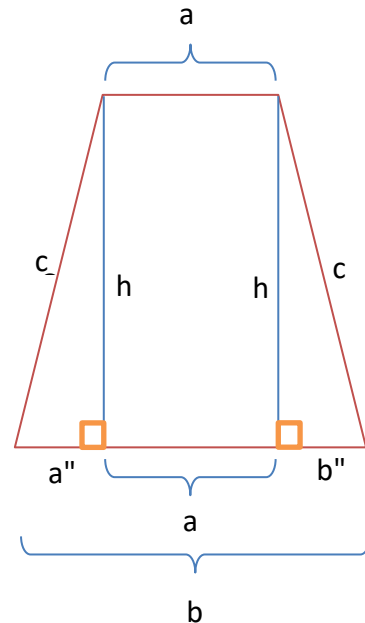
$$A = 2c + a = 2 \times 1.2007 + 0.257 = 2.6584 \text{ mm}$$

We can estimate that the value of «c» is equal to «h» because of ($c - h = 0.0007 \text{ mm}$)

This allows us to assume that

$$A = 2c + a \approx 2h + a = (2 \times 1.2) + 0.257 = 2.657 \text{ mm} \approx 2.6584 \text{ mm}$$

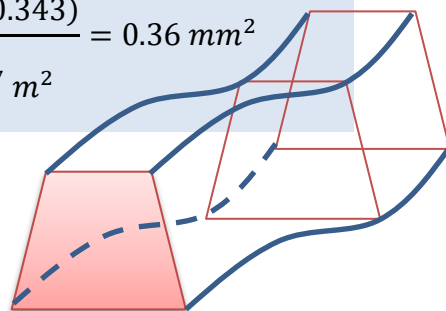
$$A = 2.657 \text{ mm}$$



Trapèze cross section

$$S = \frac{h(a+b)}{2} = \frac{1.2(0.257 + 0.343)}{2} = 0.36 \text{ mm}^2$$

$$S = 3.6 \times 10^{-7} \text{ m}^2$$



Annex II

The calculation of "Pr", "Re", " ρ ", " q_v ", " q_m "

$$\rho \text{ (electrical resistivity)} = 1.033 \times 10^{-5} \Omega m$$

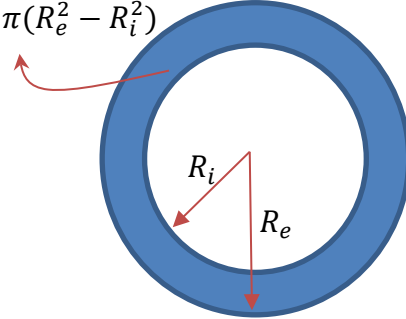
$$L \text{ (characteristic length)} = 1 m$$

$$a \text{ (cross section area)} = 6.16 \times 10^{-6} m^2$$

R (electrical resistance)

$$\rho = \frac{R * a}{L} \Rightarrow R = \frac{\rho * L}{a} = 1.67 \Omega$$

$$S = \pi(R_e^2 - R_i^2)$$



$$Pr = \frac{v}{a} = \frac{\mu/\rho}{k/(\rho Cp)} = \frac{\mu Cp}{k}$$

$$\mu \text{ (dynamic viscosity)} = 1153.94 \mu Pa \cdot s = 0.00115394 kg/m \cdot s$$

$$Cp \text{ (specific heat)} = 4.1855 kJ/kg \cdot K = 4185.5 J/kg \cdot K$$

$$k \text{ (thermal conductivity)} = 0.5889 W/m K$$

$$Pr = \frac{\mu Cp}{k} = \frac{0.00115394 \times 4185.5}{0.5889} = 8.201$$

$$Re = \frac{\rho v L}{\mu}$$

$$\mu \text{ (dynamic viscosity)} = 1153.94 \mu Pa \cdot s = 0.00115394 kg/m \cdot s$$

$$L \text{ (characteristic distance)} = 0.96 cm = 0.0096 m$$

$$V \text{ (fluid velocity)} = 7.2 \times 10^{-2} m/s$$

$$\rho_{(water)} \text{ (Saturated Liquid Water density at } 15^\circ C) = 999.079 kg/m^3$$

$$Re = \frac{\rho v L}{\mu} = \frac{999.079 \times 7.2 \times 10^{-2} \times 0.0096}{0.00115394} = 598.44$$

Contribution to the theoretical study of heat and dynamic transfers in finned and unfinned solar absorbers

Abstract: This thesis delves into the intricate world of heat transfer and fluid dynamics within solar thermal collectors, specifically focusing on the tubes that transport the heat-carrying fluid. We conducted a comprehensive investigation, employing both theoretical analysis and advanced computer simulations, to understand how different tube designs and configurations impact the efficiency and performance of these crucial components. Our journey began with a thorough review of existing research on solar thermal collectors, paying particular attention to studies on enhancing heat transfer within the tubes. We explored various methods, including the use of nanofluids, innovative tube geometries, and the integration of fins. Our focus ultimately landed on internal helical fins, a promising technology with the potential to significantly improve heat transfer efficiency. To accurately model the complex physical processes at play, we developed a robust mathematical framework. This framework incorporated essential equations governing fluid flow and heat transfer, along with relevant parameters such as pressure drop, friction factor, and the Nusselt number. We carefully considered the geometry of the annulus and the helical fins, meticulously defining their dimensions and properties. With the theoretical foundation laid, we turned to computational fluid dynamics (CFD) simulations to bring our model to life. We meticulously constructed the simulation environment, paying close attention to the mesh structure and element size to ensure accurate and reliable results. We then conducted a series of tests to investigate the impact of various factors on the system's thermo-hydraulic behavior. We carefully designed each test and investigation for this PhD thesis to answer our research questions. By examining these results closely, we aim to contribute new knowledge to our field.

Through a comprehensive examination of results, several key findings emerged: contrasting tetrahedral mesh structures; a smaller mesh element sizes yield more accurate results, they come at the cost of longer computational time, hence, a balance between accuracy and efficiency is crucial. Various parameters including fins number, helix angle, heat flux, and fluid velocity were tested, leading to significant enhancements in thermo-hydraulic performance across all configurations. Increasing fins number, helix angle, and heat flux raised fluid temperature and improved heat transfer performance, whereas decreasing fluid velocity yielded similar effects. Helical fins and higher helix angles led to reduced fluid-outer tube interface temperatures due to increased exchange surface area, while pressure drop, wall shear stress, and heat flux at the fluid-outer tube interface increased with these parameters. Additionally, the Nusselt number increased with fins number, helix angle, and fluid velocity, and decreased with rising heat flux, highlighting the intricate relationship between these factors and heat transfer efficiency. Overall, these findings deepen our understanding of solar thermal collector optimization, emphasizing the importance of parameters in enhancing performance and efficiency.

Keywords: Solar thermal collectors, heat transfer, fluid dynamics, internal helical fins, computational fluid dynamics, thermo-hydraulic behavior, pressure drop, heat flux.

المساهمة في الدراسة النظرية للانتقالات الحرارية والديناميكية في الممتصات الشمسية المزودة بأجنحة وغير المزودة بأجنحة

ملخص: تنغمس هذه الرسالة في عالم معقد من نقل الحرارة وديناميات السوائل داخل جمعيات الطاقة الشمسية الحرارية، مركزة بشكل خاص على الأنابيب التي تنقل السائل الحار. قمنا بتنفيذ تحقيق شامل، باستخدام تحليل نظري ومحاكاة حاسوبية متقدمة، لفهم كيفية تأثير تصميمات الأنابيب وتكويناتها المختلفة على كفاءة وأداء هذه العناصر الحيوية. بدأت رحلتنا بمراجعة شاملة للأبحاث الحالية حول جمعيات الطاقة الشمسية الحرارية، مولاة اهتماما خاصا للدراسات حول تعزيز نقل الحرارة داخل الأنابيب. استكشفنا طرقاً مختلفة، بما في ذلك استخدام السوائل النانوية، والهندسة المبتكرة للأنابيب، ودمج الأجنحة. تركز اهتمامنا في النهاية على الأجنحة الحلزونية الداخلية، وهي تكنولوجيا واعدة لديها القدرة على تحسين كفاءة نقل الحرارة بشكل كبير. لنمنح العمليات الفيزيائية المعقدة بدقة، قمنا بتطوير إطار رياضي قوي. تضمن هذا الإطار المعادلات الأساسية التي تحكم تدفق السائل ونقل الحرارة، بالإضافة إلى المعلمات ذات الصلة مثل الضغط الهابط وعامل الاحتكاك ورقم نوسلت. نظرنا بعناية هندسة الحلقة الخارجية والأجنحة الحلزونية، وصفنا بدقة أبعادها وخصائصها. بعد رسم الأساس النظري، تحولنا إلى محاكاة الديناميكا السائلة الحاسوبية لإعطاء حياة لنموذجنا. بنينا بعناية بيئة المحاكاة، مولين اهتماما خاصا لهيكل الشبكة وحجم العنصر لضمان النتائج الدقيقة والموثوقة. ثم قمنا بإجراء سلسلة من الاختبارات للتحقيق في تأثير عوامل مختلفة على السلوك الحراري-هيدروليكي للنظام. صممنا كل اختبار وتحقيق بعناية لهذه الرسالة لنيل درجة الدكتوراه للإجابة على أسئلة البحث. من خلال فحص هذه النتائج عن كثب، نهدف إلى إضافة معرفة جديدة إلى مجالنا.

من خلال الفحص الشامل للنتائج، ظهرت عدة نتائج رئيسية: كشفت هياكل الشبكة التتراهيدرالية المتباينة عن أداء ودقة أفضل عند اختيار أحجام العناصر الصغيرة في الشبكة، إلا أنها تأتي بتكلفة زمن الحساب الأطول، لذلك فإن التوازن بين الدقة والكفاءة أمر حاسم. تم اختبار عدة معاملات بما في ذلك عدد الأجنحة، وزاوية الحلزون، وكثافة الحرارة، وسرعة السائل، مما أدى إلى تحسينات كبيرة في الأداء الحراري-هيدروليكي عبر جميع التكوينات. زيادة عدد الأجنحة، وزاوية الحلزون، وكثافة الحرارة، رفعت درجة حرارة السائل وأعطت أداء أفضل في نقل الحرارة، في حين أن خفض سرعة السائل أدى إلى تأثيرات مماثلة. أدت الأجنحة الحلزونية وزوايا الحلزون الأعلى إلى خفض درجات حرارة السائل عند واجهة الأنبوب الخارجية بسبب زيادة مساحة التبادل، في حين أن الضغط الهابط، والضغط الجداري، وكثافة الحرارة عند واجهة الأنبوب الخارجية زادت مع هذه المعاملات. بالإضافة إلى ذلك، زاد رقم نوسلت مع عدد الأجنحة، وزاوية الحلزون، وسرعة السائل، وانخفض مع زيادة كثافة الحرارة، مما يسلط الضوء على العلاقة المعقدة بين هذه العوامل وكفاءة نقل الحرارة. بشكل عام، تعمقت هذه النتائج فهمنا لتحسين جمعيات الطاقة الشمسية الحرارية، مؤكدة أهمية المعاملات في تعزيز الأداء والكفاءة.

الكلمات المفتاحية: الطاقة الشمسية الحرارية، نقل الحرارة، ديناميات السوائل، أجنحة حلزونية داخلية، الديناميكا

السائلية الحاسوبية، السلوك الحراري-هيدروليكي، انخفاض الضغط، كثافة الحرارة.

Contribution à l'étude théorique des transferts de chaleur et dynamiques dans les absorbeurs solaires ailetés et non ailetés

Résumé: Cette thèse plonge dans le monde complexe du transfert de chaleur et de la dynamique des fluides au sein des collecteurs solaires thermiques, en se concentrant spécifiquement sur les tubes qui transportent le fluide porteur de chaleur. Nous avons mené une enquête approfondie, en utilisant à la fois une analyse théorique et des simulations informatiques avancées, pour comprendre comment différents designs et configurations de tubes impactent l'efficacité et les performances de ces composants cruciaux. Notre parcours a commencé par une revue approfondie des recherches existantes sur les collecteurs solaires thermiques, en accordant une attention particulière aux études sur l'amélioration du transfert de chaleur dans les tubes. Nous avons exploré diverses méthodes, notamment l'utilisation de nano-fluides, des géométries de tubes innovantes, et l'intégration d'ailettes. Notre attention s'est finalement portée sur les ailettes hélicoïdales internes, une technologie prometteuse ayant le potentiel d'améliorer significativement l'efficacité du transfert de chaleur. Pour modéliser avec précision les processus physiques complexes en jeu, nous avons développé un cadre mathématique robuste. Ce cadre a intégré des équations essentielles régissant l'écoulement des fluides et le transfert de chaleur, ainsi que des paramètres pertinents tels que la perte de charge, le facteur de friction et le nombre de Nusselt. Nous avons soigneusement considéré la géométrie de l'annulus et des ailettes hélicoïdales, définissant méticuleusement leurs dimensions et leurs propriétés. Avec les fondements théoriques posés, nous nous sommes tournés vers des simulations de dynamique des fluides numériques (CFD) pour donner vie à notre modèle. Nous avons soigneusement construit l'environnement de simulation, en accordant une attention particulière à la structure du maillage et à la taille des éléments pour garantir des résultats précis et fiables. Nous avons ensuite mené une série de tests pour étudier l'impact de divers facteurs sur le comportement thermo-hydraulique du système. Nous avons soigneusement conçu chaque test et enquête pour cette thèse de doctorat afin de répondre à nos questions de recherche.

À travers un examen approfondi des résultats, plusieurs conclusions clés ont émergé: les structures de maillage tétraédriques avec des tailles d'éléments de maillage plus petites donnent des résultats plus précis, ils s'accompagnent d'un temps de calcul plus long, ainsi, un équilibre entre précision et efficacité est crucial. Divers paramètres, y compris le nombre d'ailettes, l'angle d'hélice, le flux de chaleur et la vitesse du fluide, ont été testés, entraînant des améliorations significatives des performances thermo-hydrauliques dans toutes les configurations. L'augmentation du nombre d'ailettes, de l'angle d'hélice et du flux de chaleur a augmenté la température du fluide et amélioré les performances du transfert de chaleur, tandis que la diminution de la vitesse du fluide a produit des effets similaires. Les ailettes hélicoïdales et les angles d'hélice plus élevés ont conduit à des températures d'interface fluide-tube externe réduites en raison de l'augmentation de la surface d'échange, tandis que la perte de charge, la contrainte de cisaillement sur la paroi et le flux de chaleur à l'interface fluide-tube externe ont augmenté avec ces paramètres. De plus, le nombre de Nusselt a augmenté avec le nombre d'ailettes, l'angle d'hélice et la vitesse du fluide, et a diminué avec l'augmentation du flux de chaleur, soulignant la relation complexe entre ces facteurs et l'efficacité du transfert de chaleur. Dans l'ensemble, ces résultats approfondissent notre compréhension de l'optimisation des collecteurs solaires thermiques, en mettant en évidence l'importance des paramètres dans l'amélioration des performances et de l'efficacité.

Mots-clés: Collecteurs solaires thermiques, transfert de chaleur, dynamique des fluides, ailettes hélicoïdales internes, dynamique des fluides computationnelle, comportement thermo-hydraulique, perte de charge, flux de chaleur.